

University of Louisville

ThinkIR: The University of Louisville's Institutional Repository

Electronic Theses and Dissertations

8-2023

Connectivity of amygdala somatostatin-expressing neurons and their role in taste-guided behavior.

Jane Jeruto Bartonjo
University of Louisville

Follow this and additional works at: <https://ir.library.louisville.edu/etd>



Part of the [Behavioral Neurobiology Commons](#), [Molecular and Cellular Neuroscience Commons](#), and the [Systems Neuroscience Commons](#)

Recommended Citation

Bartonjo, Jane Jeruto, "Connectivity of amygdala somatostatin-expressing neurons and their role in taste-guided behavior." (2023). *Electronic Theses and Dissertations*. Paper 4158.
<https://doi.org/10.18297/etd/4158>

This Doctoral Dissertation is brought to you for free and open access by ThinkIR: The University of Louisville's Institutional Repository. It has been accepted for inclusion in Electronic Theses and Dissertations by an authorized administrator of ThinkIR: The University of Louisville's Institutional Repository. This title appears here courtesy of the author, who has retained all other copyrights. For more information, please contact thinkir@louisville.edu.

CONNECTIVITY OF AMYGDALA SOMATOSTATIN-EXPRESSING NEURONS
AND THEIR ROLE IN TASTE-GUIDED BEHAVIOR

By

Jane Jeruto Bartonjo

M.S., University of Louisville, 2023
M.S., Western Kentucky University, 2015
B.S., Western Kentucky University, 2018
B.S., Western Kentucky University, 2011

A Dissertation
Submitted to the Faculty of the
School of Medicine of the University of Louisville
in Partial Fulfillment of the Requirements
for the Degree of

Doctor of Philosophy
in Anatomical Sciences and Neurobiology

Department of Anatomical Sciences and Neurobiology
University of Louisville
Louisville, Kentucky

August 2023

Copyright 2023 by Jane Jeruto Bartonjo
All rights reserved.

CONNECTIVITY OF AMYGDALA SOMATOSTATIN-EXPRESSING NEURONS
AND THEIR ROLE IN TASTE-GUIDED BEHAVIOR

By

Jane Jeruto Bartonjo
M.S., University of Louisville, 2023
M.S., Western Kentucky University, 2015
B.S., Western Kentucky University, 2018
B.S., Western Kentucky University, 2011

A Dissertation Approved on

May 10, 2023

by the following Dissertation Committee:

Robert F Lundy, Ph.D., Dissertation Advisor

Chad L Samuelsen, Ph.D.

Martha E Bickford, Ph.D.

Robin F Krimm, Ph.D.

Cynthia Corbitt, Ph.D.

ACKNOWLEDGMENTS

I would like to take this opportunity to express my sincere gratitude to all those who have supported me throughout my research and the completion of this dissertation. First and foremost, I am deeply grateful to my advisor Dr. Robert Lundy for his invaluable guidance, expertise, and unwavering support. His insightful feedback, patience, and encouragement have been instrumental in shaping the direction of my research and enhancing my academic growth.

I would like to express my sincere gratitude to Dr. Chad Samuelsen for his invaluable support and guidance throughout the course of my dissertation. Dr. Samuelsen's unwavering availability and willingness to answer my questions played a crucial role in the success of my research. His insightful inquiries about my project not only sparked my curiosity but also pushed me to delve deeper into my topic, enabling me to gain a comprehensive understanding of the subject matter. Additionally, I am immensely grateful to Dr. Samuelsen for his invaluable presentation tips, which greatly enhanced my ability to communicate my research effectively. His guidance on creating visually engaging and impactful PowerPoint slides has been instrumental in delivering compelling presentations.

I would like to extend my heartfelt appreciation to Dr. Martha Bickford and the members of her lab for their invaluable support and contributions to my electron microscopy project. Dr. Bickford, as a committee member and an expert in electron microscopy, played a crucial role in ensuring the success of this study. Her

expertise and guidance were instrumental in refining my research procedures and methodology. I am immensely grateful to Dr. Bickford for not only providing me with a new procedure to conduct my electron microscopy study but also granting me access to the equipment in her lab, which was essential for the completion of my research.

I would also like to express my deepest appreciation to the members of Dr. Bickford's lab, Arkadiusz Slusarczyk, James Whitely, and Dr. Kyle Whyland. Their assistance and collaboration throughout various stages of the transmission electron microscopy (TEM) process were invaluable. In particular, I am profoundly grateful to Arkadiusz Slusarczyk, who provided constant guidance and support, working alongside me through the entire electron microscopy procedure, conducting experiments, and offering insightful suggestions. Much thanks to the electron microscopy core and staff training me and allowing me to use their facility. Furthermore, I would like to acknowledge Dr. Sean Masterson for his assistance with the electrophysiology experiments. His expertise in this area greatly contributed to the overall success of my research.

I would like to extend my deepest gratitude to Dr. Robin Krimm and Dr. Cynthia Corbitt, both of whom served as members of my committee, for their invaluable contributions to my dissertation. Throughout my research journey, they consistently provided valuable feedback on my presentations and posed thought-provoking questions that helped shape the direction of my work.

I am especially grateful to Dr. Robin Krimm for her unwavering availability and support during my practice presentations. Her constructive feedback and insightful

suggestions were instrumental in refining my presentation skills and effectively communicating my research findings. Her dedication to my growth as a researcher and presenter is deeply appreciated.

I would also like to express my sincere appreciation to Dr. Cynthia Corbitt for accepting the invitation to be a member of my committee, despite the logistical challenges of commuting from the main campus. I am truly grateful for her understanding and flexibility in accommodating the additional time and effort required to attend committee meetings.

Heartfelt appreciation to Dr. Steven St. John of Rollins College, FL, for his invaluable contributions to our research project. Despite being in a different state, Dr. St. John generously dedicated his time to meet with us multiple times, offering his expertise in designing behavior experiments and data analysis. Dr. St. John's guidance and feedback were instrumental in shaping the direction of our project and improving its quality. His deep understanding of experimental design helped us refine our methodologies and ensure the validity of our results. Moreover, the software he designed played a crucial role in transforming our raw data into meaningful and interpretable information.

I would like to express my heartfelt appreciation to Dr. Sanaya Stocke and Dr. Landry Konan for their unwavering moral support throughout my academic journey. Dr. Stocke's constant belief in me and her valuable feedback during practice presentations were invaluable in boosting my confidence and refining my presentation skills. Despite accepting a new position at the main campus, she

continued to make herself available to provide guidance and support, for which I am truly grateful.

I am also deeply thankful to Dr. Landry Konan for his guidance in using Adobe Suite software, including Photoshop and Illustrator. His expertise in these tools and his instruction on formatting Word documents were invaluable in enhancing the visual appeal and professionalism of my research materials. Moreover, Dr. Konan and his family's support extended beyond the academic realm, offering encouragement and assistance outside of school.

I would like to express my deep gratitude to Dr. Bill Guido, the department chair, for his exceptional dedication and care for the students. Dr. Guido's genuine concern for the students' well-being and success has had a profound impact on my academic and personal growth. His understanding of my unique circumstances and challenges allowed him to provide the necessary support and resources to help me overcome obstacles and thrive. I am particularly grateful to Dr. Guido for his financial support, which enabled me to attend conferences and present my research. His assistance went above and beyond, as he continued to provide financial support even after my funding ran out, ensuring that I could complete my dissertation without undue financial burden.

I would like to express my gratitude to my friends and family for their unconditional love, encouragement, and belief in my abilities. Their support and understanding have been a constant source of motivation throughout this challenging endeavor. Although it is not possible to name everyone who has played a role in this journey, please know that your support and encouragement

have made a significant impact on my academic and personal growth.

Thank you all for your contributions, guidance, and belief in my abilities. This dissertation would not have been possible without your support.

ABSTRACT

CONNECTIVITY OF AMYGDALA SOMATOSTATIN-EXPRESSING NEURONS AND THEIR ROLE IN TASTE-GUIDED BEHAVIOR

Jane Jeruto Bartonjo

05/10/2023

The nucleus of solitary tract (NST) and parabrachial nucleus (PBN) represent the first and second central synapses of ascending gustatory information. Neural processing in these nuclei is influenced by descending input from forebrain regions such as the central nucleus of the amygdala (CeA). In mice, we have shown that somatostatin (Sst) expressing neurons of CeA that project to NST and PBN are largely distinct cell populations and optogenetic inhibition of the CeA/Sst-to-NST subpopulation increases the intake of high concentrations of quinine with no apparent effect on sucrose intake. Synaptic connectivity of these cells is needed to understand the possible mechanisms underlying these behavioral responses. Our lab has previously demonstrated that CeA/Sst terminals within the PBN expressed GABA and made synaptic contacts largely with non-GABAergic neural elements. To determine whether CeA/sst terminals within the NST also express GABA, we used electron microscopy combined with cre-dependent anterograde transported virus injections (AAV9-DIO-dApex2) into the CeA of Sst-cre mice and post-embedding immunogold labelling for GABA. We found that majority of

CeA/sst terminals in NST express GABA and synapsed with non-GABAergic targets. These results suggest that CeA/Sst cells provide monosynaptic input to second order NST projection neurons (non-GABAergic) and that this direct feedback inhibition is necessary for appropriate responding to bitter taste quality.

TABLE OF CONTENTS

ACKNOWLEDGMENTS.....	iii
ABSTRACT.....	viii
LIST OF FIGURES.....	xiii
LIST OF TABLES.....	xvi
CHAPTER 1 GENERAL INTRODUCTION.....	1
1.1 Organization of the Peripheral Gustatory System.....	1
1.2 Afferent Gustatory Pathways.....	2
1.3 Attributes of Taste.....	4
1.4 Role of Brainstem Nuclei in Taste Guided Behavior.....	5
1.5 Ventral Forebrain Modulation of Brainstem Taste Processing.....	6
1.6 Methods to Study Intake Driven by Orosensory Stimulation.....	7
1.6.1 Taste Reactivity Tests.....	7
1.6.2 Brief Access Tasks.....	8
1.7 Gaps in Knowledge.....	9
CHAPTER 2 DISTINCT POPULATIONS OF AMYGDALA SOMATOSTATIN- EXPRESSING NEURONS PROJECT TO THE NUCLEUS OF THE SOLITARY TRACT AND PARABRACHIAL NUCLEUS.....	14
2.1 Introduction.....	14
2.2 Material and Methods.....	16
2.2.1 Tract tracing using cholera toxin subunit B injections (non-viral).....	16
2.2.2 HSV injections.....	19
2.2.3 Transmission electron microscopy.....	21
2.3 Results.....	26
2.3.1 CT-b injections.....	26
2.3.2 HSV injections.....	28
2.3.3 Electron microscopy.....	30
2.4 Discussion.....	53

CHAPTER 3 PERTURBATION OF AMYGDALA/SOMATOSTATIN-NUCLEUS OF THE SOLITARY TRACT PROJECTIONS REDUCES SENSITIVITY TO QUININE IN A BRIEF-ACCESS TEST	57
3.1 Introduction.....	57
3.2 Materials and Methods.....	59
3.2.1 Subjects.....	59
3.2.2 Surgeries	60
3.2.3 Virus injections	61
3.2.4 Cannula implantation.....	62
3.2.5 Apparatus	63
3.2.6 Procedure for water and food restriction.....	64
3.2.7 Water training	65
3.2.8 Procedures for concentration-dependent licking to sucrose and QHCl	65
3.2.9 In Vitro slice recording.....	66
3.2.10 Immunohistochemistry	68
3.2.11 Data analysis.....	69
3.3 Results.....	71
3.3.1 Anatomy and physiology	71
3.3.2 Body weight and water training.....	73
3.3.3 Sucrose water restricted.....	74
3.3.4 Sucrose water replete	75
3.3.5 QHCl water restricted.....	77
3.4 Discussion	90
CHAPTER 4 TARGET SPECIFIC PROJECTIONS OF AMYGDALA SOMATOSTATIN-EXPRESSING NEURONS TO THE HYPOTHALAMUS AND BRAINSTEM.....	96
4.1 Introduction.....	96
4.2 Materials and Methods.....	98
4.2.1 Subjects.....	98
4.2.2 Surgery	99
4.2.3 HSV injections	99
4.2.4 Immunohistochemistry and confocal microscopy	101
4.2.5 Data analysis	101
4.3 Results.....	103
4.3.1 NST-LH injections	103

4.3.2 PBN-LH injections	105
4.4 Discussion	120
CHAPTER 5 GENERAL DISCUSSION	123
REFERENCES	129
CURRICULUM VITAE	143

LIST OF FIGURES

Figure 1.1: Anatomy of the gustatory system.....	12
Figure 1.2: Ventral limbic structures: key players in affecting responding to taste.	13
Figure 2.1: Example of the process for automated cell counts using Image J software.	32
Figure 2.2: Taste evoked responses and CT-b injection sites in NST and PBN.....	33
Figure 2.3: Fill patterns of tracers in sections of NST and PBN.	35
Figure 2.4: Representative photomicrographs CeA neurons projecting to NST and PBN.	36
Figure 2.5.: Representative high-power photomicrographs of the CeA neurons projecting to NST and PBN	38
Figure 2.6: Graph showing the average number of retrograde labeled neurons in CeA sections.	39
Figure 2.7: Graph showing the percentage of CeA Sst-positive and Sst-negative cells projecting to NST and PBN.....	40
Figure 2.8: Representative fluorescent images of viral injection into NST and PBN	41
Figure 2.9: Photomicrographs showing retrograde labelled cells in CeA.....	43
Figure 2.10: Graph showing the number of retrograde labelled cells in CeA sections. ..	45
Figure 2.11: Graph showing percentage of double labelled and single labelled cells in CeA sections.	46
Figure 2.12: Photomicrograph showing peroxidase labeling in a CeA tissue section.....	47
Figure 2.13: Photomicrograph showing peroxidase labelled Sst axon terminals in the NST	48

Figure 2.14: A representative electron micrograph of a DAB labelled terminal and its post-synaptic target.....	49
Figure 2.15: Mean gold particle density of pre- and post-synaptic profiles relative to the background	50
Figure 2.16: Histogram of normalized gold particle densities relative to background	51
Figure 2.17: Cumulative histogram of raw gold particle densities	52
Figure 3.1: Representative fluorescent images of NST injections sites, retrograde labelled cells in CeA and cannula placement above CeA.	80
Figure 3.2: Weekly hydrated body weights	82
Figure 3.3: Lick performance during water training.....	83
Figure 3.4: Behavioral responses to water and sucrose under water restricted conditions.	84
Figure 3.5: Behavioral responses to sucrose under hydrated conditions.....	85
Figure 3.6: Behavioral responses to water and QHCl under water restricted conditions.	86
Figure 3.7: Individual mouse performance during QHCl trials.....	87
Figure 4.1: Representative fluorescent images of the viral injections into the NST and LH.	108
Figure 4.2: Representative photomicrographs of CeA/Sst neurons projections to NST and LH.....	110
Figure 4.3: The number of retrograde labeled Sst neurons in the CeA projecting into the NST and LH.	112
Figure 4.4: Representative fluorescent images of PBN and LH viral injection sites.	114
Figure 4.5: Representative photomicrographs showing retrograde labelled cells in CeA.	116

Figure 4.6: The number of retrograde labeled Sst neurons in CeA projecting to PBN
and/or LH. 118

Figure 5.1: Possible mechanisms through which CeA/Sst-to-NST pathway influencing
licking in mice..... 128

LIST OF TABLES

Table 3.1: Summary of behavioral procedures	88
Table 3.2: Average nonlinear regression parameters for quinine (water restricted) and sucrose (water replete) lick-concentration functions.....	89

CHAPTER 1

GENERAL INTRODUCTION

1.1 Organization of the Peripheral Gustatory System

Food intake is necessary for meeting an animal's metabolic energy requirements for survival. For this reason, animals must be able to select between nutritious and potentially toxic chemical stimuli. As the initial sensor of the gastrointestinal tract, the role of the gustatory system is to detect a wide range of soluble chemicals and trigger appropriate responses resulting in either ingestion or rejection. These taste-guided behaviors are mediated by taste receptor cells (TRCs) within taste buds in the oral cavity. Considered peripheral organs of gustation, taste buds are clusters of TRCs embedded within the epithelium of the tongue, palate, and epiglottis. In mammals, lingual taste buds reside in three specialized structures on the dorsal surface of the tongue called papillae: fungiform papillae on the rostral two thirds of the tongue, single circumvallate papillae in the midline of the posterior tongue (in rodents), and foliate papillae on the posterior lateral edges of the tongue (Fujimoto et al., 1993; Stone et al., 1995). Each taste bud consists of 50-100 columnar TRCs which originate from an interrupted basal membrane and converge at the tip forming an onion-like structure. Microvilli at the apical ends of the TRCs extend into the taste pore where they interact with chemical components of taste stimuli via receptors or ion channels. In general, organic molecules such as sugars, amino acids, and alkaloids use G protein-

coupled receptors (GPCR) for signal transduction. Binding of these molecules to the GPCRs in apical microvilli results in conformational change that triggers a cascade of intracellular reactions leading to depolarization of taste cells. For acids and salts, taste transduction is mediated by ion channels in apical microvilli. Flow of ions such as Na^+ or H^+ across the apical membrane directly depolarizes TRC's (Gravina et al., 2013; Pallante et al., 2021). These interactions increase intracellular calcium and transmitter release from TRC's onto afferent gustatory nerve fibers.

While neural coding of taste information is still not clearly understood, the fact that different soluble molecules use distinct receptor mechanisms forms the basis for the labeled-line coding hypothesis. That is, specific TRCs detect specific molecules and synapse with specific afferent fibers. This dedicated line of transmission is then maintained through the gustatory neuraxis (Barretto et al., 2015). An alternative theory, across-fiber (combinatorial) coding, suggests that coding is achieved by ensembles of neurons that are broadly responsive to different soluble molecules (Wu et al., 2015). Although available evidence is still debated, it is likely that elements of both theories are used to encode gustatory information (Ohla et al., 2019).

1.2 Afferent Gustatory Pathways

Taste receptor cells are innervated by peripheral axons from neurons located in the geniculate (chorda tympani and greater superficial petrosal nerves), petrosal (glossopharyngeal nerve), and nodose (vagus nerve) ganglia. Briefly, the chorda tympani nerve (branch of CN VII) supplies fungiform papillae located on the rostral

two thirds of the tongue (Lopez and Krimm, 2006; Miller Jr., 1974) and part of foliate (anterior) papillae (Lehman et al., 1995; Whitside, 1927). The greater superficial petrosal nerve (another branch of CN VII) supplies taste buds of the palate (Miller and Spangler, 1982). Foliate and circumvallate papillae are supplied by the glossopharyngeal nerve (branch of CN IX) (Frank, 1991; Whitside, 1927), while taste buds of the epiglottis are supplied by the superior laryngeal nerve (branch CN X) (Contreras et al., 1982b; Sato and Koyano, 1987). Epiglottal taste buds are, however, not associated with papillae (Jowett and Shrestha, 1998) and do not appear to play a role in gustatory evaluation (Bradley, 2000).

The central branches of first order gustatory neurons synapse with second order neurons in the rostral portion of the nucleus of solitary tract (rNST) (Corson et al., 2012c; Hamilton and Norgren, 1984b). In rodents (Figure 1.1), ascending projections from the rNST synapse with third order neurons in the pontine parabrachial nucleus (PBN) (Cho et al., 2002a; Halsell et al., 1996; Monroe and Lorenzo, 1995; Ogawa et al., 1984b). From the PBN, gustatory information reaches higher order nuclei through two pathways. One pathway projects to the parvocellular component of the ventrobasal complex of the thalamus (VPMpc) and then to gustatory cortex (GC). The second pathway, ventral/limbic pathway, projects from the PBN to ventral forebrain nuclei such as the lateral hypothalamus (LH), central nucleus of amygdala (CeA), and bed nucleus of stria terminalis (BNST) (Halsell, 1992a; Nakashima et al., 2000; Norgren and Leonard, 1971; Norgren and Leonard, 1973b; Tokita et al., 2010).

1.3 Attributes of Taste

The TRCs transduce chemical information into neural signals used for the perception of taste attributes such as stimulus intensity (concentration), quality (identity), and hedonic value (palatability). Quality refers to the identity of the taste. In general, sugars such as sucrose tend to be described as "sweet", alkaloids such as quinine as "bitter", amino acids such as monosodium glutamate as "umami", acids such as citric acid as "sour", and salts such as NaCl as "salty". For each taste, the gustatory system can distinguish the respective intensities which are represented by concentrations. Although previous studies demonstrated that the intensity of a tastant can be characterized by changes in action potential rate (Maier and Katz, 2013; Wu et al., 2015), it was recently shown that intensity also can be represented by spike timing (Fonseca et al., 2018). Lastly, taste stimuli are also described in terms of hedonic value (e.g., palatable vs aversive) that varies with intensity and quality. In general, sweet, umami and low concentrations of salt stimuli are considered palatable and ingested, while sour, bitter and high concentrations of salt stimuli are considered aversive and rejected. Whether a taste quality is ingested or rejected is, therefore, strongly influenced by its hedonic value.

The influence of gustatory hedonic value on feeding behavior, however, is dynamic because factors such as learning (Bernstein, 1978) and physiological state (e.g., hyponatremia, illness) (Cross-Mellor et al., 2005; Kutscher and Steilen, 1973) can switch the behavioral response to a taste stimulus from rejection to ingestion or vice versa. For example, a normally palatable taste such as sucrose

becomes aversive when paired with a toxic substance such as lithium chloride that induces gastrointestinal malaise. This learned taste/visceral association is known as conditioned taste aversion (CTA). (Nachman and Ashe, 1973). Contrary to CTA, a switch from avoidance of concentrated sodium salt to avid ingestion occurs when animals have a negative body sodium balance (e.g. sodium appetite) (Berridge et al., 1984). These adaptive changes in ingestive behavior appear to involve alteration of gustatory hedonic value rather than taste quality or intensity (Fonseca et al., 2020; Wang et al., 2018).

1.4 Role of Brainstem Nuclei in Taste Guided Behavior

As mentioned earlier, in many mammalian species, the rostral nucleus of the solitary tract (rNST) and the parabrachial nucleus (PBN) contain the first and second central neurons for the ascending gustatory system, respectively. As would be expected, input to the rNST and PBN are important for an animal's ability to use taste information to guide behavior. In rats with bilateral lesions of rNST, concentration dependent intake of taste stimuli was severely impaired. Nevertheless, the same lesioned animals were able to alter gustatory hedonic value following induction of CTA or sodium appetite. (Grigson et al., 1997a; Shimura et al., 1997c). In contrast, rats with bilateral damage to PBN are unable to acquire CTA or express sodium appetite. However, concentration dependent intake was not severely affected (Flynn et al., 1991b; Scalera et al., 1995a; Spector et al., 1992a; Spector et al., 1993a). Thus, lesion-behavior studies suggest that neural processing in rNST is particularly important for unconditioned responding to different concentrations of a taste stimulus, while that in PBN is more involved

in assignment of new hedonic value to taste stimuli (Grigson et al., 1998b; Reilly et al., 1993b).

Importantly, when connections between the brainstem and forebrain were severed (Figure 1.2) (e.g. decerebrate preparation), animals were able to generate discriminatory responses to taste stimuli but unable to acquire CTA or express sodium appetite (Grill et al., 1986; Kaplan et al., 2000). These results imply that reciprocal interactions between the brainstem and forebrain are critical for adaptive alteration of gustatory hedonic value and consequent ingestive behavior. Importantly, lesions of the thalamic taste area (Figure 1.2) do not disrupt CTA learning or sodium appetite. This result suggests that the critical interactions involve direct connections between the brainstem and ventral forebrain structures (Scalera et al., 1997).

1.5 Ventral Forebrain Modulation of Brainstem Taste Processing

Taste responses in rNST and PBN are not static but can be modulated by factors such as learning and physiological state. For example, salt-responsive neurons in rNST and PBN exhibited decreased responses to oral stimulation with hypertonic sodium chloride solution following induction of sodium appetite (Jacobs et al., 1988; McCaughey and Scott, 2000; Shimura et al., 1997b). In contrast, responses to the conditioned stimulus are enhanced in both rNST and PBN after CTA acquisition (Chang and Scott, 1984a; Shimura et al., 1997e). These results indicate that changes in taste-evoked responses recorded in the brainstem are coincident with conditions that alter gustatory hedonic value and intake. Interestingly, the changes in PBN taste-evoked responses following induction of

CTA are abolished when connections between the brainstem and forebrain are severed (Tokita et al., 2007).

Ventral forebrain nuclei such as the central nucleus of the amygdala (CeA), bed nucleus of stria terminalis (BNST), and lateral hypothalamus (LH) not only receive taste information directly from the PBN but also project back to the gustatory rNST and PBN (Figure 1.1) (Kang and Lundy, 2009c; Moga et al., 1989b; Moga et al., 1990a; Moga et al., 1990c; Saggiu and Lundy, 2008b). Indeed, electrical stimulation of the BNST, CeA, and LH produce varied effects on tastant-evoked responses recorded in the rNST and PBN. Activation of the BNST and CeA predominately inhibited PBN taste responses, while inhibition and excitation occurred equally often during LH activation. For rNST neurons, however, the most common effect of CeA and LH activation was excitatory, whereas BNST activation was predominately inhibitory (Cho et al., 2003a; Kang and Lundy, 2010a; Li et al., 2002a; Li et al., 2005a; Li and Cho, 2006a; Lundy and Norgren, 2001b; Lundy and Norgren, 2004b). Taken together, it is clear that activity in brainstem taste neurons is not simply the result of afferent input but subject to descending modulation. Such neural modulation likely contributes to ingestive behavior that varies as a function of taste stimulus intensity and hedonic value.

1.6 Methods to Study Intake Driven by Orosensory Stimulation

1.6.1 Taste Reactivity Tests

Behavioral responses to taste stimuli in the oral cavity can be categorized into what are called ingestive or aversive sequences. Ingestive sequences are elicited by palatable stimuli such as sucrose and consist of three orofacial responses:

rhythmic mouth movements, rhythmic symmetric tongue protrusions, and lateral tongue protrusions. In contrast, unpalatable stimuli such as quinine evoke aversive sequences and consist of one orofacial response, gaping; and an additional five somatic responses: chin rubbing, headshaking, face washing, flailing of the forelimbs and paw wiping. These response patterns have been observed in both neurologically intact and decerebrate rats (Grill and Norgren, 1978a; Grill and Norgren, 1978b). Because taste reactivity patterns are not quality-specific (e.g. one cannot tell the quality of the tastant simply by observing orofacial responses), they reflect the hedonic value of a taste stimulus. These orofacial responses also are conserved across species making it a reliable method for assessing palatability (Berridge, 2000). However, taste reactivity tests are labor-intensive and often involve direct infusion of taste stimuli into the oral cavity bypassing normal approach behavior. An alternative method to assess orosensory driven intake that includes both approach and consummatory behaviors is brief-access licking.

1.6.2 Brief Access Tasks

Food intake is controlled by oral (taste) and post-oral signals (visceral) (Beeler et al., 2012; Eisen et al., 2001). For example, concentration-dependent intake of carbohydrates such as sucrose result in an inverted-U shaped concentration function whether assessed in long-term (>1 hr) or short-term (30min-1hr) tests (Davis et al., 1995; Ernits and Corbit, 1973; McCleary, 1953; Shuford, 1959). The descending limb of the concentration-response function is attributed to negative post-ingestive feedback. The ascending limb of the concentration-response function, on the other hand, is attributed to the orosensory properties of the taste

stimulus (Davis and Smith, 1990; Mook et al., 1991; Mook et al., 1993). Thus, to assess the influence of only orosensory stimulation on ingestive behavior, inhibitory visceral feedback must be minimized. A simple way to achieve this is by allowing only brief exposure to taste stimuli. Specifically, brief access intake tests involve recording the number of licks to different taste stimuli during a small period of time (often 5 to 10s trials), which limits the accumulation of ingesta in the gastrointestinal tract. This procedure results in a monotonic function to palatable stimuli such as sucrose that increases with increasing concentration (Davis, 1973), while that to unpalatable taste stimuli such as quinine decreases with increasing concentration (Boughter et al., 2002).

1.7 Gaps in Knowledge

The molecular identity of neuromodulator pathways to gustatory regions of the brainstem and their contributions to ingestive behavior are critical knowledge gaps. This dissertation focuses on descending input that originates from the central nucleus of the amygdala (CeA). Historically, the CeA is best known for its role in emotion and motivation (Botta et al., 2015; Ciochi et al., 2010; Han et al., 2017). However, the CeA also contributes to ingestive behavior (Fekete et al., 2002; Fekete et al., 2007). Not surprisingly, it is a major source of descending input to both the gustatory rNST and PBN (Kang and Lundy, 2009b; Tokita et al., 2009). Given the diverse genetic identities of CeA cells (Kim et al., 2017; McCullough et al., 2018a), work is needed to identify which population(s) innervate the rNST and/or PBN.

This dissertation focused on somatostatin (Sst) cells in the CeA because: 1) its expression marks a major population in CeA cells (McCullough et al., 2018b), 2) CeA/Sst cells constitute a major source of descending input to the PBN compared to CeA cells that express corticotrophin-releasing hormone (Magableh and Lundy, 2014; Panguluri et al., 2009), and 3) brain Sst has been implicated in the control of ingestive behavior (Kim et al., 2017; Stengel et al., 2010). We also know that populations of CeA neurons projecting to the rNST and PBN are largely distinct (Kang and Lundy, 2009c). Whether CeA/Sst neurons also project to the rNST and are distinct from those projecting to the PBN is unknown. If so, the contribution(s) of these descending pathways to taste processing and ingestive behavior could be assessed independently.

To the best of our knowledge only two prior studies have assessed the role of CeA/Sst neurons, as a whole population, on ingestive behavior. In one study, optogenetic activation of CeA/Sst neurons was shown to suppress licking to water that was rapidly reversed upon cessation of laser light (Yu et al., 2016a). In contrast, the other study showed that optogenetic inhibition of CeA/Sst neurons decreased time spent drinking water during a 5-minute test (Kim et al., 2017). Despite these inconsistencies, that might be due to procedural differences among the studies, CeA/Sst neurons seem to influence licking behavior to water and, thus might additionally contribute to intake of taste stimuli. To address gaps in knowledge, we propose to further characterize neural input from CeA/Sst neurons to the brainstem and assess the contribution of CeA/Sst neurons to taste-guided behavior.

Briefly, Chapter II will focus on the anatomical and synaptic connectivity of CeA/Sst cells using a combination of viral tract tracing and electron microscopy. Chapter III involves optogenetic manipulation of CeA/Sst cells to determine the role on intake driven by orosensory signals using brief access intake tests. Chapter IV examines the possibility that the influence of CeA/Sst cells on intake can be attributed, in part, to an indirect pathway to the brainstem via the lateral hypothalamus.

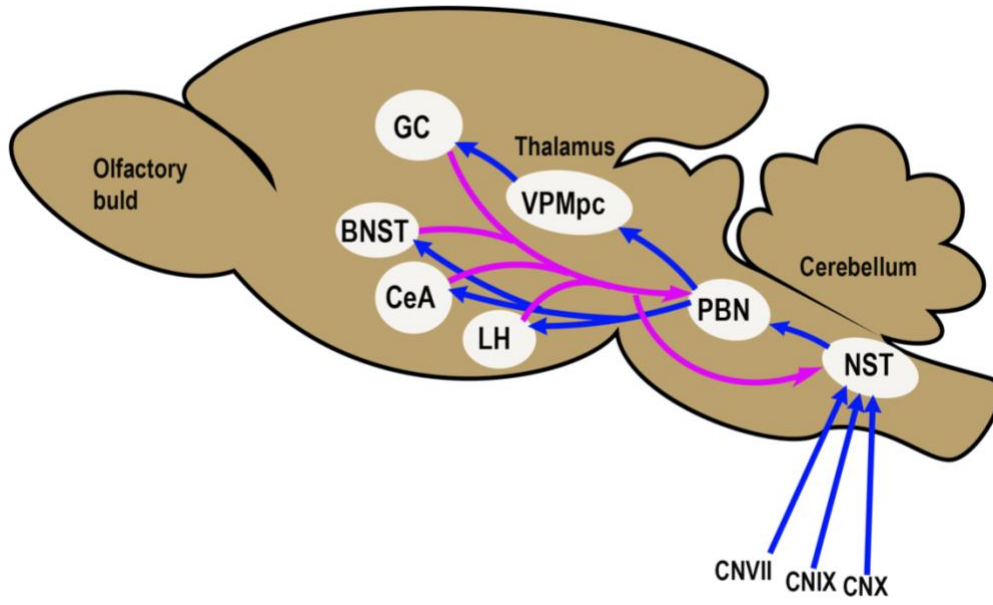


Figure 1.1: Anatomy of the gustatory system

Simplified schematic illustrating the flow of information through the gustatory system of a mouse. The solid, blue arrows represent ascending information, magenta arrows represent descending information. Abbreviations: NST, nucleus of solitary tract; PBN, parabrachial nucleus; VPMpc, ventrobasal complex of the thalamus; parvocellular part; LH, lateral hypothalamus; CeA, central nucleus of amygdala, BNST, bed nucleus of stria terminalis; GC, gustatory cortex; CNVII, cranial nerve VII; CNIX, cranial nerve IX; CNX, cranial nerve X.

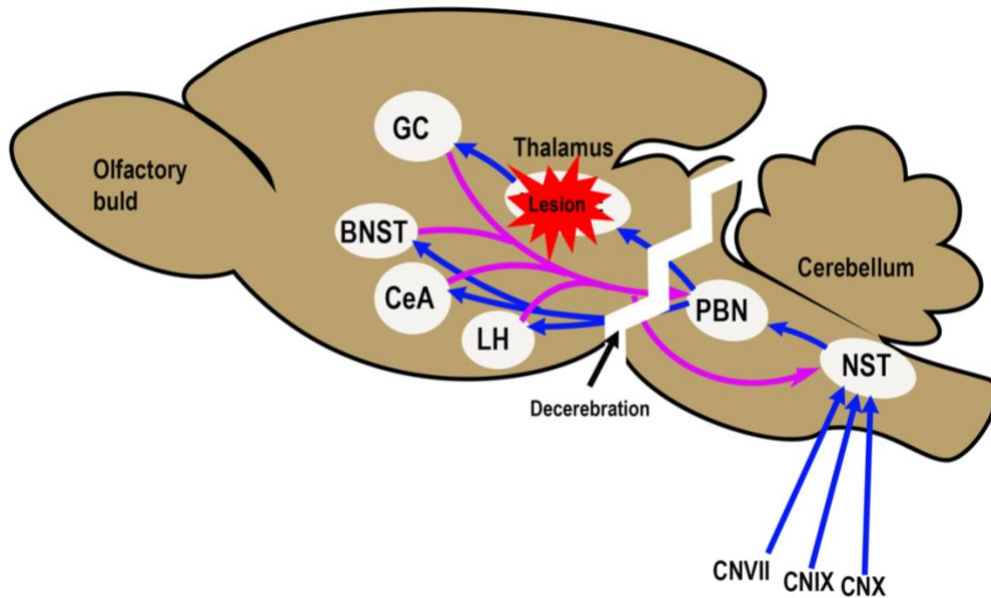


Figure 1.2: Ventral limbic structures: key players in affecting responding to taste. Illustration of a mouse brain highlighting ventral limbic structures crucial for affective response to taste stimuli. Supracollicular decerebration (black arrow) does not affect discriminatory responses to taste stimuli, but it disrupts affective responding. Lesioning the thalamic taste area (shaded red) does not affect discriminatory responses or affective responding. Abbreviations: NST, nucleus of solitary tract; PBN, parabrachial nucleus; VPMpc, ventrobasal complex of the thalamus; parvocellular part; LH, lateral hypothalamus; CeA, central nucleus of amygdala, BNST, bed nucleus of stria terminalis; GC, gustatory cortex; CNVII, cranial nerve VII; CNIX, cranial nerve IX; CNX, cranial nerve X.

CHAPTER 2
DISTINCT POPULATIONS OF AMYGDALA SOMATOSTATIN-
EXPRESSING NEURONS PROJECT TO THE NUCLEUS OF THE
SOLITARY TRACT AND PARABRACHIAL NUCLEUS.

2.1 Introduction

In rodents, gustatory information from taste receptor cells in the tongue and palate is carried by branches of the facial (chorda tympani and greater superficial petrosal) and glossopharyngeal nerves to the rostral third of the medullary nucleus of the solitary tract (NST) (Contreras et al., 1982a; Corson et al., 2012b; Hamilton and Norgren, 1984a). From the NST, ascending gustatory information reaches the pontine parabrachial nucleus (PBN) (Cho et al., 2002b; Dilorenzo and Monroe, 1995; Ogawa et al., 1984a). Not surprisingly, neural processing in these 2 brainstem nuclei is critical for an animal's ability to use gustatory information to guide ingestive behavior (Grigson et al., 1997b; Grigson et al., 1997c; Reilly et al., 1993a; Shimura et al., 1997d; Spector et al., 1993b).

It is well established that neural processing of gustatory information in the NST and PBN is not static but subject to modulation by many factors (Baird et al., 2001; Chang and Scott, 1984b; Giza et al., 1992; Hajnal et al., 1999; Lundy and Norgren, 2004a; Nakamura and Norgren, 1995; Shimura et al., 1997a). For example, the PBN conveys gustatory information to ventral forebrain structures such as the bed nucleus of the stria terminalis (BNST), central nucleus of the amygdala (CeA), and

lateral hypothalamus (LH) (Li and Cho, 2006b; Norgren, 1976). These forebrain areas, in turn, send projections back to the gustatory NST and PBN (Kang and Lundy, 2009a; Moga et al., 1989a; Moga et al., 1990a; Moga et al., 1990b; Saggi and Lundy, 2008a; Tokita et al., 2010). Electrical stimulation of the BNST, CeA, and LH produce varied effects on tastant-evoked responses recorded in the NST and PBN. Activation of the BNST and CeA predominately inhibited PBN taste responses, while inhibition and excitation occurred equally often during LH activation (Li et al., 2005b; Li and Cho, 2006b; Lundy and Norgren, 2001a; Lundy and Norgren, 2004a). For NST neurons, however, the most common effect of CeA and LH activation was excitatory, whereas BNST activation was predominately inhibitory (Cho et al., 2003b; Kang and Lundy, 2010b; Li et al., 2002b). Thus, a single forebrain region can differentially affect gustatory processing depending on the whether the targeted neurons are in the NST or PBN.

One possibility is that distinct populations of forebrain neurons project to the NST and PBN. Indeed, previous research from our lab using rats demonstrated that largely separate populations of BNST, CeA, and LH neurons project to the NST and PBN (Kang and Lundy, 2009a) with the largest source of descending input originating from the CeA (Kang and Lundy, 2009a; Tokita et al., 2010). The molecular identity of forebrain neurons that give rise to this descending input remains an area of active research. The CeA, for instance, is a remarkably heterogeneous nucleus consisting of cells expressing neurochemical markers such as somatostatin (Sst), neurotensin (Nts), corticotropin-releasing factor (Crf), tachykinin 2 (Tac2), protein kinase c-delta (Prkcd), and dopamine receptor 2

(Drd2) (McCullough et al., 2018a). Our lab has shown both in rats and mice that CeA neurons marked by somatostatin expression (Sst) are a major source of descending input to the gustatory region of the PBN compared to those marked by corticotrophin-releasing hormone (Crh) expression (Magableh and Lundy, 2014; Panguluri et al., 2009). In addition, the axon terminals of CeA/Sst neurons in PBN co-express the neurotransmitter Gamma-aminobutyric acid (GABA) (Lundy, 2020a). Whether the NST and PBN of mice are targeted by non-overlapping populations of CeA/Sst-expressing neurons and whether the axon terminals of CeA/Sst terminals in NST also co-express GABA remains unknown. To address these gaps in knowledge, we performed retrograde viral and non-viral tracer injections into the NST and PBN of transgenic mice followed by analysis of co-localization in CeA. To determine whether the terminals in NST express GABA, we used an anterograde virus injected into the CeA of transgenic mice to label Sst neurons in CeA and axon terminals in NST combined with post-embedding immunogold staining of for GABA and electrom microscopy analyses.

2.2 Material and Methods

2.2.1 Tract tracing using cholera toxin subunit B injections (non-viral)

2.2.1.1 Subjects

For cholera toxin subunit B retrograde tracer injections (CTb), Sst-cre mice (Jackson Laboratories, Sst) were bred with floxed-TdTomato mice (Jackson Laboratories, B6.Cg-Gt(ROSA)26Sor) to generate a reporter line that expressed TdTomato in Sst cell types (Sst/TdTomato line). Two male and one female reporter mice weighing 20-25 g were used. All procedures conformed to the

National Institutes of Health guidelines and were approved by the University of Louisville Institutional Animal Care and Use Committee.

2.2.1.2 Surgery

The mice were anesthetized with an intraperitoneal injection of Ketamine/Xylazine [(100mg/kg (K)/10mg/kg (X)]. If needed, an additional dose of Ketamine (50mg/kg) was administered to continue a deep level of anesthesia. The animals were placed on a feedback-controlled heating pad, and rectal temperature was monitored to maintain body temperature at $35\pm 1^{\circ}\text{C}$. Animals were secured in a stereotaxic instrument and the skull leveled with reference to bregma and lambda cranial sutures. Two small holes were drilled through the bone overlying the cerebellum to allow access to the nucleus of the solitary tract (NST) and parabrachial nucleus (PBN). The analgesic meloxicam (3mg/kg) was administered prior to wound incision and again for at least 2 days post-surgery.

2.2.1.3 Electrophysiological recording

Gustatory NST and PBN neurons were identified by recording multiunit activity through a glass-coated tungsten microelectrode (resistance: 1-2 $\text{M}\Omega$) while stimulating the anterior tongue with 0.1 M NaCl. Only the anterior 2/3 of the tongue was stimulated because numerous prior studies have demonstrated that CeA activation has a profound influence on brainstem taste cells that receive input via the chorda tympani nerve (Cho et al., 2002c; Cho et al., 2003b; Kang and Lundy, 2010b; Lundy and Norgren, 2001a; Lundy and Norgren, 2004a). Further, the concentration of NaCl used has been shown to produce a significant neural response in each “best-stimulus” class of NST and PBN neurons (Kang and Lundy, 2010b; Lundy and Norgren, 2001a; Lundy and Norgren, 2004a). For access to the

NST, the electrode was lowered at coordinates ranging from 6.0-6.2 mm posterior to bregma and 1.1-1.3 mm lateral to the midline according to mouse stereotaxic atlas (Paxinos and Franklin, 2001). Typically, taste-evoked activity was encountered 3.7-3.9 mm ventral to the surface of the cerebellum. The coordinates for the PBN recordings were 5.1-5.3 mm posterior to bregma, 1.1-1.3 mm lateral to the midline and 2.7-3.0 mm below the surface of the inferior colliculus. The surface of the brain was kept moist throughout surgery with physiological saline.

2.2.1.4 CTb tracer injections

Once the gustatory region was identified, the tungsten electrode was replaced by a 10 μ L nanofil syringe (34-g beveled needle, World Precision Instruments) mounted in a microprocessor-controlled injector (UltraMicroPump, World Precision Instruments) attached to the stereotaxic instrument. The syringe was first front-loaded with light mineral oil followed by either a 0.2% solution of CTb AlexaFluor-488 conjugate (Invitrogen, cat#C34775) in phosphate-buffered saline or a 0.2% solution of CTb AlexaFluor-647 conjugate (Invitrogen, cat#C34778). A different syringe was used for each tracer conjugate. The microprocessor was set to deliver 75nL of CTb to each site at a rate of 40nL/min, and the syringe was retracted 5 minutes post-injection. Five to 6 days following tracer injections, the animals were administered a lethal dose of Ketamine/Xylazine [(300mg/kg (K)/30mg/kg (X))] and perfused through the ascending aorta with 10mL of 4% paraformaldehyde. The brains were removed, blocked just rostral to the PBN, and post-fixed overnight at 4°C in the same fixative. Coronal sections (70 μ m) were cut using a vibrating microtome.

2.2.2 HSV injections

2.2.2.1 Subjects

For retrograde Herpes Simplex Virus injections (HSV), we used two female and one male Sst-cre heterozygous mice (18-24 g). The animals were maintained in a temperature-controlled colony room on a 12-h light/dark cycle and allowed free access to normal rodent chow and distilled water. All procedures conformed to the National Institutes of Health guidelines and were approved by the University of Louisville Institutional Animal Care and Use Committee.

2.2.2.2 HSV injections

Animals were prepped for surgeries as described in section 2.2.1.2. The coordinates from electrophysiological recordings in the CTb experiments were used for injection of HSV into the NST (6.1 mm posterior to bregma, 1.3 mm lateral to the midline, 3.9 mm ventral to the surface of the cerebellum) and PBN (5.2 mm posterior to bregma, 1.3 mm lateral to the midline, 2.9 mm ventral to the surface of the inferior colliculus). The 10 μ L nanofil syringe was first front-loaded with light mineral oil followed by either HSV-EF1alpha-DIO-mCherry (RN413, 2.5 x 10⁹ infectious units/ml) or HSV-EF1alpha-DIO-EYFP (RN415, 2.5 x 10⁹ infectious units/ml) [Rachael Neve, Massachusetts General Hospital]. Because the mCherry and EYFP genes are preceded by DIO, a *double-floxed inverse open reading* frame, expression of transgene is restricted to Sst-expressing neurons. A different syringe was used for each virus. The microprocessor was set to deliver 300nL of HSV to each site at a rate of 40nL/min, and the syringe was retracted 5 minutes post-injection. Three weeks following virus injections, the animals were administered a lethal dose of Ketamine/Xylazine [(300mg/kg (K)/30mg/kg (X))] and

perfused through the ascending aorta with 10ml of 4% paraformaldehyde. The brains were removed, blocked just rostral to the PBN, and post-fixed overnight at 4°C in the same fixative. Coronal sections (70 µm) were cut using a vibrating microtome.

2.2.2.3 Immunohistochemistry and confocal microscopy

Every other section was collected, blocked with 10% normal donkey serum (NDS) in 0.1% triton-x phosphate buffered saline (TPBS) followed by incubation at 4 °C overnight on a shaker in 1:1000 dilution (in 0.1% TPBS and 5% NDS) of goat anti-GFP (Novus Biologicals) and rabbit anti-DsRed (Novus Biologicals) primary antibodies. After four rinses in TPBS (10min each), the tissue sections were incubated (at room temperature) for 1hr in 1:100 dilution (in 0.1% TPBS and 5% NDS) of Alexa Fluor-488 donkey anti-goat and Alexa Fluor-546 donkey anti-rabbit (Fisher Scientific). After rinsing 3 times in phosphate buffered saline and once in phosphate buffer (10min each), the sections were mounted on microscope slides (HistoBond Adhesive Microscope Slides, VWR) and allowed to dry for 1hr. The sections were rehydrated with deionized water followed by Fluoromount-G® mounting medium and coverslips. Images were obtained using Olympus confocal microscope.

2.2.2.4 Data analysis (CTb and HSV injections)

Cell bodies in the CeA positive for CTb-488, CTb-647, and TdTomato (Sst-reporter mice) or mCherry and EYFP (virus injected Sst-cre mice) were identified using sequential scanning with an Olympus confocal microscope. In every other section (8 sections/mouse), the number of fluorescent positive cells in each Z stack (3µm/slice) was calculated and used for statistical analyses. The color

segmentation function in Image J software was used to separate and count labeled neurons. The separate color channels were converted to 8-bit images (Figure 2.1A&B), auto threshold adjusted (white objects on black background, otsu or triangle method), and a Gaussian blur applied (sigma radius = 1) (Figure 2.1C&D). The appropriate scale was set (1.4 pixels/um (40x magnification) or 0.85 pixels/um (10x magnification)) and the analyze particles function used to count labeled cells in each channel (size $\geq 20\mu\text{m}^2$) (Figure 2.1E&F). The image calculator function “AND” was used to identify overlapping pixels in the separate channels. Using the analyze particles function on the resultant image, overlapping elements with size $\geq 20\mu\text{m}^2$ were considered to be a double (Figure 2.1G) or triple labeled cells (only for CTb injections; not shown). Manual counts on select sections were similar to automated calculations. Nonparametric two-independent samples tests (Kolmogorov-Smirnov) were used for statistical analyses (SPSS 17.0). The results are presented as mean \pm s.e. and a value of $p < 0.05$ was considered statistically significant.

2.2.3 Transmission electron microscopy

2.2.3.1 Subjects

Transgenic mice homozygous for cre recombinase in somatostatin (Sst-cre) expressing neurons (Sstm2.1(cre) Zjh/J) and wild type mice (C57BL/J6) were obtained from Jackson Laboratories. The two strains were bred at the University of Louisville to generate mice heterozygous for cre recombinase expression in Sst neurons. The mice were maintained in a temperature-controlled colony room on a 12h light/dark cycle with free access to normal rodent chow and distilled water unless otherwise noted. Two mice (male and female), 104 days old weighing 21-

27g, were used for this study. All procedures conformed to NIH guidelines and were approved by the University of Louisville Institutional Animal Care and Use Committee.

2.2.3.2 Surgeries and viral injections

Animals were prepped for surgeries as described in section 2.2.1.2. The viral vector AAV9-Ef1 α -DIO-dAPEX2 was bilaterally injected in the CeA. This anterograde transported cre-dependent virus allows peroxidase reporter enzyme to be expressed in the cytosol and nucleus of cells expressing cre-recombinase (Zhang et al., 2019). The microprocessor was set to 300 nL of the virus at a rate of 30nL/min. The stereotaxic coordinates used for CeA, relative to bregma, were: -1.2 posterior, \pm 2.8 lateral, and -4.3 ventral to dura. The analgesic Rimadyl (5mg/kg) was administered prior to wound incision and again for at least 2 days post-surgery. Two to three weeks were allowed for transgene expression.

2.2.3.3 Perfusion and DAB staining

Mice received an intraperitoneal injection of a lethal dose of Ketamine/Anased mixture (300 mg/kg [Ketamine]/30 mg/kg [Anased]) followed by thoracotomy and transcardial perfusion using a mixture 2% EM grade glutaraldehyde and 2% paraformaldehyde (freshly depolymerized, pH 7.4). The brains were extracted and post-fixed overnight at 4 °C in the same fixative. Two brain blocks containing NST and CeA were made and 70 μ m sections were cut using a Leica vibrating microtome. The resulting thin sections were reacted in nickel enhanced DAB (3,3'-Diaminobenzidine) working solution for 30mins by adding 15 μ l of 30% hydrogen peroxide. Nickel enhanced DAB was prepared by first dissolving two 25mg tablets in 25ml of water then adding 25ml of 0.1M Nickel ammonium sulphate in 0.1M

sodium acetate buffer (pH 6.0). The solution was passed through a filter paper to remove any undissolved DAB. The DAB reaction was stopped by incubating the sections in sodium acetate buffer (pH 6.0) for 10mins followed by two washes (10mins each) in 0.1M PB. After DAB staining, the NST sections were further processed for electron microscopy (see section below), while the CeA sections underwent optical tissue clearing for light microscopy. Optical clearing was achieved by first mounting the CeA containing sections in subbed slides. The sections were then dehydrated by immersing in graded alcohols followed by clearing in Hemo-D® organic solvent and subsequent mounting in the resin mounting media, DPX.

2.2.3.4 Embedding

Following DAB staining, the NST tissue sections were incubated in 1% OsO₄ in 0.1M PB for 30mins at room temperature and washed three times (10mins each) in 0.1M PB. The sections were dehydrated by incubation in increasing concentrations of ethanol (50%, 70%, 95%) for 10 mins each and three times in 100% ethanol (5mins each). After dehydration, sections were infiltrated with durcupan resin by first incubating them in 1part 100% ethanol/1part durcupan resin (for one hour in a rotor), followed by another incubation in 1 part ethanol/3 parts durcupan resin and finally in 100 % durcupan resin overnight in a vacuum. After infiltration, sections were flat embedded in the durcupan resin between two aclar sheets and baked at 60°C for 72 hours. With the aid of a light microscope, the rNST containing the DAB labelling was cut out and secured to resin blocks with crazy® glue. Ultrathin sections (60 nm, silver-gray interference color) were made

in ultramicrotome using a diamond knife (Diatome, Fort Washington, PA), and every tenth section was collected on Formvar-coated nickel slot grids.

2.2.3.5 Post-embedding immunohistochemistry

Grids were washed in 0.1 % triton X-100 in 0.1M tris buffered saline (TBST, pH 7.6) for 5 mins followed by an overnight incubation (at 4°C) in rabbit anti-GABA (Sigma-Aldrich, A2052) diluted (1:2000) in TBST (pH 7.6). After incubation, the grids were washed twice in TBST (5 min each) followed by incubation in TBST for 30 mins. The grids were conditioned for 5 mins in TBST pH 8.2 then incubated (1 hr at room temperature) in goat anti-rabbit gold-conjugated secondary antibody diluted (1:25) in TBST (pH 8.2). The gold solution had been vortexed and allowed to sit for at least one hour before use to allow clumps to settle; only the topmost solution was used. After incubation, grids were washed twice in TBST (5mins each) followed by two washes in deionized water (5mins each). The grids were transferred to a grid staining matrix and allowed to dry. Once dry, the grids were stained in uranyl acetate in methanol (30mins) then rinsed by dipping in three separate containers of 100% methanol (20 times each). All solutions used during this staining process were filtered through a 0.22µm Millipore® membrane filters and tissue-containing grids were either floated face-down on the droplet or submerged face-up in the droplet on silicon rubber pad. Between steps, excess solution on the grid and forceps tip was blotted using filter paper wedges. After immersion in methanol, the grids were allowed to dry, and tissues were imaged using Hitachi TEM (HT7700).

2.2.3.6 Data analysis

The pre- and post-synaptic profiles were characterized based on area and GABA content (represented by gold particle densities). By using Image J, the area of each DAB labelled Sst-positive presynaptic terminal and its post synaptic target(s) were measured, and gold particle densities (number of particles per unit area) were calculated. Profiles were categorized as GABAergic or non-GABAergic based on their gold densities relative to background gold density for each staining session (single staining session per animal). The background density for each staining session was determined by calculating the gold particle density within the entire area of an image that contained at least 1 DAB labelled Sst-positive presynaptic terminal. The background level of gold particle density for each image in a staining session was set at a mean value +2.33 standard deviations above background. The gold particle density for each labeled terminal and its postsynaptic target was divided by their respective background density to derive a normalized fold difference score. A value of 2 indicates a density twice that of background, while values less than 1 indicate density less background. Presynaptic terminals and their postsynaptic targets in which the gold particle density was greater than 1 were considered GABA positive. Nonparametric 2-independent samples tests (Mann-Whitney Rank Sum) were used for statistical analyses (Sigmaplot). The results are presented as mean \pm se and a value of $p < 0.05$ was considered statistically significant (Lundy, 2020a).

2.3 Results

2.3.1 CT-b injections

In each animal, the taste responsive region of the NST (Figure 2.2 A) and PBN (Figure 2.2 F) was electrophysiologically located by applying 0.1M NaCl to the anterior tongue. Figure 2.2 B, C, D, and E show photomicrograph examples of CTb-647 (white fluorescence) injected into the taste-responsive NST of an Sst-TdTomato reporter mouse. Neurons and fibers expressing Sst (red fluorescence) filled the rostrocaudal extent of the NST. Microscopic examination of medullary tissue revealed that CTb injections were concentrated in the medial subdivisions of the NST with minimal spread into the ventrally located reticular formation or laterally located dorsomedial spinal trigeminal nucleus. Numerous labelled neurons were observed in the medial vestibular nucleus immediately dorsal to the NST. This might be the result of tracer spread along the injection needle tract or reflect vestibular input to the NST (Balaban and Beryozkin, 1994). Nevertheless, we have not observed retrograde labeled cells in the CeA when injections were misplaced in the medial vestibular nucleus dorsal to the NST. Photomicrograph examples of CTb-488 (green fluorescence) injected into the taste-responsive PBN of the same mouse are shown in Figure 2.2G, H, and I. Neurons and fibers expressing Sst (red fluorescence) surrounded the medial, central lateral, ventral lateral and waist portions of the PBN. Microscopic examination of pontine tissue revealed that CTb injections predominately targeted the above PBN sub nuclei with minimal spread into the rostral and external regions. A summary diagram of the CTb injections and their relative spread are shown in Figure 2.3.

Robust retrograde labeling was observed throughout the rostral caudal extent of the CeA. The CeA was identified as the area approximately 0.7 to 1.9 mm posterior to bregma, ventral to the striatum, medial to the basolateral nucleus of the amygdala, and lateral to the optic tract. Low power photomicrograph examples of retrograde-labeled (CeA-to-PBN, white fluorescence; CeA-to-NST, green fluorescence) and Sst-expressing neurons (red fluorescence) at 4 different levels of the CeA are shown in Figure 2.4 A, B, C, and D. Panels E-H show corresponding stereotaxic atlas drawings depicting the general location of CeA neurons projecting to the NST (green) and PBN (blue). No attempt was made to signify double-labeled neurons or provide an exact representation of the total number of cells in each photomicrograph. Consistent with previous tracing studies, Sst neurons are densely packed throughout the rostrocaudal extent of the CeA where neurons projecting to the NST and PBN are largely intermingled (Kang and Lundy, 2009a; Magableh and Lundy, 2014; Panguluri et al., 2009).

We counted a total of 1,233 CeA neurons that projected to the NST and 1,362 to the PBN. Retrograde labeled cells fell into one of six groups: NST only Sst positive, NST only Sst negative, PBN only Sst positive, PBN only Sst negative, NST/PBN Sst positive, and NST/PBN Sst negative (Figure 2.5A-D). The average number of retrograde-labeled CeA cells was comparable between injection sites (Figure 2.6Total; Kolmogorov-Smirnov $F = 0.57$, $p = 0.89$). The majority of the CeA-to-NST population was Sst negative (Kolmogorov-Smirnov $F = 2.0$, $p < 0.01$), while the CeA-to-PBN population was more equally split between Sst-negative and Sst-positive cells (Kolmogorov-Smirnov $F = 0.86$, $p = 0.44$).

Expressed as a percentage of their respective population, a significantly greater proportion of CeA-to-PBN neurons expressed Sst (~40%) compared to CeA-to-NST neurons (~23%) (Figure 2.7A, Kolmogorov-Smirnov $F = 1.73$, $p < 0.01$). A statistically significant difference between injection site also was evident for the remaining Sst-negative portion of the populations (Figure 2.7B, Kolmogorov-Smirnov $F = 1.58$, $p = 0.01$). For both the CeA Sst-positive (Figure 2.7A) and -negative populations (Figure 2.7B), the vast majority had a single target (i.e. NST only or PBN only) with a smaller proportion being dual-target cells. Statistically significant differences were not observed between injection sites for single- or dual-target neurons (Kolmogorov-Smirnov F 's ≥ 0.44 , p 's ≥ 0.4).

2.3.2 HSV injections

To confirm the above results obtained from CTb injections, we injected cre-dependent HSV's into the NST and PBN of Sst-cre mice. Figure 2.8A, B, C, and D show photomicrograph examples of *HSV-Ef1 α -DIO-EYFP* injected into the NST. Microscopic examination of each injection site revealed that green fluorescence (cells, axons, dendrites) largely filled the NST at each level. The green fluorescent cells in the NST likely reflect Sst-expressing interneurons, while those in surrounding areas indicate Sst neurons that project to the NST or possibly virus spread outside the NST (Balaban and Beryozkin, 1994; Beckman and Whitehead, 1991; Corson et al., 2012b; Travers, 1988). The red fluorescent cells represent Sst neurons that project to the PBN (Dallel et al., 2004; Murakami et al., 2002; Travers, 1988). A few cells were positive for both EYFP and mCherry (yellow

fluorescence) indicative of Sst neurons that project to or within the NST as well as to the PBN.

Photomicrograph examples of *HSV-Ef1 α -DIO-mCherry* injected into the PBN of the same mouse are shown in Figure 2.8E, F, G, and H where red fluorescence (cells, axons, dendrites) largely surrounded the superior cerebellar peduncle (scp) at each level. The red fluorescent cells in the PBN likely reflect Sst-expressing interneurons, while those in surrounding areas such as LC indicate Sst neurons that project to the PBN or possibly virus spread outside the PBN (Giehl and Mestres, 1995; Luppi et al., 1995). The green fluorescent cells represent Sst-positive PBN-to-NST projection neurons (Karimnamazi and Travers, 1998), while green fluorescent fibers likely represent retrograde-labeled axons from higher structures. Despite greater spread of the larger volume virus injections relative to CTb injections, the resulting label in the CeA was remarkably similar.

Dense expression of fluorescent markers was observed throughout the rostrocaudal extent of the amygdala. Low power photomicrograph examples of retrograde-labeled Sst-expressing neurons at 4 different levels of the CeA are shown in Figure 2.9A, B, C, and D. Panels E-H show corresponding stereotaxic atlas drawings depicting the general location of CeA/Sst neurons projecting to the NST (green) and PBN (red). No attempt was made to signify double-labeled neurons (yellow in Figure 2.9A-D) or provide an exact representation of the total number of cells in each photomicrograph. We counted a total of 241 CeA/Sst neurons that projected to the NST and 469 projecting to the PBN. On average, a greater number of CeA/Sst neurons projected to the PBN (16.1 ± 1.3 cells per

section) compared to the NST (8.3 ± 1.6 cells per section) (Figure 2.10; Kolmogorov-Smirnov $F = 2.2$, $p < 0.01$). Out of the 710 retrograde labeled neurons, only 28 contained both fluorescent markers and were considered dual-target neurons (Figure 2.10; 0.9 ± 0.2 cells per section). Expressed as a percentage of their respective population, greater than 90% of CeA/Sst cells project either to the NST or PBN (Figure 2.11A). Statistically significant differences were not observed between injection sites for single- or dual-target neurons (Kolmogorov-Smirnov F 's = 0.65, p 's = 0.78). Comparison of both experimental methods used in the present report revealed a similarly small percentage of CeA/Sst neurons that project to both brainstem gustatory nuclei (Figure 2.11B; Kolmogorov-Smirnov F 's ≥ 0.5 , p 's ≥ 0.8). Thus, CeA cells mostly project either to the NST or PBN and a subset of each population expresses Sst.

2.3.3 Electron microscopy

Dense peroxidase labelling of somatostatin cell bodies filled the rostrocaudal extent of the CeA (Figure 2.12). The axon terminals of these cells, represented by dark puncti, were observed through the rostrocaudal extent of the NST (Figure 2.13A). With the aid of a light microscope, the portions of NST showing peroxidase labeled axon terminals were excised and glued to a resin block. Based on tissue landmarks, a trapezoid sketch showing the approximate areas that were cut around NST is shown in Figure 2.13B (solid line). The block was further trimmed as shown in Figure 2.13B (dashed line) and ultrathin sections were made. The thin sections were stained for GABA and images were obtained using a transmission electron microscope. A representative electron micrograph of a Sst-positive

terminal (dark reaction product) and its post synaptic target (shaded light green) is shown in Figure 2.14. A total of 102 Sst presynaptic terminals and 120 post-synaptic targets were analyzed (some presynaptic terminals had more than one post-synaptic target). On average, Sst axon terminals had gold particle densities significantly above background (Figure 2.15, black bar, Mann-Whitney Rank Sum=213; $p \leq 0.001$), while their post-synaptic targets had gold particle densities below background (Figure 2.15, black bar, Mann-Whitney Rank Sum=2812; $p \leq 0.001$). A histogram of normalized gold particle densities of pre- and post-synaptic terminals relative to the background shows a bimodal distribution (Figure 2.16). The gold particle density in 93% of Sst presynaptic terminals was above background (e.g. >1) and considered to be GABAergic. In contrast, the gold particle density in 98% of post-synaptic targets was less than background (e.g., <1) and were considered to be non-GABAergic. This distribution also can be seen by examining the cumulative histogram of raw gold particle densities shown in Figure 2.17. The majority of the Sst-positive presynaptic terminals (89%) had a density above the mean background level of 18.5 particles/ μm^2 , while nearly all of the postsynaptic targets (98%) had a density below this background level. Together, these data indicate that CeA/Sst terminals in NST co-express GABA and primarily synapse with non-GABAergic neural elements.

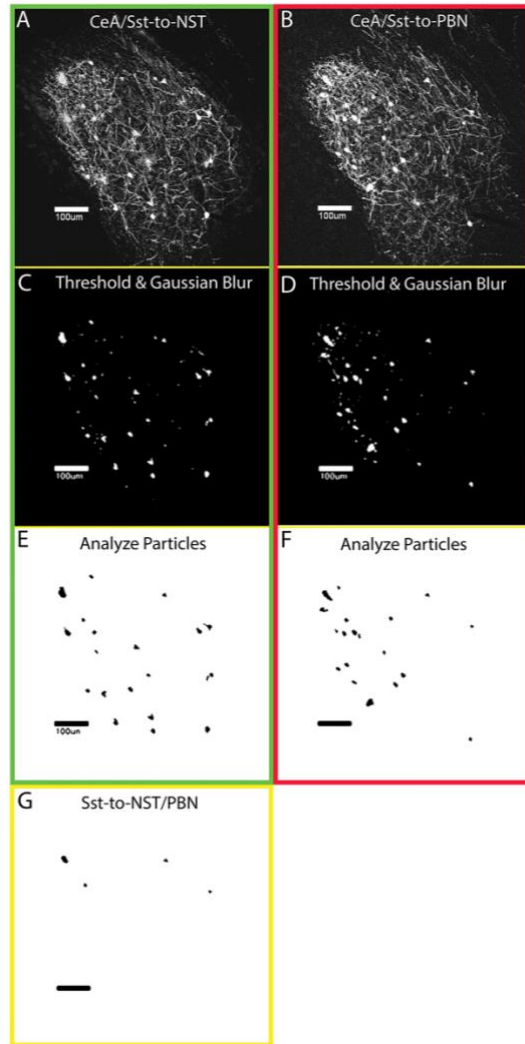


Figure 2.1: Example of the process for automated cell counts using Image J software.

Height-bit images of separate color channels depicting retrograde labeled Sst cells in the CeA resulting from HSV-Ef1 α -DIO-EYFP injected into the NST (A) and HSV-Ef1 α -DIO-mCherry into the PBN (B). The black and white images were auto threshold adjusted (otsu or triangle method) and a Gaussian blur applied (sigma radius = 1) (C&D). The analyze particles function was used to create a mask of labeled cells in each channel (size > 20 μ m²) (E&F). In this example with 2 color channels, the number of double-labeled cells was calculated using the image calculator function “AND” to identify overlapping pixels in the separate channels. Using the analyze particles function on the resultant image, overlapping elements with size > 20 μ m² were considered to be double labeled (G).

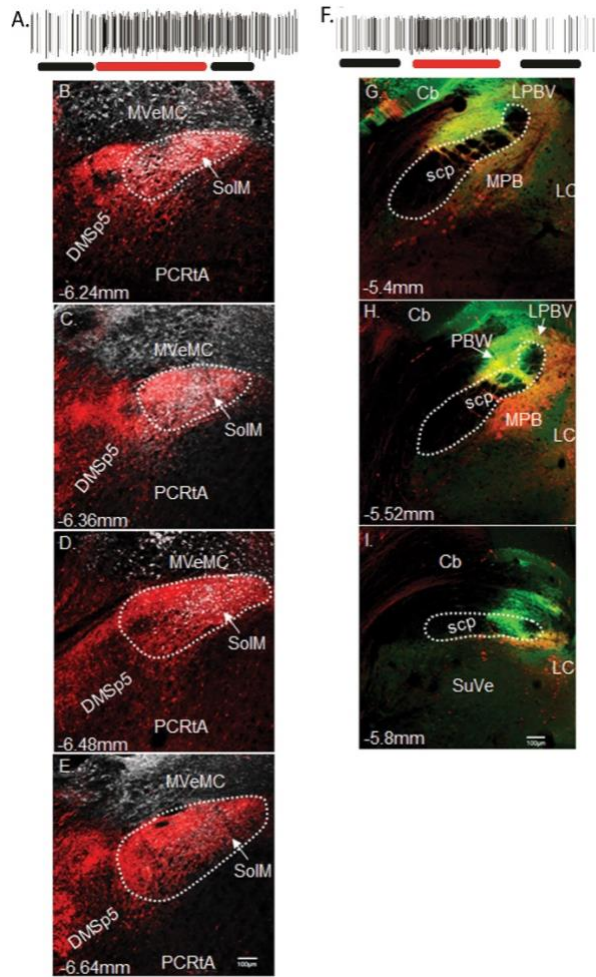


Figure 2.2: Taste evoked responses and CT-b injection sites in NST and PBN

Electrophysiological recordings of taste-evoked responses to 0.1M NaCl in NST (A) and PBN (F). Red lines show neural activity during application of NaCl to the anterior tongue while black lines indicate water application. Fluorescent images of CTb-647 (white) injection in the gustatory responsive NST (**B-F**) and CTb-488 (green) in the gustatory responsive PBN (**G-I**) from case #1704. Sections are arranged from rostral (top) to caudal (bottom). White dots outline the approximate boundaries of the NST and the superior cerebellar peduncle (scp) in the PBN. Red fluorescence indicates Sst-expressing fibers and neurons. Yellow fluorescence (**G-I**) indicates overlap between Sst-expressing neural elements and CTb-488 injection. The approximate level relative to bregma is shown at the bottom left of each photomicrograph. Magnification was 10x (0.85 pixels/micron). Abbreviations: Cb, cerebellum; DMsp5, dorsomedial spinal trigeminal nucleus; anterior part; LC, locus coeruleus; LPBV, lateral parabrachial nucleus, ventral part; MPB, medial parabrachial nucleus; MVeMC, medial vestibular nucleus, magnocellular part; PCRtA, parvicellular reticular nucleus, alpha part; PBW,

parabrachial nucleus, waist part; scp, superior cerebellar peduncle; SolM, nucleus of the solitary tract, medial part; SuVe, superior vestibular nucleus.

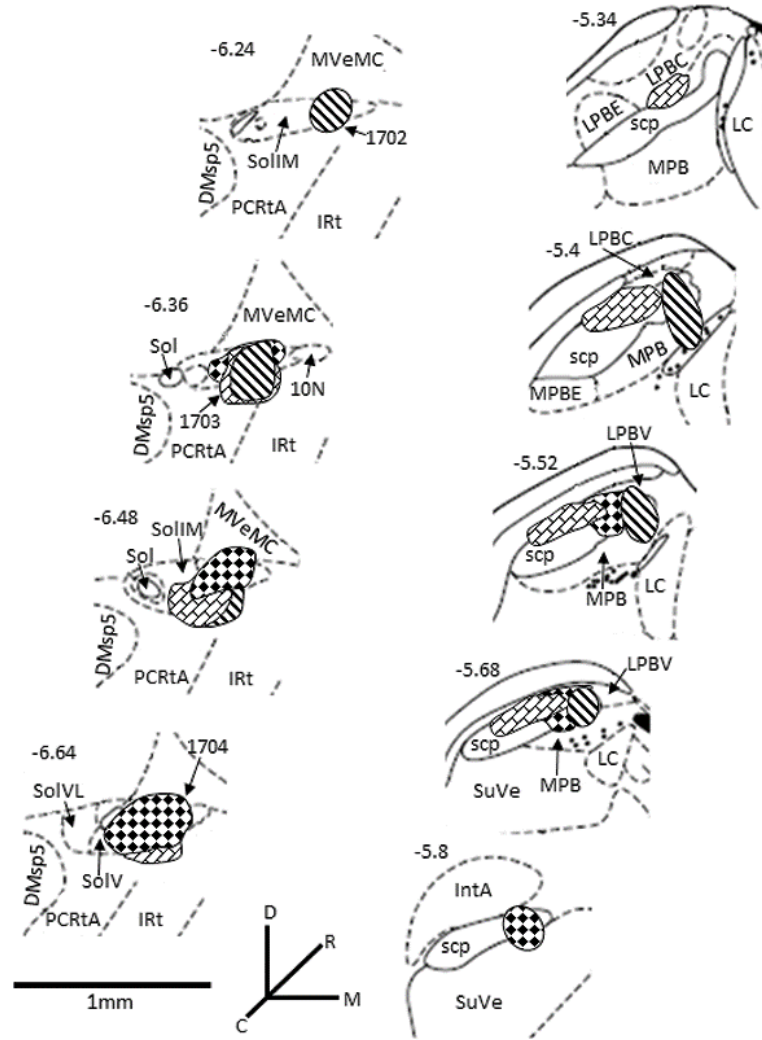


Figure 2.3: Fill patterns of tracers in sections of NST and PBN.

The different fill patterns represent the extent of individual tracer injections concentrated in the rostral regions of the NST (left panels) and caudal regions of PBN (right panels). Sections are arranged from rostral (top) to caudal (bottom) and medial is to the right. The approximate levels relative to bregma are indicated at the top left of each image (Paxinos and Franklin, 2001).

Abbreviations: DMsp5, dorsomedial spinal trigeminal nucleus; anterior part; IRT, intermediate reticular nucleus; IntA, interposed cerebellar nucleus, anterior part; LC, locus coeruleus; LPBC, lateral parabrachial nucleus, central part; LPBE, lateral parabrachial nucleus, external part; LPBV, lateral parabrachial nucleus, ventral part; MPB, medial parabrachial nucleus; MPBE, medial parabrachial nucleus external part; MVeMC, medial vestibular nucleus, magnocellular part; PCRtA, parvicellular reticular nucleus, alpha part; scp, superior cerebellar peduncle; Sol, solitary tract; SoliM, nucleus of the solitary tract, intermediate.

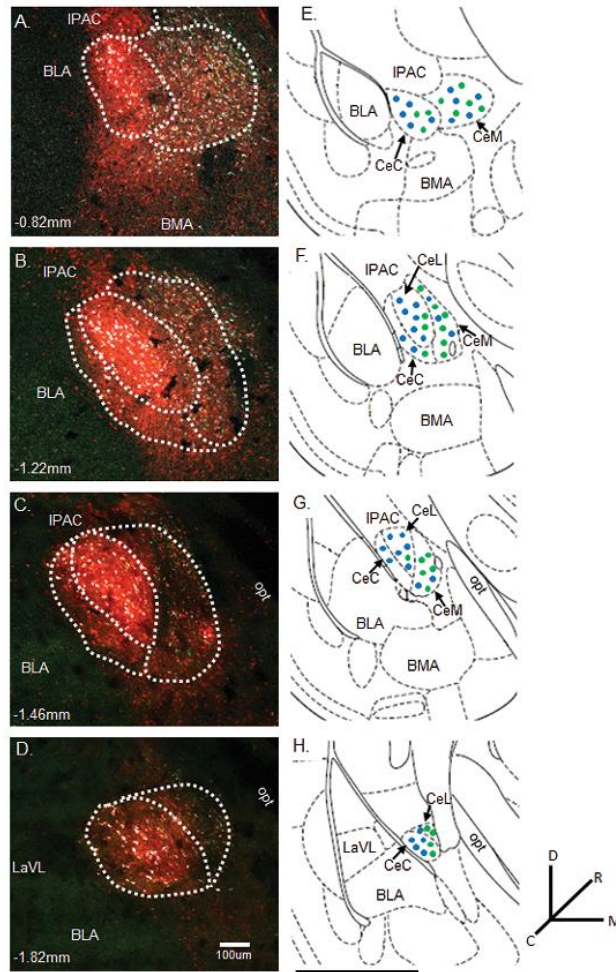


Figure 2.4: Representative photomicrographs CeA neurons projecting to NST and PBN.

(A-D) Representative photomicrographs of CeA/Sst neurons (red) and neurons projecting to the NST (green) and PBN (white) from case #1702. The white dotted lines outline the approximate boundaries of the CeC, CeL, and CeM divisions of the CeA. The approximate levels relative to bregma are indicated at the bottom left corner in each photomicrograph (Paxinos and Franklin, 2001). Magnification of fluorescent images was 10x (0.85 pixels/micron). **(E-H)** Corresponding diagrams labeled with amygdala subnuclei as defined in Paxinos and Franklin (2001). The general location of retrograde labeled neurons are represented by green (NST projecting) and blue (PBN projecting) dots. The black scale bar below the atlas drawings is 1mm. Abbreviations: BLA, basolateral amygdaloid nucleus, anterior part; BMA, basomedial amygdaloid nucleus, anterior part; CeC, central amygdaloid nucleus, capsular part; CeL, central amygdaloid nucleus, lateral division; CeM, central amygdaloid nucleus,

medial division; IPAC, interstitial nucleus of the posterior limb of the anterior commissure; LaVL, lateral amygdaloid nucleus, ventrolateral part; opt, optic tract.

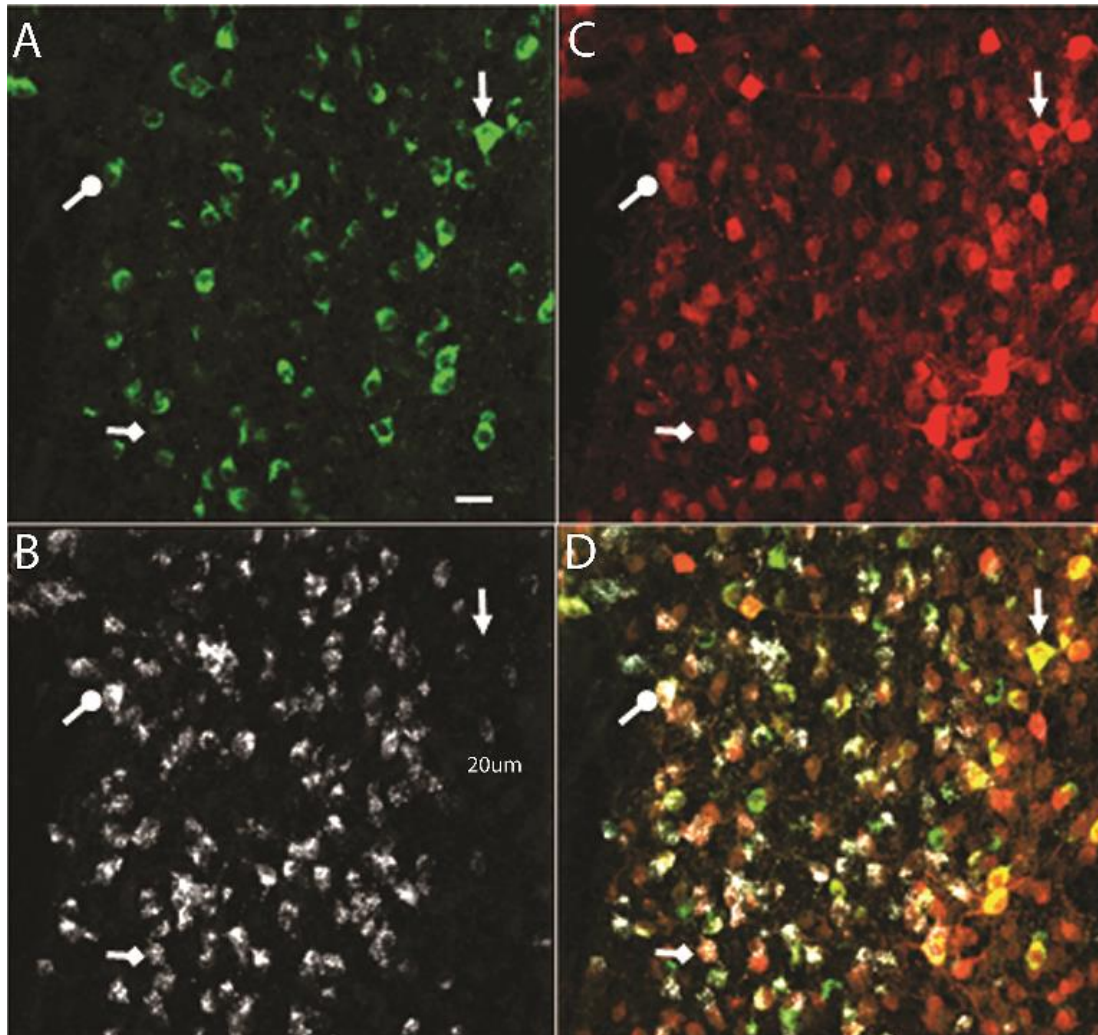


Figure 2.5: Representative high-power photomicrographs of the CeA neurons projecting to NST and PBN

Representative high-power photomicrographs of the CeA showing fluorescent labeling from CTb-488 (A, green PBN projecting neurons) and CTb-647 (B, white NST projecting neurons) injections in case #1704. (C) Sst-positive neurons marked by TdTomato reporter expression (red). (D) Merged image of separate color channels. Filled arrowhead: example of Sst-positive neuron that only projects to the PBN (yellow). Filled diamond: example of Sst-positive neuron that only projects to the NST. Filled circle: example of Sst-positive neuron that projects both to the NST and PBN. Magnification was 40x (1.40 pixels/micron). The white scale bar at bottom right in panel A is 20um.

Figure 2.5. Representative high-power photomicrographs of the CeA showing fluorescent labeling from CTb-488 (A, green PBN projecting neurons) and CTb-647 (B, white NST projecting neurons) injections in case #1704. (C) Sst-positive neurons marked by TdTomato.

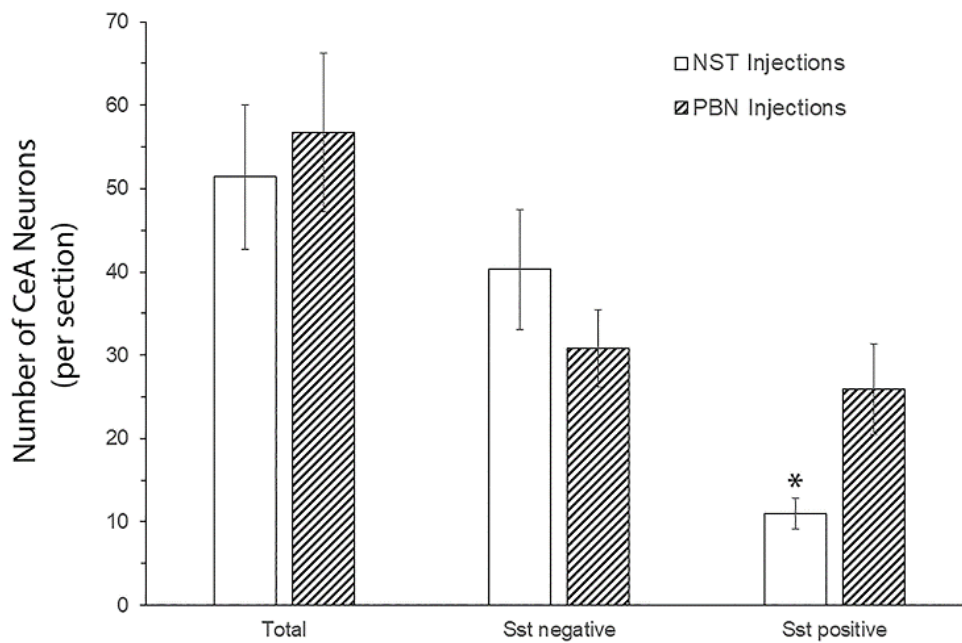


Figure 2.6: Graph showing the average number of retrograde labeled neurons in CeA sections.

Figure 2.7 The per section average of retrograde labeled neurons in the CeA following injections of CTb into the gustatory NST (open bars) and PBN (cross-hatched bars) of Sst/TdTomato reporter mice. *, significantly different from PBN Sst positive.

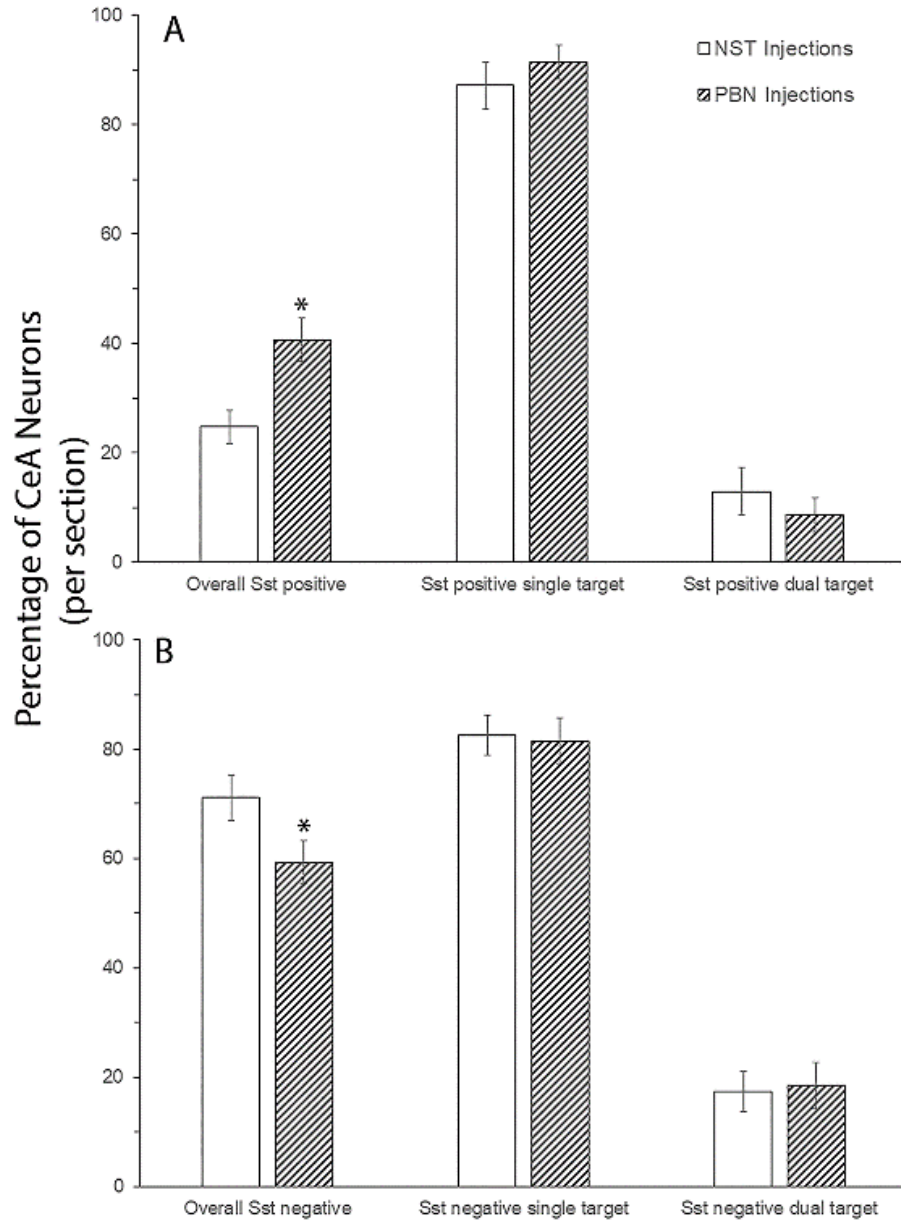


Figure 2.7: Graph showing the percentage of CeA Sst-positive and Sst-negative cells projecting to NST and PBN

The mean percentage of CeA Sst-positive **(A)** and –negative **(B)** neurons following injections of CTb into the gustatory NST (open bars) and PBN (cross-hatched bars) of Sst/TdTomato reporter mice. Relative to the overall number of NST and PBN projecting cells, the majority of Sst-positive and –negative neurons projected to a single target (i.e. either the NST or PBN). *, significantly different from NST overall Sst positive.

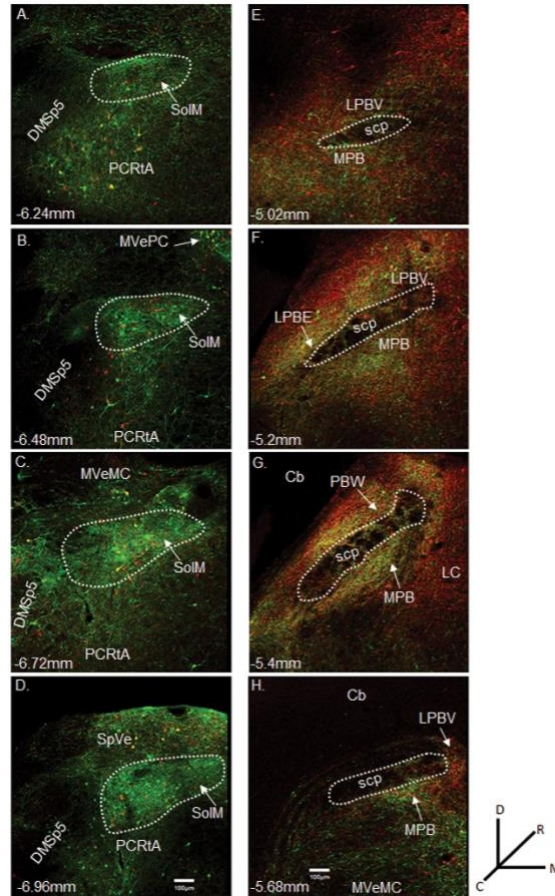


Figure 2.8: Representative fluorescent images of viral injection into NST and PBN

Representative fluorescent images resulting from the injection of HSV-Ef1 α -DIO-EYFP into the NST (**A-D**, green) and HSV-Ef1 α -DIO-mCherry into the PBN (**E-H**, red) of a Sst-cre mouse. Sections are arranged from rostral (top) to caudal (bottom). White dots outline the approximate boundaries of the NST and the superior cerebellar peduncle (scp) in the PBN. Within the NST, red fluorescence indicates Sst-expressing neurons that project to the PBN, while yellow fluorescence indicates Sst-expressing neurons that project to the PBN and locally within the NST. Within the PBN, the red fluorescent cells in the PBN indicate Sst-expressing interneurons, while those in surrounding areas such as LC indicate Sst neurons that project to the PBN. The green, fluorescent cells represent Sst-positive PBN-to-NST projection neurons, while green, fluorescent fibers likely represent retrograde-labeled axons from higher structures. The approximate level relative to bregma is shown at the bottom left of each photomicrograph. Magnification was 10x (0.85 pixels/micron). Abbreviations: Cb, cerebellum; DMsp5, dorsomedial spinal trigeminal nucleus; anterior part; LC, locus coeruleus; LPBE, lateral parabrachial nucleus, external part; LPBV, lateral parabrachial nucleus, ventral part; MPB, medial parabrachial nucleus; MVeMC,

medial vestibular nucleus, magnocellular part; MVePC, medial vestibular nucleus, parvicellular part; PCRtA, parvicellular reticular nucleus, alpha part; PBW, parabrachial nucleus, waist part; SolM, nucleus of the solitary tract, medial part; scp; superior cerebellar peduncle; SpVe, spinal vestibular nucleus.

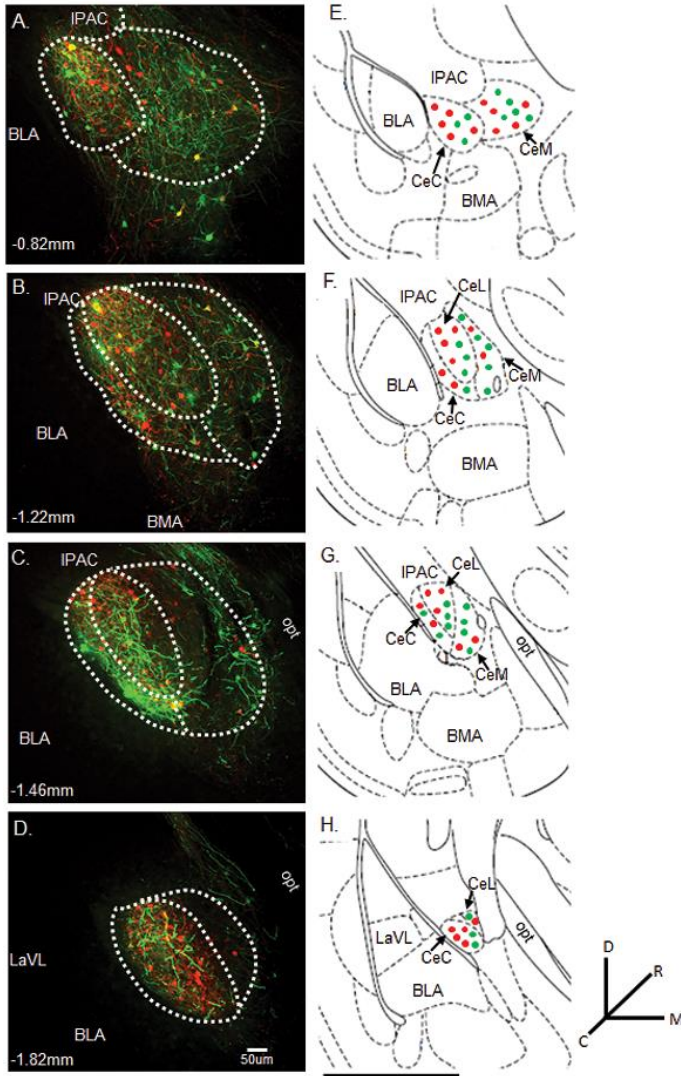


Figure 2.9: Photomicrographs showing retrograde labelled cells in CeA.

(A-D) Representative photomicrographs of CeA/Sst neurons projecting to the NST (green) and PBN (red) from HSV injections depicted in Figure 2.8. Yellow fluorescence indicates Sst neurons that project both to the NST and PBN. The white dotted lines outline the approximate boundaries of the CeC, CeL, and CeM divisions of the CeA. The approximate levels relative to bregma are indicated at the bottom left corner in each photomicrograph (Paxinos and Franklin 2001). Magnification of fluorescent images was 10x (0.85 pixels/micron). (E-H) Corresponding diagrams labeled with amygdala sub nuclei as defined in Paxinos and Franklin (2001). The general location of retrograde labeled neurons are represented by green (NST projecting) and red (PBN projecting) dots. The black scale bar below the atlas drawings is 1mm. Abbreviations: BLA, basolateral amygdaloid nucleus, anterior part; BMA, basomedial amygdaloid nucleus,

anterior part; CeC, central amygdaloid nucleus, capsular part; CeL, central amygdaloid nucleus, lateral division; CeM, central amygdaloid nucleus, medial division; IPAC, interstitial nucleus of the posterior limb of the anterior commissure; LaVL, lateral amygdaloid nucleus, ventrolateral part; opt, optic tract.

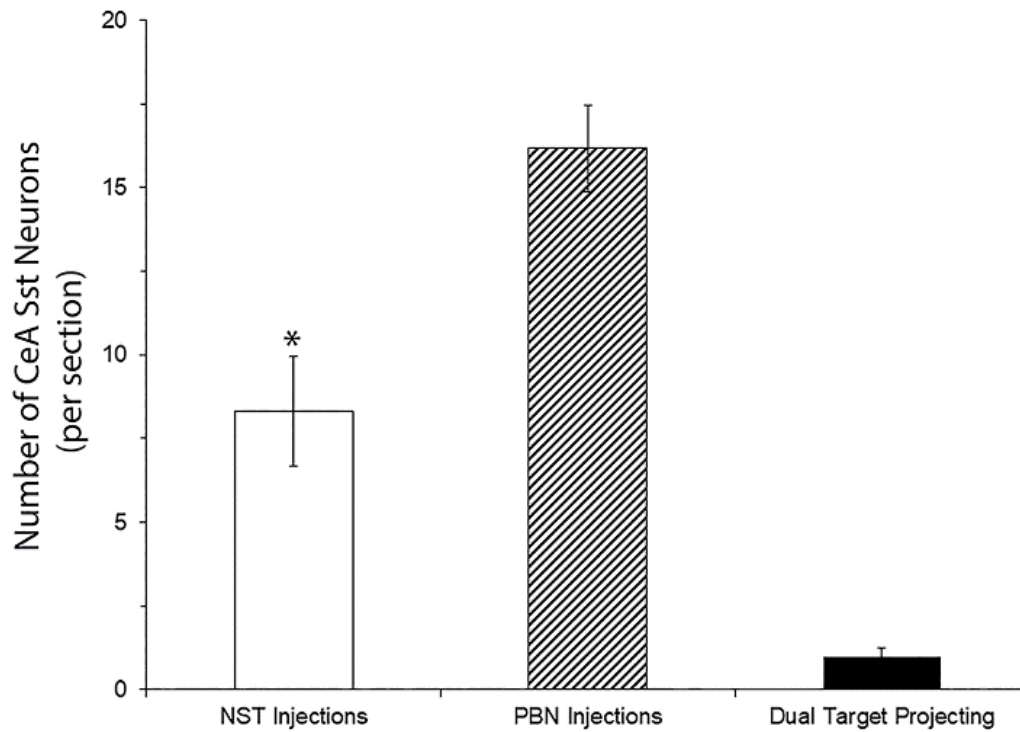


Figure 2.10: Graph showing the number of retrograde labelled cells in CeA sections.

The per section average of retrograde labeled Sst neurons in the CeA following HSV injections of into the NST and PBN of a Sst-cre mice. Open bar represents the average number of Sst cells that only projected to the NST, cross-hatched bar Sst cells that only projected to the PBN and filled bar Sst cells that projected both to the NST and PBN. *, significantly different from PBN injections.

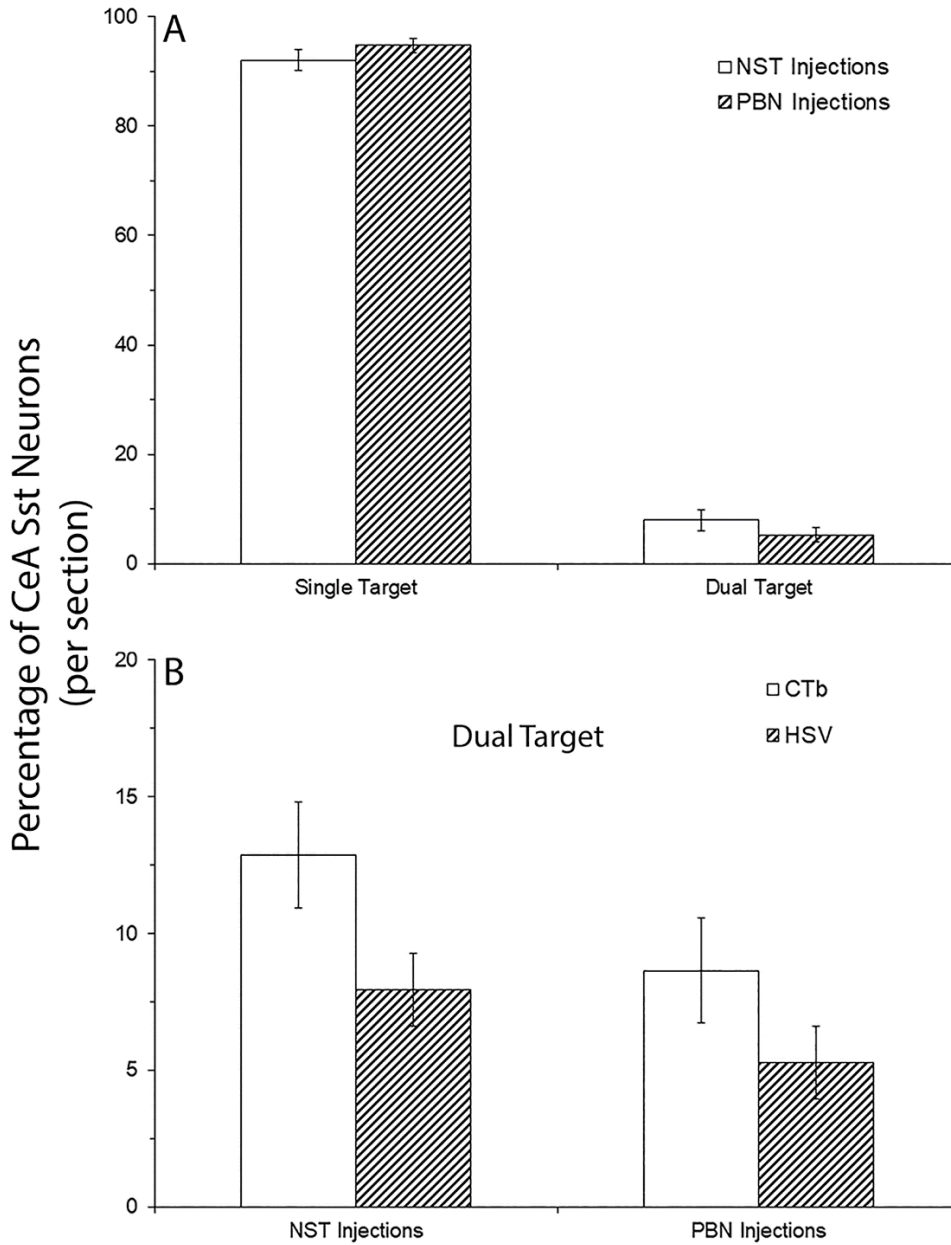


Figure 2.11: Graph showing percentage of double labelled and single labelled cells in CeA sections.

(A) The mean percentage of single- and double-labeled Sst neurons in the CeA following HSV injections into the NST (open bars) and PBN (cross-hatched bars). (B) Comparison of the percentage of dual-target Sst neurons calculated following CTb (open bars) and HSV (cross-hatched bars) injections into the NST and PBN. Both experimental methods resulted in a low percentage of CeA/Sst neurons that projected both nuclei.

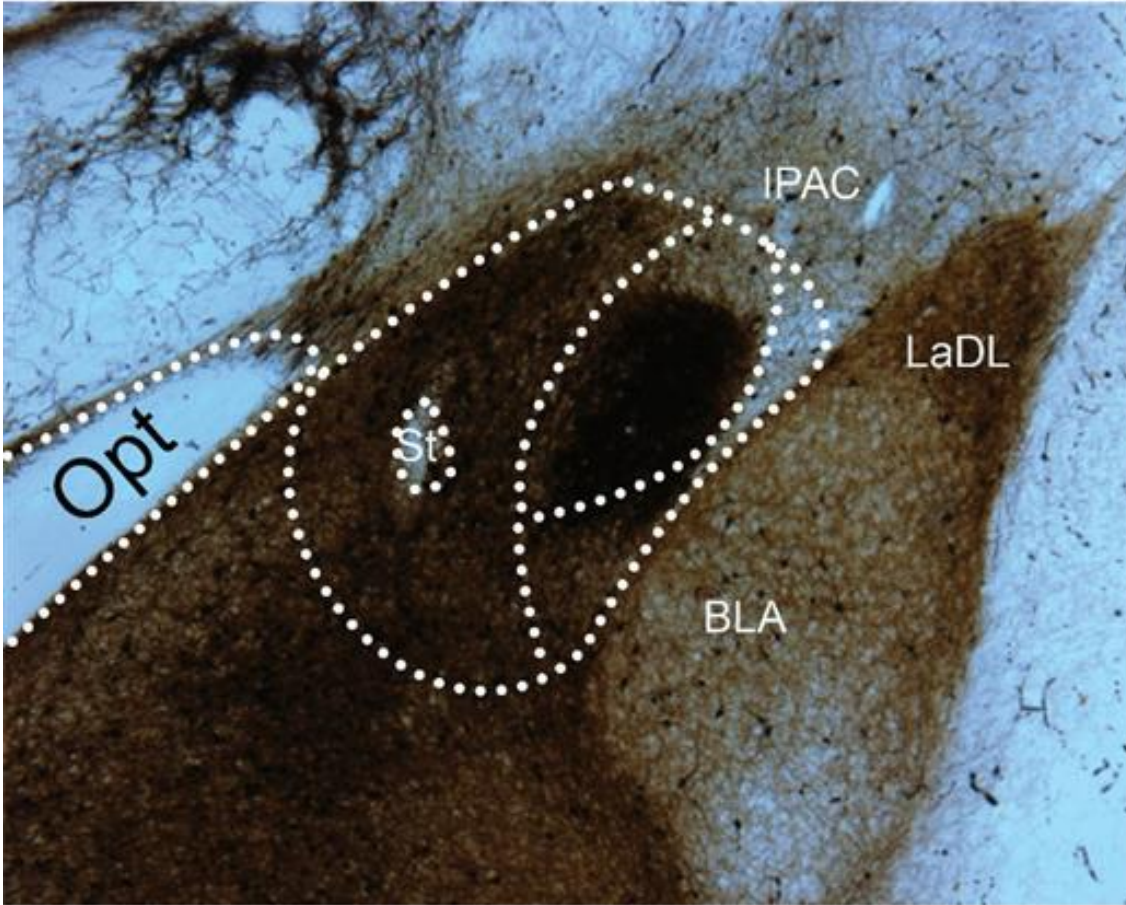


Figure 2.12: Photomicrograph showing peroxidase labeling in a CeA tissue section.

Peroxidase labelling of Sst-cell bodies in the CeA injection site following the injection of AAV9-Ef1 α -DIO-dAPEX2. White dots outline the CeA.

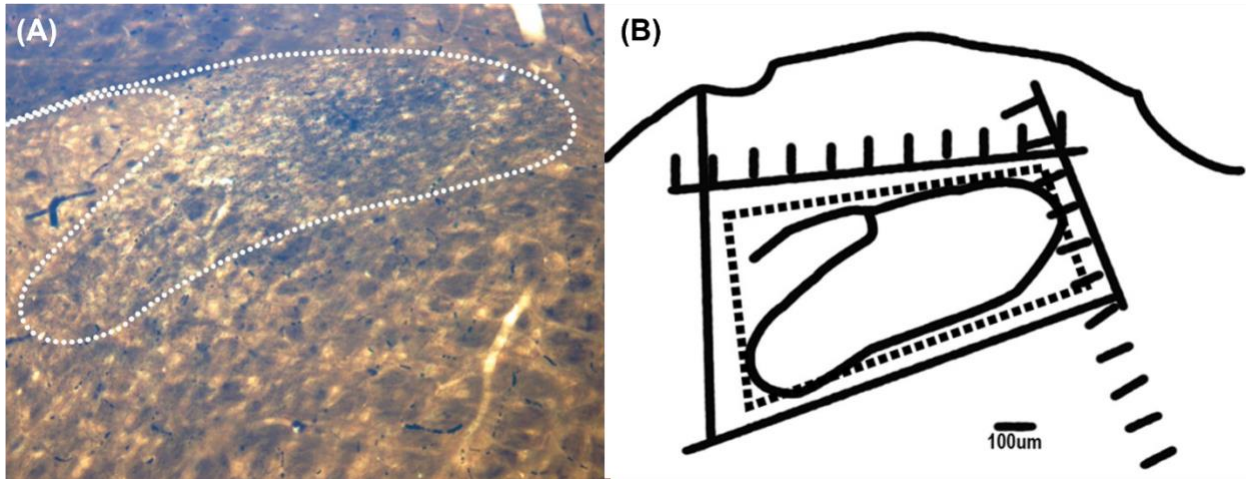


Figure 2.13:Photomicrograph showing peroxidase labelled Sst axon terminals in the NST.

(A) Peroxidase labelling of Sst axon terminals in the NST (outlined by white dots) resulting from the injection of AAV9-Ef1 α -DIO-dAPEX2 into the CeA. (B) A sketch of the NST region that was excised (solid line) for electron microscope analyses. Further trimming (Dashed line) was done before thin sections were cut using an ultramicrotome.

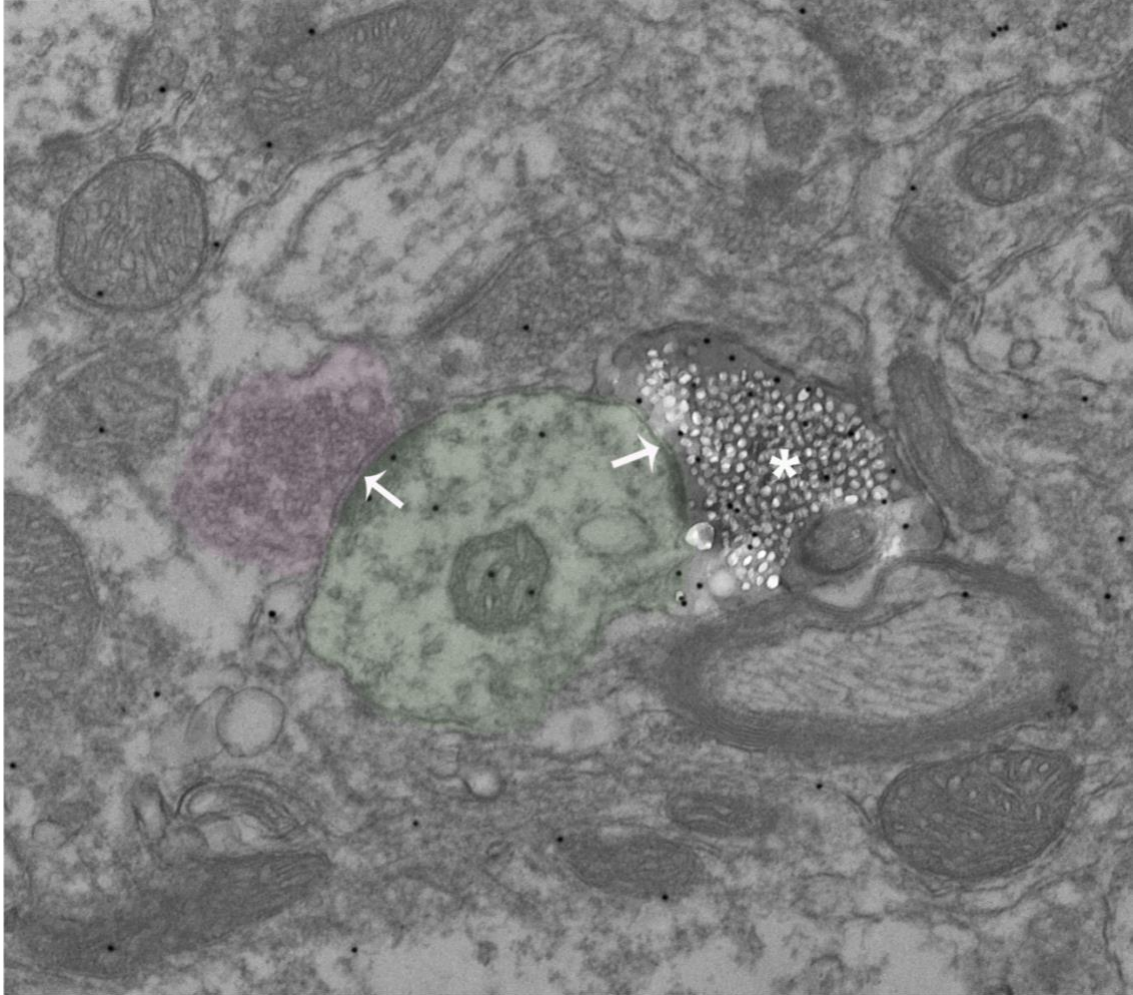


Figure 2.14: A representative electron micrograph of a DAB labelled terminal and its post-synaptic target

A representative electron microscope image showing a dendrite (shaded light green) receiving input from two presynaptic terminals: a DAB-labeled Sst-positive terminal (white star) and a Sst-negative terminal (shaded purple). White arrows indicate synaptic contacts. Black dots represent GABA immunoreactivity.

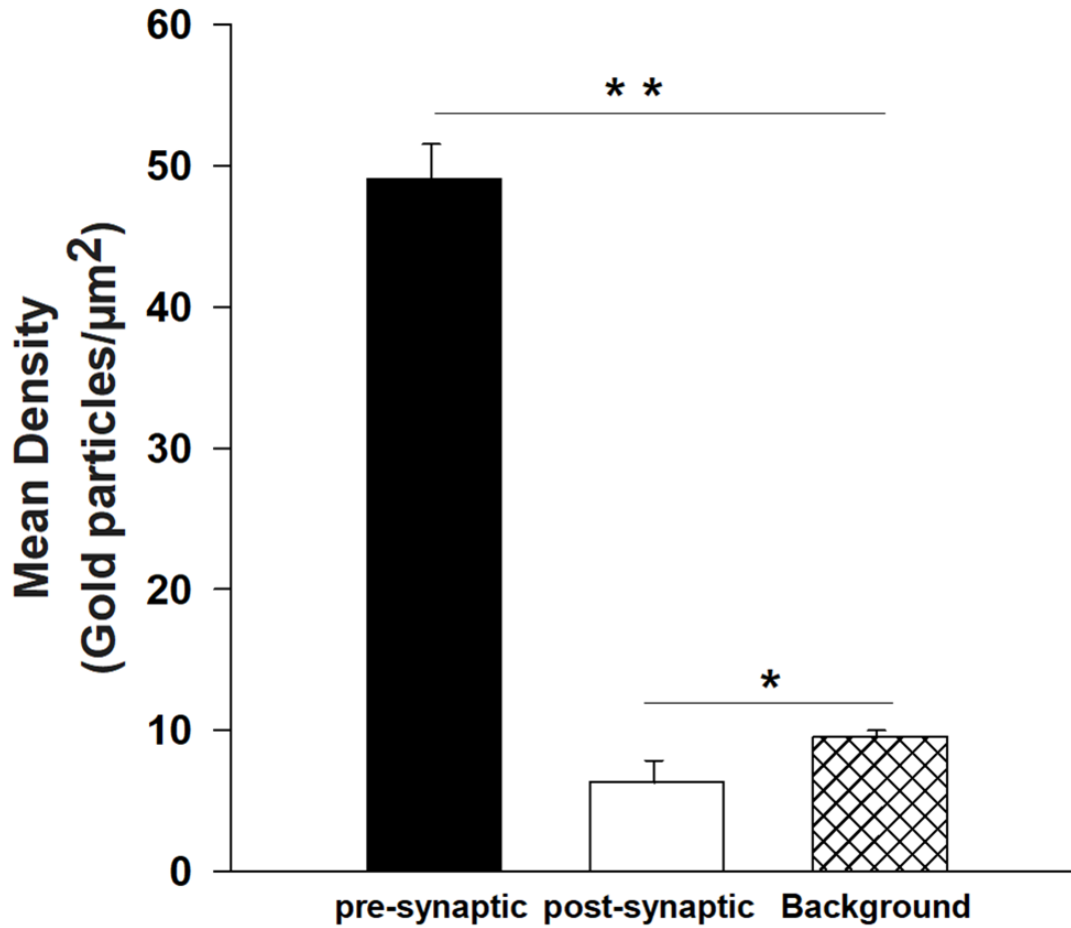


Figure 2.15: Mean gold particle density of pre- and post-synaptic profiles relative to the background

Mean gold particle density for Sst-positive pre-synaptic terminals (filled bar) and post-synaptic targets (open bar). The cross hatched bar represents the mean background density. ** significantly different from post-synaptic and background density. * Significantly different from background density.

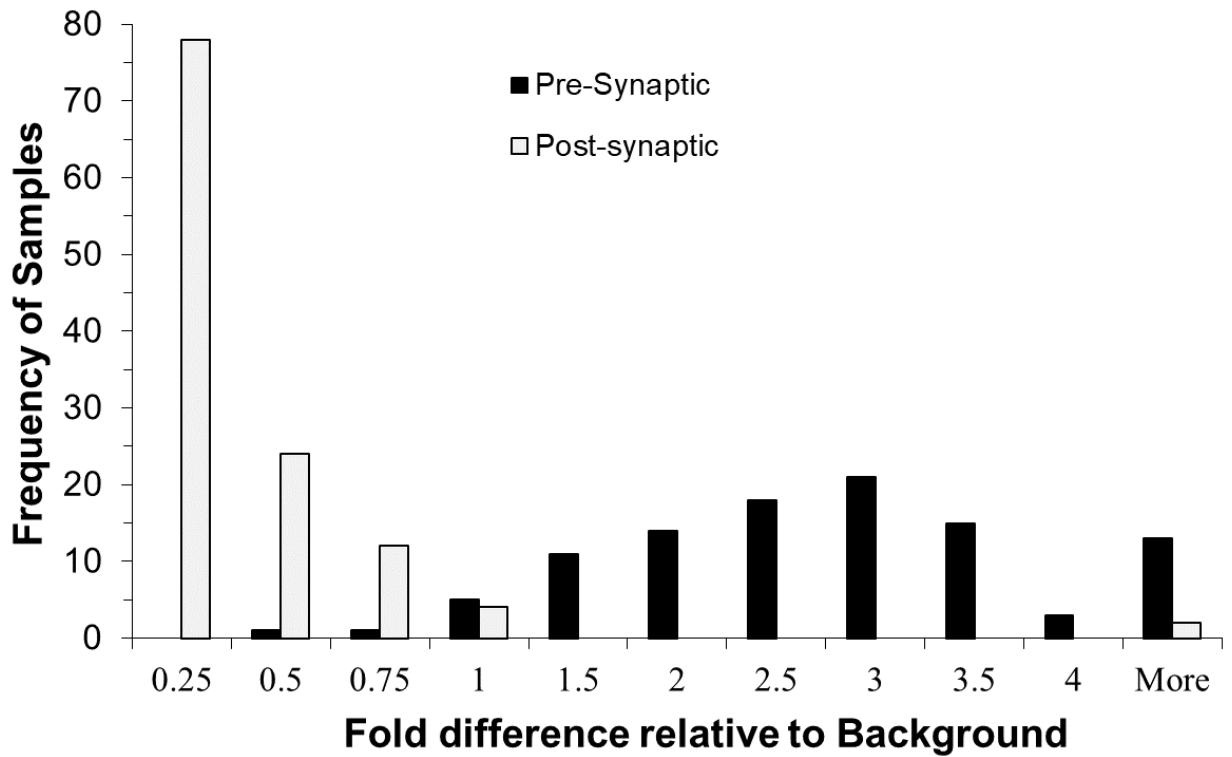


Figure 2.16: Histogram of normalized gold particle densities relative to background

Histogram of normalized gold particle densities relative to background in Sst-positive presynaptic terminals (filled bars) and postsynaptic targets (open bars). Presynaptic terminals and their postsynaptic targets in which the gold particle density was greater than 1 were considered to be GABA positive. Background density for the 2 staining sessions was 14.13 and 23.60 particles/ μm^2 .

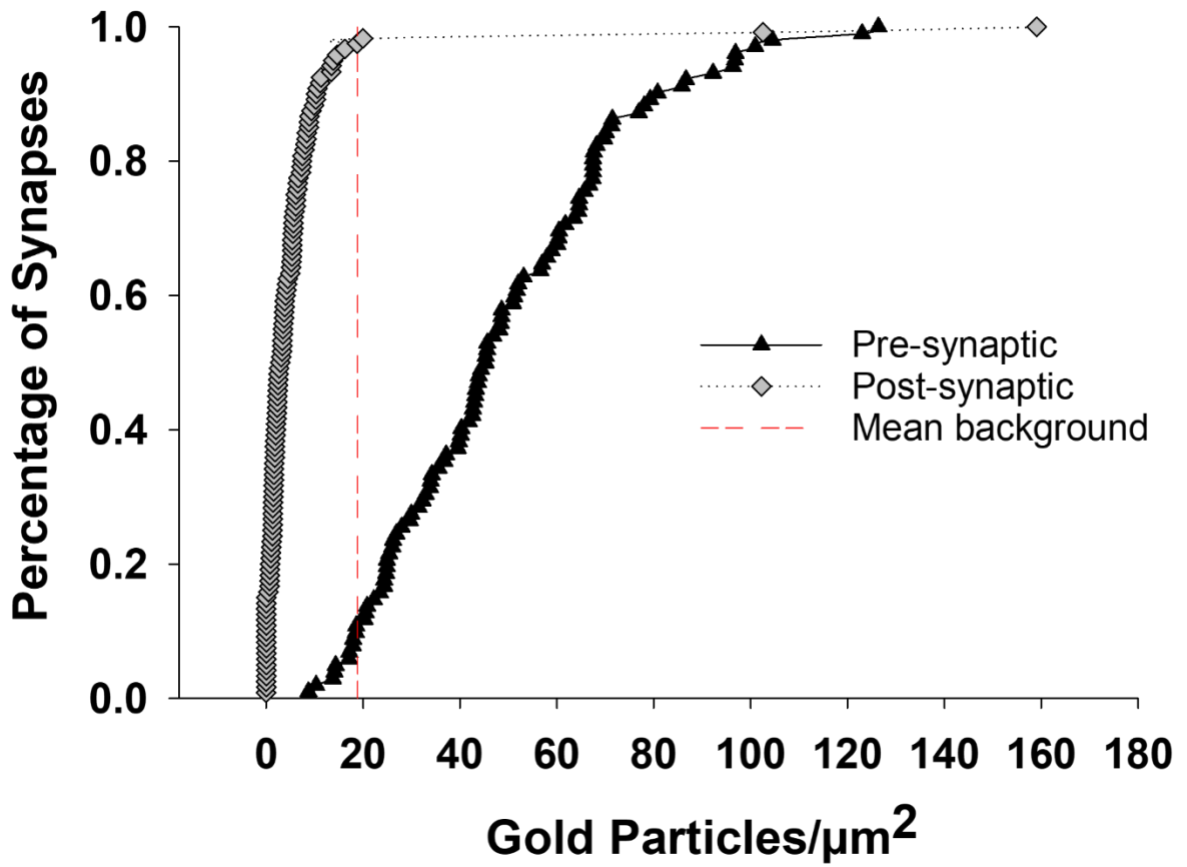


Figure 2.17: Cumulative histogram of raw gold particle densities

Cumulative histogram of raw gold particle densities of Sst-positive pre-synaptic terminals and post-synaptic targets. Mean background densities for the two staining sessions was 18.86 ± 4.73 gold particles/μm².

2.4 Discussion

The objective of the present experiments was to further delineate neural populations in the CeA that project to the gustatory regions of the NST and PBN. The present findings mirror results from previous studies showing that the NST and PBN are largely innervated by distinct populations of CeA neurons (Kang and Lundy, 2009a) and, at least for the PBN, a large portion of CeA-to-PBN neurons co-express Sst and GABA (Magableh and Lundy, 2014; Panguluri et al., 2009). The present results extend these observations by demonstrating that a subset of CeA-to-NST neurons also express Sst, are largely distinct from CeA-to-PBN Sst neurons, and co-express GABA.

Although the HSV injections produced greater spread in the rostrocaudal orientation compared to the CTb injections, the resultant retrograde labeling was overall in agreement. Retrograde labeled Sst neurons were observed throughout the rostrocaudal extent of the CeA and most were found to be single-target cells projecting to either the NST or PBN with a much smaller population projecting to both brainstem nuclei. One difference between these CeA/Sst populations was that a significantly higher proportion innervated the PBN compared to the NST. Approximately 45% of CeA-to-PBN neurons were Sst positive whereas Sst expression only accounted for about 25% of CeA-to-NST neurons. A previous study in mice reported an identical percentage of CeA-to-PBN neurons that express Sst (Magableh and Lundy, 2014). Despite this difference in the extent to which Sst neurons contribute to CeA-to-NST and CeA-to-PBN pathways, they likely influence neural processing of taste information in the brainstem.

Prior investigations in rats and/or hamsters demonstrate that the CeA modulates taste responsive neurons in the NST and PBN, which is often differential. In rats and hamsters, the most common effect of CeA stimulation on NST taste cells was excitatory (Cho et al., 2003b; Kang and Lundy, 2010b). One synapse further along in the PBN, inhibition of taste cells in response to CeA stimulation predominated (Li et al., 2005b; Lundy and Norgren, 2001a; Lundy and Norgren, 2004a). The present results showing that separate populations of CeA neurons project to the NST and PBN but express a common neuropeptide suggests that differential modulation of taste processing might rely on differences in local brainstem/forebrain synaptic connections. However, the present results show that CeA/Sst neurons that project to the NST, like those that innervate the PBN (Lundy, 2020b), predominately co-express GABA and synapse with non-GABAergic neural elements. This arrangement also is consistent with previous research showing that CeA axon terminals in the caudal visceral sensitive NST co-express Sst and GABA and synapse with non-GABAergic neural elements (Batten et al., 2002; Saha et al., 2000). Thus, it is unlikely that CeA/Sst-to-NST cells underlie the predominately excitatory effect on NST taste neurons observed during electrical stimulation of CeA (Kang and Lundy, 2010a; Li et al., 2002c). Rather, this cell population likely mediates, at least in part, the observation that a small proportion of NST taste cells are inhibited by electrical activation of the CeA. Future research is needed to determine whether the postsynaptic targets of CeA/Sst/GABA neurons contribute to the ascending gustatory pathway and/or project locally within the NST.

Although our research demonstrates that Sst/GABA neurons of CeA origin represent one component of descending input to the NST and PBN, the molecular identity of the Sst-negative population remains unclear. This group of neurons also largely projected to either the NST or PBN as well as constituted the bulk of projections to the NST (~75%) and more than 50% of the projections to the PBN. At least for the CeA-to-PBN neurons, we have previously shown that a small subset of neurons express corticotrophin-releasing hormone (Magableh and Lundy, 2014; Panguluri et al., 2009). The molecular identity of the remaining CeA-to-NST and CeA-to-PBN neurons could include one or more of the other numerous neurochemicals present in the CeA (McCullough et al., 2018a; Moga and Gray, 1985). For example, CeA-serotonin receptor Htr2a and CeA-neurotensin expressing neurons contribute to ingestive behavior via interactions with the PBN (Douglass et al., 2017; Torruella-Suarez et al., 2020). If and how any of these CeA cell types influence neural processing of taste information in the brainstem remains unknown. Clearly, additional research is needed to understand the neurochemicals and neural circuitry that mediates top-down modulation of central taste processing and its impact on taste-guided behavior.

In conclusion, a clear understanding of the true impact that centrifugal regulation of taste processing has on taste-guided behavior awaits experiments that independently manipulate the relevant descending neurochemical pathways. Our studies shed light on one candidate neurochemical demonstrating that CeA/Sst-to-PBN and CeA/Sst-to-NST pathways arise from largely distinct neural populations. That these cell populations are distinct provides the opportunity for

future investigations to delineate their contribution(s) to taste processing and ingestive behaviors.

CHAPTER 3
PERTURBATION OF AMYGDALA/SOMATOSTATIN-NUCLEUS OF THE
SOLITARY TRACT PROJECTIONS REDUCES SENSITIVITY TO QUININE
IN A BRIEF-ACCESS TEST

3.1 Introduction

A fundamental role of the gustatory system is to identify the components of foods and fluids to promote favorable dietary selection. In many mammalian species, the nucleus of the solitary tract (NST) and the parabrachial nucleus (PBN) contain the first and second central neurons for the ascending gustatory system (Halsell, 1992b; Norgren and Leonard, 1973a). As would be expected, neural processing in the NST and PBN are important for an animal's ability to use taste information to guide behavior.

Following bilateral damage to the gustatory region of the NST, concentration-dependent intake of normally preferred and avoided taste stimuli is abolished (Shimura et al., 1997d). Altered affective licking to taste stimuli is not due simply to an inability to modify ingestive behavior because the same NST lesioned animals responded normally to increases in the concentration of the trigeminal stimulus capsaicin. Despite a substantial deficit in affective responding to taste stimuli, these same animals were competent in other taste-guided behaviors like acquisition of a conditioned taste aversion (CTA) and expression of sodium appetite (Grigson et al., 1997b).

In contrast to lesions of the NST, bilateral damage to the gustatory PBN blunted concentration-dependent intake of normally preferred and avoided taste stimuli but failed to eliminate them (Flynn et al., 1991a; Scalera et al., 1995b; Spector et al., 1992b; Spector et al., 1993b). Nevertheless, the lesion animals were unable to acquire a CTA or express sodium appetite (Grigson et al., 1998c; Reilly et al., 1993a; Spector et al., 1992b). Together, lesion-behavior studies suggest that the NST is particularly important for appropriate behavioral responses to changes in the affective value of a gustatory stimulus, while the PBN is more involved in taste-visceral associations that assign affective value (Grigson et al., 1997b; Grigson et al., 1998a; Scalera et al., 1995b; Shimura et al., 1997d; Spector et al., 1993b; Spector, 1995). Yet, the neural mechanisms that mediate the seemingly distinct behavioral functions of the gustatory regions of the NST and PBN are poorly understood.

Importantly, several ventral forebrain regions that receive gustatory information like the central nucleus of the amygdala (CeA), lateral hypothalamus (LH), and bed nucleus of the stria terminalis (BNST) send projections back to the NST and PBN (Kang and Lundy, 2009a; van der et al., 1984; Veening et al., 1984) and, thus, provide an anatomical substrate for critical forebrain/brainstem interactions. Indeed, chemical or electrical stimulation of the CeA, LH, and BNST modulates responsiveness of NST and PBN neurons to sapid stimuli indicating active filtering of gustatory information (Kang et al., 2004; Kang and Lundy, 2010b; Li et al., 2005b; Lundy and Norgren, 2004a). Of these forebrain regions, prior research has shown that largely distinct populations of CeA neurons marked by expression of

somatostatin (Sst) project to the gustatory NST and PBN (Bartonjo and Lundy, 2020; Kang and Lundy, 2009a; Magableh and Lundy, 2014; Panguluri et al., 2009). The functional role, if any, of the CeA/Sst-to-NST and CeA/Sst-to-PBN pathways is unknown.

To begin addressing this gap in knowledge, the present experiments optogenetically targeted the CeA/Sst-to-NST pathway and assessed its role in brief-access licking to normally preferred sucrose solutions and normally avoided QHCl solutions. This was accomplished by using replication-deficient Herpes Simplex Virus (HSV) for retrograde transport of transgenes (Neve et al., 2005). Only a subpopulation of CeA-to-NST neurons express Sst (Bartonjo and Lundy, 2020), thus, our approach allowed selective manipulation of these neurons rather than the entire population of CeA-to-NST neurons. Previous research highlights the importance of targeting defined projections beyond simply targeting neuron types (Cai et al., 2014; Tye et al., 2011). Our results show that neither activation nor inhibition of this pathway influenced affective responding to sucrose. In contrast, optogenetic inhibition, but not excitation, of the CeA/Sst-to-NST pathway increased licking to high concentrations of QHCl suggesting that this subpopulation of CeA-to-NST neurons must be active for normal affective responding to an aversive gustatory stimulus.

3.2 Materials and Methods

3.2.1 Subjects

Transgenic mice homozygous for cre recombinase in somatostatin (Sst-cre) expressing neurons (Sstm2.1(cre) Zjh/J) and wild type mice (C57BL/J6) were

obtained from Jackson Laboratories. The two strains were bred at the University of Louisville to generate mice heterozygous for cre recombinase expression in Sst neurons. The mice were maintained in a temperature-controlled colony room on a 12h light/dark cycle with free access to normal rodent chow and distilled water unless otherwise noted. All procedures conformed to NIH guidelines and were approved by the University of Louisville Institutional Animal Care and Use Committee. A total of 28 male and female Sst-cre heterozygous mice were used for data analysis.

3.2.2 Surgeries

The mice were anesthetized with an intraperitoneal injection of Ketamine (100mg/kg) and Anased (10mg/kg) mixture. If needed, an additional dose of Ketamine (50mg/kg) was administered to maintain a deep level of anesthesia, which was determined using toe pinch reflex. The scalp was shaved and disinfected using Prevacics Swab (Professional Disposables International). Mice were secured in a stereotaxic apparatus and ophthalmic ointment was applied to both eyes. Body temperature was maintained at $35\pm 1^{\circ}\text{C}$ by a feedback-controlled heating pad and rectal temperature probe. A midline incision was made to expose the skull, and the skull was leveled with reference to bregma and lambda cranial sutures. Four small holes were drilled through the skull to allow bilateral access to the nucleus of solitary tract (NST) and the central nucleus of amygdala (CeA). The analgesic Rimadyl or Meloxicam (5mg/kg) was administered prior to wound incision and again for at least 2 days post-surgery.

3.2.3 Virus injections

The coordinates used for the virus injections into the NST were 6.1 mm posterior to bregma, ± 1.3 mm lateral to midline, and 3.9 mm ventral to the surface of the cerebellum (Bartonjo and Lundy, 2020). Viral injections were performed using a 10- μ L nanofil syringe (34 g beveled needle, WPI) mounted in a microprocessor-controlled injector (UltraMicroPump, WPI) attached to the stereotaxic instrument. The syringe was first front-filled with light mineral oil followed by either HSV-EF1alpha-DIO-EYFP (RN415, 2.5×10^9 infectious units/mL) [**EYFP control group**], HSV-EF1alpha-DIO-eNpHR3-EYFP (RN417, 2.5×10^9 infectious units/m) [**eNpHR3 inhibitory opsin group**], or HSV-EF1alpha-DIO-hChR2(H134R)-EYFP (RN416, 2.5×10^9 infectious units/m) [**ChR2 excitatory opsin group**]. Viruses were obtained from Dr. Rachael Neve at the Gene Delivery Technology Core, Massachusetts General Hospital. A different syringe was used for each virus. The microprocessor was set to deliver 400 nL of virus at a rate of 40 nL/min, and the syringe retracted 5 min post-injection. Each group consisted of 8 virus-injected mice (control group: 3 males and 5 females; eNpHR3 inhibitory opsin group: 5 males and 3 females; ChR2 excitatory opsin group: 2 males and 6 females). The control group included 4 mice in which injections of opsin containing viruses were misplaced and, thus, no retrograde labeled cells were observed in the CeA.

Cell bodies positive for EYFP were identified using sequential scanning with an Olympus confocal microscope. In alternate tissue sections (8 per animal), the

number of fluorescent positive cells in each Z stack (3um/slice) was manually calculated (Olympus FluoView software) and used for statistical analyses.

To assess the potential neural toxicity of HSV injections over the time frame of behavioral testing, we took advantage of the ipsilateral nature of projections from the CeA to the NST. Additional Sst-cre heterozygous mice received unilateral injection of HSV-EYFP into the NST as described above (n = 2). Tissue sections were subsequently stained for NeuN to quantify the number of neurons present in the NST and CeA ipsilateral and contralateral to the injection. Cell bodies positive for NeuN expression (Alexa Fluor-546) were identified using a confocal microscope and counted as described above (4 sections per animal).

3.2.4 Cannula implantation

Following virus injections, a dual fiber-optic cannula (Doric Lenses, 200um core, 0.26NA, 5.6 mm pitch) was implanted above the CeA and secured to the skull using UV cured epoxy (GrandioSO Flow, Dental Wholesale Direct). The coordinates for the CeA were 1.1 mm posterior to bregma, ± 2.8 mm lateral to midline, and 3.6 mm ventral to the brain surface. Once ambulatory, the mice were placed in their home cages and provided with soft diet (DietGel 76A) for 2-3 days post-surgery. Animals recovered for 2 weeks before behavioral testing began.

Our rationale for a between-subjects light-on design rather than a counter-balanced light-on during some trials and light-off during other trials design is as follows. First, a counter-balanced design raised the possibility that the number of trials initiated during light-on and light-off conditions would be limited and negatively impact the generation of robust and reliable concentration-response

functions necessary for the assessment of brief-access affective licking (Glendinning et al., 2002; Glendinning et al., 2005). To ensure an adequate number of trials across concentrations, we would have needed to extend the duration of the experiments that already took 5 weeks to complete from day of surgery, raising the possibility that fewer animals would complete all behavioral sessions. Second, mice can habituate to the aversiveness of quinine, raising the possibility that order effects (light on or off first) would contribute to differences between conditions (Lin et al., 2012; Mura et al., 2018). This could have been assessed by counterbalancing, but counterbalancing comes with the cost of increasing the necessary number of subjects. Thus, we decided it would be prudent to streamline the design and chose to emphasize getting robust concentration-response functions and minimize the prospect of order effects.

3.2.5 Apparatus

A commercially available 16-bottle gustometer (mouse Davis Rig, Med Associates Inc.) was used to record the licking behavior of each mouse to taste stimuli and deionized water presentations. All behavioral tests were performed during the light cycle. Taste stimuli were dissolved in deionized water and included 5 concentrations each of sucrose (0.0625, 0.125, 0.25, 0.5, and 1.0 M) and quinine hydrochloride (QHCl: 0.01, 0.03, 0.1, 0.3, and 1 mM). Once a mouse was placed in the test chamber a motorized shutter opened allowing access to a sipper tube via a small slot in the chamber wall. The gustometer automatically centered the appropriate sipper tube in the slot by moving the sipper tube carriage. Throughout the experiments, a small fan was used to pass air across the line of sipper tubes

to minimize olfactory cues. The software provided with the gustometer controlled the presentation schedule of each stimulus as well as recorded the latency to the first lick, the interlick intervals (ILI) between licks (and therefore the number of licks), stimulus identification, and session number. These data points were stored in a sequential file that was later extracted for data analyses using a custom software program written by Dr. Steven St. John. Dr. St. John was blinded to injection group identification until the completion of statistical analyses of licking behavior.

3.2.6 Procedure for water and food restriction

Water restriction was used to motivate the mice to sample from the sipper tubes during training and testing with QHCl (see below). Water bottles were removed from the home cages 23 hr before each water training and QHCl session. In this manner, fluid intake was limited to the 20- or 30-min sessions as well as for an additional 3 min of water access in the home cage immediately after each session.

During taste testing with sucrose, mice were tested under two conditions: (1) water restricted as described above and (2) food restricted with ad libitum water (see below). For food restriction, the mice were placed in new home cages with water but no food pellets to instate ~18 hr of food restriction. Immediately after each gustometer session, a 2 g food pellet was placed in the home cage for 6 hr.

Water training and taste test sessions occurred once per day during 3 blocks of 5 days (Mon-Fri). Between each block of sessions, mice were allowed ad libitum access to food and water. All mice remained at or above 85% of their baseline body weight during restricted access to water or food and regained 95-100% of

their baseline weight during the recovery days (i.e. relative to Sunday body weights prior to instatement or re instatement of water restriction). The timetable for behavioral testing is shown in Table 3.1.

3.2.7 Water training

On days 2 and 3, mice were acclimated to the gustometer and allowed free access to a single stationary sipper tube containing water. The shutter was permanently open, and the session lasted for 30 min following the first lick. During the next 3 days, each session lasted 20 min and the mice were trained with six sipper tubes of water presented semi-randomly. The shutter would open for 10 s during which time the mouse could initiate a 5 s trial by licking the spout. At the end of a trial or the 10 s in which a trial was not initiated, the shutter closed for 7.5 s while another sipper tube containing water was positioned in the slot. A mouse could initiate as many trials as possible within a session. These session parameters remained constant for subsequent taste test sessions. During the last 2 water training sessions, the mice were acclimated to licking while tethered to one of the laser light sources using a commutator and patch cables. Laser light illumination was not delivered during water training sessions.

3.2.8 Procedures for concentration-dependent licking to sucrose and QHCl

Prior to being placed in the test chamber, mice were connected to the appropriate laser light source. A computer programmable TTL pulse-train generator (Pulser, Prizmatix) was used to control laser light illumination. Two licks to water or a taste stimulus were required to trigger the pulse generator via a TTL out signal from the gustometer. A 100mW 473nm laser (LaserGlow Technologies)

was used to activate CeA/Sst neurons expressing ChR2. The parameters were 20 ms pulse duration at 20 Hz for 5 s (6.4 ± 0.8 mW/mm²). A 100mW 589nm laser (LaserGlow Technologies) was used to inhibit CeA/Sst neurons expressing eNpHR3 with 5 s constant illumination (5.6 ± 1.0 mW/mm²). Half of the mice in the control group received 473nm laser light illumination and the other half received 589nm illumination. For each animal, laser power was measured at the cannula tips following euthanasia using an optical power meter (ThorLabs, PM200).

After water training, water-restricted mice were first tested over 2 consecutive days with water and 5 concentrations of sucrose (laser triggered). For these and all subsequent sessions, the gustometer computer software was programmed to present stimuli in a semi-random order without replacement (e.g. no stimulus was presented twice in a row). Trial structure was identical to water training – the mouse had 10 s to initiate a 5 s taste trial and trials were separated by a 7.5 s intertrial interval during which the shutter was closed. Over the next 3 days, the rehydrated but hungry mice were tested with the 5 concentrations of sucrose only (laser triggered). Next, mice were again water restricted and tested with one session of water only (laser off) followed by three sessions with water and 5 concentrations of QHCl (laser triggered). In these last sessions, the water tube was presented between each QHCl trial for 2.25 s and served as a rinse to encourage initiation of subsequent QHCl trials.

3.2.9 In Vitro slice recording

Within two weeks of weaning, 1 Sst-cre heterozygous mouse received an injection of HSV- ChR2-EYFP into the NST as described above, while a second

mouse was injected with HSV- eNpHR3-EYFP. Three-week post-injection, animals were deeply anesthetized by placing them in a 500cc jar that contained a gauze pad wetted with 1cc of 20% isoflurane (v/v in propylene glycol). The brain was removed from the cranial cavity and chilled for 2 minutes in cold slicing solution containing the following (in mM): 2.5 KCl, 26 NaHCO₃, 2.5 KCl, 1.25 NaH₂PO₄, 10 MgCl₂, 2 CaCl₂, 234 sucrose, and 11 glucose. Coronal slices (275µm) were cut in room temperature slicing solution using a vibratome (Leica VT1000 S). Then slices were transferred into an incubation solution of oxygenated (95%O₂/5%CO₂) artificial cerebrospinal fluid (ACSF) containing (in mM): 126 NaCl, 26 NaHCO₃, 2.5 KCl, 1.25 NaH₂PO₄, 2 MgCl₂, 2 CaCl₂, and 10 glucose at 32°C for 30 min, and later maintained at room temperature.

Individual slices were transferred into a recording chamber, which was maintained at 32°C by an inline heater and continuously perfused with room temperature oxygenated ACSF (2.5ml/min, 95%O₂/5%CO₂). Slices were stabilized by a slice anchor or harp (Warner Instruments 64–0252). Neurons were visualized on an upright microscope (Olympus BX51WI) equipped with both differential interference contrast optics and a filter set for visualizing YFP (Chroma 49002) using a 4x or 60x water-immersion objective (Olympus) and a CCD camera. Recording electrodes were pulled from borosilicate glass capillaries (World Precision Instrument Inc.) by using a MODEL P-97 puller (Sutter Instrument Co., Novato, CA). The electrode tip resistance was 4–6 MΩ when filled with an intracellular solution containing the following (in mM): 117 K-gluconate, 13.0 KCl, 1 MgCl₂, 0.07 CaCl₂, 0.1 EGTA, 10 HEPES, 2 Na₂-ATP, and 0.4 Na₂-GTP with PH

adjusted to 7.3 with KOH and osmolarity 290–295 mOsm. Biocytin (0.5%) was added to this intracellular solution to allow subsequent identification of the recorded CeA/Sst neurons. Briefly, brain slices were fixed in 4% paraformaldehyde overnight then rinsed and incubated in Alexa-Fluor 546 streptavidin diluted (1:100) in 1% triton-x for 1 hr.

Recordings were obtained with an AxoClamp 2B amplifier (Axon Instruments, Foster City, CA) and a Digidata 1440A was used to acquire electrophysiological signals. The stimulation trigger was controlled by Clampex 10.3 software (Molecular Devices). The signals were sampled at 20 kHz and data were analyzed offline by pClamp 10.0 (Molecular Devices). Series resistance was compensated and only recordings with stable series resistance and overshooting action potentials were included in the analysis. For current clamp recordings, voltage signals were obtained from cells with resting potentials of -50mV to -65mV .

For photoactivation, light from a blue light emitting diode (Prizmatix UHP 460) or red light emitting diode (Prizmatix UHP 630) was reflected into a 60X water immersion objective. This produced a spot of light onto the submerged slice with an approximate diameter of 0.3 mm.

3.2.10 Immunohistochemistry

Following the last behavioral test session, the mice received an intraperitoneal injection of a lethal dose of Ketamine/Anased mixture (300 mg/kg [Ketamine]/30 mg/kg [Anased]) followed by thoracotomy and transcardial perfusion with 4% paraformaldehyde. Extracted brains were post fixed overnight in 4% paraformaldehyde at 4 °C. Brain blocks containing the NST and CeA were cut (60

um) using a vibrating microtome (Leica). Every other section was collected, blocked with 10% normal donkey serum (NDS) in 0.1% triton-x phosphate buffered saline (TPBS) followed by overnight incubation in 1:1,000 dilution of goat anti-GFP (Novus Biologicals) and rabbit anti-RBFOX3/NeuN (1:500, Novus Biologicals) or goat anti-GFP and rabbit anti-P2X2 (1:750, Alomone Labs) [all in TPBS plus 2% NDS]. Following rinses in TPBS (four times, 10min each), the tissue sections were incubated for 1hr in 1:100 dilutions of Alexa Fluor-488 donkey anti-goat (Fisher Scientific) or Alexa Fluor-488 donkey anti-goat and Alexa Fluor-546 donkey anti-rabbit [all in TPBS and 5% NDS]. After rinsing 3 times in phosphate buffered saline and once in phosphate buffer (10min each), the sections were mounted on microscope slides (HistoBond Adhesive Microscope Slides, VWR) and allowed to dry for 1hr. The sections were rehydrated with deionized water followed by Fluoromount-G mounting medium and coverslips.

3.2.11 Data analysis

To assess the potential toxicity of HSV injections, the number of NST and CeA neurons on each side of the brain were compared using paired *t*-tests. To assess the efficacy of retrograde transport across groups, the number of retrograde labeled CeA neurons on each side of the brain were compared using paired *t*-tests, while the total number of retrograde labeled neurons were compared using 1-way ANOVAs.

To assess the effects of laser light activation of inhibitory and excitatory opsins on licking to water and taste stimuli, a standardized lick ratio (SLR) was calculated for each stimulus by dividing the number of licks to water or a tastant by the

theoretical maximum possible licks during a 5 s trial; [Max Licks: $(1/ILI) \times 5000$] (Eylam et al., 2005). ILI was the inter-lick interval of each mouse to water (in ms) during the second day of stationary tube training (laser off). Only ILI's greater than 40ms but less than 160ms were used (Boughter et al., 2012). Since the water trials during the QHCI sessions served as a rinse and were 2.25s in duration, the SLR was calculated using $(1/ILI) \times 2250$.

The brief-access water training ILI, licks, trials, and licks per trial for EYFP control virus and misplaced opsin virus injected mice were compared using *t*-tests. ANOVAS (1-way) were used to compare Control, eNpHR3, and ChR2 group differences for trials, ILI, max lick rate, and SLR to water. Repeated-measures ANOVA (2-way) was used to compare body weights (group X weekly block) as well as taste stimulus trials and SLR's (group X concentration). All results are presented as mean \pm s.e. and a value of $p < 0.05$ was considered statistically significant.

In order to estimate differences in sensitivity to quinine or sucrose, a 2-parameter logistic function was fit to the concentration-SLR data for individual mice using the equation (St John and Boughter, 2004): $f(x) = 1 / (1 + (x/c)^b)$ where *b* represents the slope and *c* represents the inflection point (the concentration of quinine or sucrose generating an SLR of 0.5) . In particular, the inflection point (*c*) parameter is a useful index of taste sensitivity. A one-way ANOVA was used to compare group differences in the slope (*b*) and the logarithm of the inflection point (*c*) of the behavioral concentration-response function. Only mice with symmetrical

retrograde label in the CeA and placement of cannulas above the CeA were included in the analyses.

The software package RStudio was used to calculate estimates of effect size (t-tests: Hedges' g (g); ANOVA's: partial omega-squared, (ω^2_p)) and corresponding confidence intervals (effect size $g = 95\%$; effect size $\omega^2_p = 90\%$) (Lakens, 2013; Yigit and Mendes, 2018). Hedges' g is considered less biased compared to Cohen's d for smaller sample sizes and represents the difference of the means in units of the pooled standard deviation. Partial omega-squared is considered less biased compared to partial eta-squared and represents the variance in the dependent variable accounted for by a particular independent variable, with the effects of the other independent variables partialled out. The 90% CI is used for ω^2_p because a F -test is one-sided, and the 90% CI excludes 0 when the F -test is statistically significant, while the 95% CI does not (Steiger, 2004).

3.3 Results

3.3.1 Anatomy and physiology

Because the light-activated opsins and EYFP genes are preceded by DIO, a double-floxed inverse open reading frame, expression of transgene is restricted to Sst-expressing neurons. Figure 3.1A, C, and E show photomicrograph examples of HSV-EYFP, HSV-eNpHR3-EYFP, and HSV-ChR2-EYFP virus injections, respectively, into the left and right NST. Similar to our recent report, microscopic examination of NST tissue revealed that green fluorescence (cells, axons, dendrites) largely filled the rostral two-thirds of the NST (Bartonjo and Lundy, 2020).

Dense expression of neuronal EYFP was observed throughout the rostrocaudal extent of the CeA. Figure 3.1B, D, and F show photomicrograph examples of retrograde-labeled Sst neurons in the left and right CeA of the same mice as described above. Within each injection group, the per section mean of retrograde-labeled neurons in the left and right CeA were comparable (Control group: $t(6) = 0.57$, $P = 0.58$, $g = 0.35$, 95% CI = (-1.23, 2.27); eNpHR3 group: $t(14) = -0.29$, $P = 0.77$, $g = -0.15$, 95% CI = (-1.24, 0.90); ChR2 group: $t(14) = -1.24$, $P = 0.23$, $g = -0.59$, 95% CI = (-1.79, 0.41). The overall mean number of retrograde-labeled CeA/Sst neurons was similar between the different virus injection groups ($F_{2,17} = 0.56$, $P = 0.58$, $\omega^2_p = -0.05$, 90% CI = (0, 0); Figure 3.1G). Figure 3.1H, I, and J show photomicrograph examples of bilateral placement of fiber optic cannula above the CeA.

To determine the efficacy of the eNpHR3 and ChR2 opsins to influence neuronal activity, we patched CeA cells in slices prepared from Sst-cre mice in which the NST had been injected with HSV-EF1alpha-DIO-ChR2-EYFP or HSV-EF1alpha-DIO-eNpHR3-EYFP virus. Recordings made from ChR2 expressing cells revealed short-latency action potentials driven by the onset of blue light pulses (20 ms PD at 20 Hz for 5 s, Figure 3.1K). In contrast, eNpHR3 expressing cells exhibited sustained hyperpolarization during red light delivery (5s constant) that was able to inhibit action potentials induced by adding positive current (Figure 3.1L).

Potential toxicity from prolonged HSV infection was assessed by comparing the number of NeuN positive cells at the NST injection site and ipsilateral CeA to the

corresponding contralateral areas (not shown). The per section mean of NeuN positive cells in the NST on the side injected with HSV-EYFP (134.5 ± 15.6) was comparable to the number present on the contralateral non injected side (129.6 ± 17.4 ; $t(14) = 0.20$, $P = 0.83$, $g = 0.11$, $95\% \text{ CI} = (-1.19, 0.96)$). The same was observed for the per section mean of cells in the CeA (ipsilateral, 261.5 ± 37.8 ; contralateral, 272.2 ± 38.7 ; $t(14) = -0.19$, $P = 0.84$, $g = 0.10$, $95\% \text{ CI} = (-1.18, 0.96)$). The lack of toxicity in the present study is consistent with previous research using these HSV's (Carlezon et al., 1997; Neve et al., 2005).

3.3.2 Body weight and water training

First, we compared Sunday rehydrated body weights between control EYFP ($n=4$) and misplaced opsin virus ($n=4$) injected mice. A repeated measures ANOVA (2 way) revealed that body weight was associated with an increase across weeks ($F_{2,12} = 6.64$, $P = 0.01$, $\omega^2_p = 0.43$, $90\% \text{ CI} = (0.03, 0.65)$) but not between groups ($F_{1,12} = 0.83$, $P = 0.39$, $\omega^2_p = -0.02$, $90\% \text{ CI} = (0, 0)$) or an interaction ($F_{2,12} = 0.21$, $P = 0.81$, $\omega^2_p = -0.12$, $90\% \text{ CI} = (0, 0)$). Post-hoc analysis (Tukey) suggested that body weights were comparable for weeks 2 and 3 ($P = 0.84$) but greater than week 1 (P 's ≤ 0.03). Next, we compared inter-lick intervals (ILI) during the second day of stationary water training as well as several behavioral measures during brief-access water training. Laser light stimulation was not administered during any water training sessions. Separate t-tests revealed that mean ILI ($t(6) = 0.26$, $P = 0.79$, $g = 0.17$, $95\% \text{ CI} = (-1.49, 1.98)$), number of licks ($t(6) = -0.03$, $P = 0.97$, $g = -0.03$, $95\% \text{ CI} = (-1.76, 1.70)$), trials ($t(6) = 0.48$, $P = 0.64$, $g = 0.31$, $95\% \text{ CI} = (-1.31, 2.18)$), and licks per trial ($t(6) = -0.93$, $P = 0.38$, $g = -0.59$, $95\% \text{ CI} = (-$

2.63, 0.94)) were comparable between EYFP and misplaced opsin virus injected mice. Thus, these mice were combined to form the Control group for subsequent analyses.

A repeated measures ANOVA (2 way) on Sunday rehydrated body weights of Control, eNpHR3, and ChR2 mice indicated comparable body mass between groups ($F_{2,21} = 2.1$, $P = 0.14$, $\omega^2_p = 0.09$, 90% CI = (0, 0.27)) and across weeks ($F_{2,42} = 1.71$, $P = 0.19$, $\omega^2_p = 0.03$, 90% CI = (0, 0.13); Figure 3.2). Body weights also were not associated with a Group x Week interaction ($F_{4,42} = 1.05$, $P = 0.39$, $\omega^2_p = 0$, 90% CI = (0, 0)). Similarly, one-way ANOVAs revealed that the mean ILI ($F_{2,21} = 0.93$, $P = 0.4$, $\omega^2_p = 0$, 90% CI = (0, 0)) and Max Licks ($F_{2,21} = 0.86$, $P = 0.43$, $\omega^2_p = -0.01$, 90% CI = (0, 0)) during the second stationary water day were comparable (Figure 3.3A). For brief-access water training, additional one-way ANOVA's indicated that group membership (i.e. Control, eNpHR3, and ChR2) was not associated with changes in the mean number of trials ($F_{2,21} = 0.4$, $P = 0.67$, $\omega^2_p = -0.05$, 90% CI = (0, 0)) or standardized lick ratio for water ($F_{2,21} = 0.07$, $P = 0.93$, $\omega^2_p = -0.08$, 90% CI = (0, 0); Figure 3.3B). These results indicate that the behavioral performance of the three groups licking to water, in the absence of laser light stimulation, were equivalent.

3.3.3 Sucrose water restricted

While water-restricted, all mice were highly motivated to sample from the sipper tube irrespective of whether the tube contained water or one of the 5 concentrations of sucrose. Two-way repeated-measures ANOVAs were used to compare the effects of concentration and optogenetic manipulation on licking to

sucrose. Sucrose concentration was not associated with changes in the number of trials ($F_{4,84} = 1.62$, $P = 0.17$, $\omega^2_p = 0.03$, 90% CI = (0, 0.06); Figure 3.4A) or standardized lick ratio ($F_{4,84} = 0.20$, $P = 0.93$, $\omega^2_p = -0.04$, 90% CI = (0, 0); Figure 3.4B). While group membership was not associated with changes in the number of trials (Group: $F_{2,21} = 0.31$, $P = 0.73$, $\omega^2_p = -0.06$, 90% CI = (0, 0); Interaction: $F_{8,84} = 1.21$, $P = 0.30$, $\omega^2_p = 0.02$, 90% CI = (0, 0)), examination of Figure 3.4B suggests that group membership (i.e. eNpHR3 and ChR2) might be associated with a reduction in standardized lick ratio (Group: $F_{2,21} = 3.15$, $P = 0.06$, $\omega^2_p = 0.15$, 90% CI = (0, 0.36); Interaction: $F_{8,84} = 1.52$, $P = 0.16$, $\omega^2_p = 0.04$, 90% CI = (0, 0.03)). Although the $P = 0.06$ was close to our set level of $P < 0.05$, estimates of effect size and CI weaken the argument for an effect on behavioral sensitivity to sucrose.

In terms of water licking, one-way ANOVA's revealed that group membership was associated with an increase in trials ($F_{2,21} = 3.49$, $P = 0.04$, $\omega^2_p = 0.17$, 90% CI = (0, 0.38); Figure 3.4A), but not standardized lick ratio ($F_{2,21} = 1.03$, $P = 0.37$, $\omega^2_p = 0$, 90% CI = (0, 0); Figure 3.4B). Post-hoc analysis (Tukey) showed that the eNpHR3 inhibitory group took more water trials compared to the Control group ($P = 0.04$). Although the $P = 0.04$ was below our set level of $P < 0.05$, estimates of effect size and CI weaken the argument for an effect on water trials.

3.3.4 Sucrose water replete

When the same mice were hydrated but hungry, an increase in sucrose concentration was associated with an increase in the number of sucrose trials ($F_{4,84} = 6.29$, $P < 0.01$, $\omega^2_p = 0.19$, 90% CI = (0.06, 0.29); Figure 3.5A) and standardized lick ratio ($F_{4,84} = 173.2$, $P < 0.01$, $\omega^2_p = 0.89$, 90% CI = (0.85, 0.91); Figure 3.5B).

Group membership was not associated with changes in the number of trials ($F_{2,21} = 0.82$, $P = 0.45$, $\omega^2_p = -0.01$, 90% CI = (0, 0)) or standardized lick ratio ($F_{2,21} = 1.47$, $P = 0.25$, $\omega^2_p = 0.04$, 90% CI = (0, 0.08)). Again, the Group x Concentration interaction was not associated with changes in these behavioral measures (trials: $F_{8,84} = 0.74$, $P = 0.65$, $\omega^2_p = -0.02$, 90% CI = (0, 0); SLR: $F_{8,84} = 2.04$, $P = 0.05$, $\omega^2_p = 0.08$, 90% CI = (0, 0.11)). Overall, these results suggest that manipulating the activity of CeA/Sst-to-NST neurons had little impact on brief-access licking to sucrose by water restricted or water replete mice.

Nevertheless, there was some evidence for an effect of optogenetic activation and inhibition from the analysis of the logistic regressions for water-replete mice (Table 3.2). One mouse in the activation group was eliminated from this analysis due to a linear concentration-response function that was poorly modeled by a logistic function ($r^2 = 0.23$). While the slope of the concentration-response functions did not vary by group ($F_{2,20} = 0.78$, $P = 0.47$, $\omega^2_p = -0.02$, 90% CI = (0, 0)), group membership was associated with altered inflection point ($F_{2,20} = 4.00$, $P = 0.03$, $\omega^2_p = 0.21$, 90% CI = (0, 0.42)). Post-hoc tests (Tukey) indicated that the experimental groups differed from one another ($P = 0.02$) but not from the control group (P 's ≥ 0.20). The magnitude of the difference was relatively small, with inhibition of the CeA/Sst-to-NST pathway resulting in greater sensitivity to sucrose ($c = 0.204$ M) than activation ($c = 0.318$ M), a difference of a fifth of a log unit. Again, however, the estimates of effect size and CI weaken the argument for an effect on behavioral sensitivity to sucrose.

3.3.5 QHCl water restricted.

When thirsty mice were tested with quinine, an increase in concentration was associated with a decrease in the number of trials ($F_{4,84} = 19.21$, $P < 0.01$, $\omega^2_p = 0.45$, 90% CI = (0.31, 0.55); Figure 3.6A) and standardized lick ratio ($F_{4,84} = 147.77$, $P < 0.01$, $\omega^2_p = 0.87$, 90% CI = (0.83, 0.90); Figure 3.6B). Optogenetic activation or inhibition of CeA/Sst-to-NST neurons was not associated with changes in the number of trials ($F_{2,21} = 0.74$, $P = 0.49$, $\omega^2_p = -0.02$, 90% CI = (0, 0)), but was associated with changes in standardized lick ratio ($F_{2,21} = 12.55$, $P < 0.01$; $\omega^2_p = 0.49$, 90% CI = (0.20, 0.66)). Moreover, the changes in standardized lick ratio were associated with group membership and QHCl concentration ($F_{8,84} = 2.79$, $P < 0.01$, $\omega^2_p = 0.13$, 90% CI = (0, 0.19)). Post-hoc tests (Tukey) revealed that the eNpHR3 inhibitory group licked more to the 3 highest QHCl concentrations compared to the Control and ChR2 activation groups (P 's ≤ 0.04). When the estimates of effect size and CI are considered, the argument for an interaction is weakened and, thus, the increase in standardized lick ratio associated with the inhibitory eNpHR3 opsin might involve even lower concentrations of QHCl.

In terms of water licking, one-way ANOVA's indicated that manipulating CeA/Sst-to-NST neural activity was not associated with changes in the number of trials ($F_{2,21} = 0.11$, $P = 0.89$, $\omega^2_p = -0.08$, 90% CI = (0, 0); Figure 3.6A) or standardized lick ratio ($F_{2,21} = 2.55$, $P = 0.1$, $\omega^2_p = 0.11$, 90% CI = (0, 0.31); Figure 3.6B). Thus, manipulating the neural activity the CeA/Sst-to-NST neurons was associated with changes in brief-access licking to quinine but not to water.

The association between inhibition of CeA/Sst-to-NST neurons and increased licking to QHCl was further strengthened when individual data were fit with logistic regression functions (Figure 3.7A-C and Table 3.2). While the slope of the concentration-response functions did not vary by group ($F_{2,21} = 1.07$, $P = 0.36$, $\omega^2_p = -0.01$, 90% CI = (0, 0.02); Figure 3.7D), group membership was associated with altered inflection point ($F_{2,21} = 15.22$, $P < 0.0001$, $\omega^2_p = 0.54$, 90% CI = (0.26, 0.70); Figure 3.7E). Post-hoc tests (Tukey) indicated that the experimental groups differed from one another ($P < 0.01$) and that the inhibition group differed from the control group ($P < 0.0001$). The magnitude of shift in quinine sensitivity was considerable with the inhibition group tolerating higher concentrations of quinine ($c = 0.781$ mM) than the other groups ($c = 0.151$ mM for controls and 0.221 mM for the activation group), a difference of 0.5 to 0.75 of a log unit. Further evidence of the disruptive effect of laser inhibition of CeA/Sst-to-NST neurons were the flatter slopes of the concentration response functions of 2 mice (1819 and 2043, see Figure 3.7B). Although these mice might be particularly impressive examples of the effectiveness of the laser manipulation, the goodness-of-fit of the logistic functions were poor ($r^2 = 0.423$ and 0.622 respectively). If these mice are conservatively removed from the analysis, the magnitude of the differences decreases (see Table 3.2) but the change in inflection point associated with group membership remains robust ($F_{2,19} = 10.00$, $P < 0.001$, $\omega^2_p = 0.45$, 90% CI = (0.14, 0.63)) as does the difference between the inhibition group and the other 2 groups (Tukey p-values < 0.02).

In summary, the present analyses indicate that inhibiting the neural activity of CeA/Sst-to-NST neurons altered behavioral sensitivity to QHCl but not to sucrose or water. A caveat to this interpretation is the p-value of 0.06 for sucrose standardized lick ratio under the water-restricted condition and the p-value of 0.04 for sucrose inflection point under the water-replete condition. Despite these values being near our set value of $P < 0.05$, the associated estimates of effect size and corresponding CI's weaken a statistical argument for an effect on behavioral sensitivity to sucrose. For instance, the Group effect size for standardized lick ratio to QHCl ($\omega^2_p = 0.49$, 90% CI = (0.20, 0.66)) was over 2x larger compared to that for sucrose ($\omega^2_p = 0.21$, 90% CI = (0, 0.42)), while the Group effect size for QHCl inflection point ($\omega^2_p = 0.54$, 90% CI = (0.26, 0.70)) was over 3x larger compared to that for sucrose ($\omega^2_p = 0.15$, 90% CI = (0, 0.36)). That is, 49% and 54% of variation in QHCl SLR and inflection point, respectively, was attributable to Group membership (i.e., no opsin, inhibitory opsin, excitatory opsin). When sucrose was the stimulus, a considerably smaller proportion of variance in sucrose SLR (21%) and inflection point (15%) was accounted for by Group membership. Together with the 90% CI's for sucrose being compatible with no difference (i.e. value of 0), we do not have sufficient statistical evidence to conclude that the experimental treatments were associated with a specific change in sucrose sensitivity.

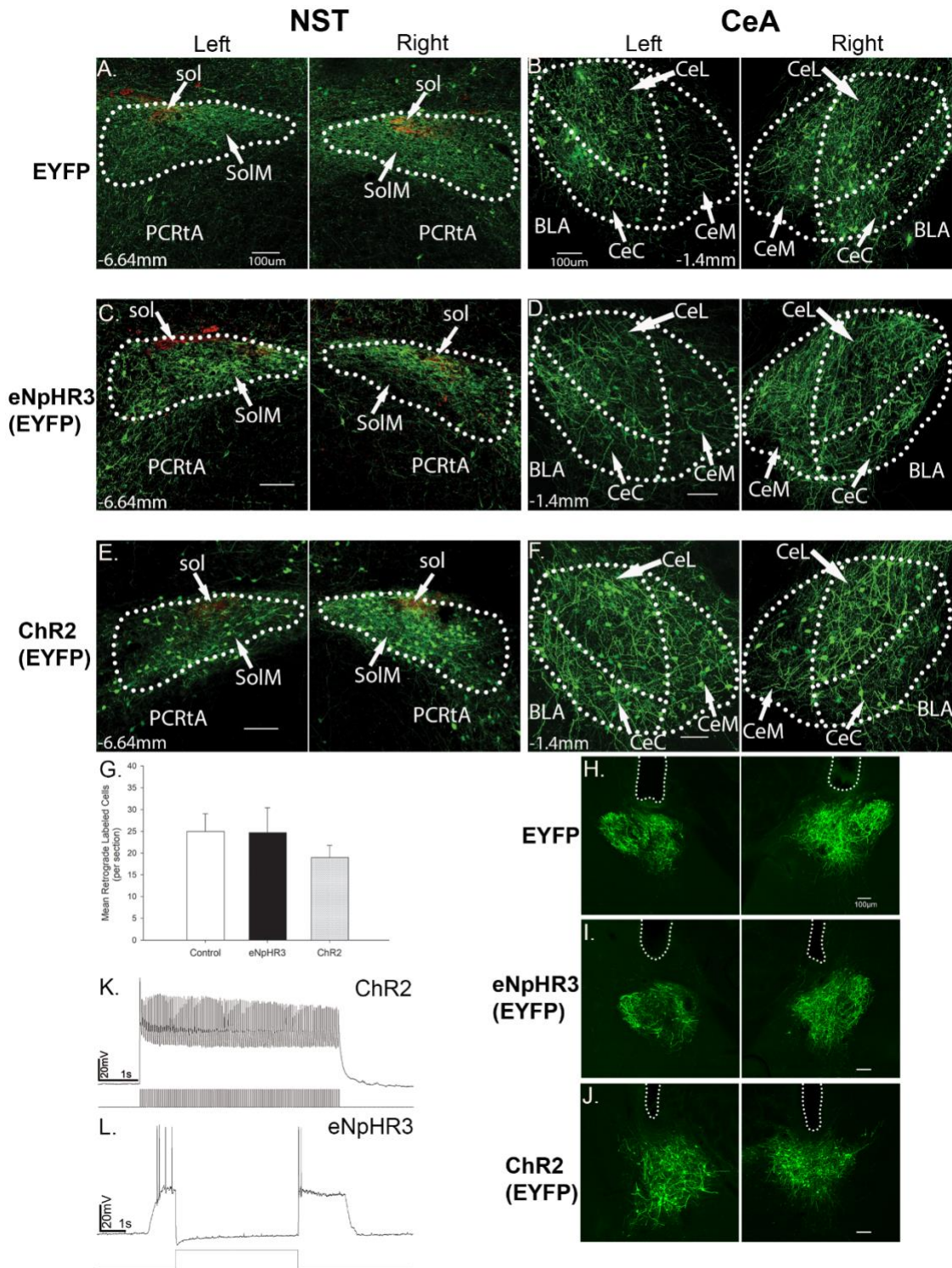


Figure 3.1: Representative fluorescent images of NST injection sites, retrograde labelled cells in CeA and cannula placement above CeA.

Representative fluorescent images resulting from the injection of HSV-Ef1 α -DIO-EYFP (**A**, green), HSV-EF1 α -DIO-eNpHR3-EYFP (**C**, green), and HSV-EF1 α -DIO-hChR2(H134R)-EYFP (**E**, green) into the Left and Right NST of Sst-cre mice. White dots outline the approximate boundaries of the NST. Within the NST, green fluorescence indicates Sst-expressing neurons that project locally within the NST. The red fluorescence indicates P2X2 axons of the nucleus of the solitary tract (sol) that mark gustatory responsive regions of the NST (Breza and Travers, 2016). Representative fluorescent images of retrograde-labeled CeA/Sst neurons resulting from each NST injection are shown in **B**, **D**, and **F**. White dots outline the approximate boundaries of CeC, CeL, and CeM divisions of the CeA. The approximate level relative to bregma is shown at the bottom of the Left NST and Left CeA photomicrographs. The white scale bar in the Left NST and Left CeA images equals 100 μ m. Magnification was 10x (0.85 pixels/micron). **G**, the per section average of retrograde-labeled Sst neurons in the CeA following injections of EYFP (**Control**, open bar), eNpHR3-EYFP (**eNpHR3**, solid bar), and ChR2-EYFP (**ChR2**, stippled bar) into the NST of Sst-cre mice. **H-J**. Representative fluorescent images of bilateral fiber optic cannula placement above the CeA in EYFP, eNpHR3-EYFP, and ChR2-EYFP injected mice. White dots outline the approximate boundaries of the cannula tracts. **K**, Neural excitation of a retrograde-labeled CeA/Sst neuron expressing ChR2 in response to blue-light pulses (1.33mW, 60x lens) of 20ms duration at 20Hz for 5s (upward deflections in the bottom trace). Short-latency action potentials were faithfully driven by the onset of each blue light pulse. **L**, Neural inhibition of a retrograde-labeled CeA/Sst neuron expressing eNpHR3 in response to red-light pulses (0.33mW, 60x lens) of 5s duration (upward deflection in the bottom trace). Neural hyperpolarization inhibited action potentials induced by adding positive current. Abbreviations: BLA, basolateral amygdaloid nucleus, anterior part; CeC, central amygdaloid nucleus, capsular part; CeL, central amygdaloid nucleus, lateral division; CeM, central amygdaloid nucleus, medial division; PCRtA, parvicellular reticular nucleus, alpha part; SolM, nucleus of the solitary tract, medial part.

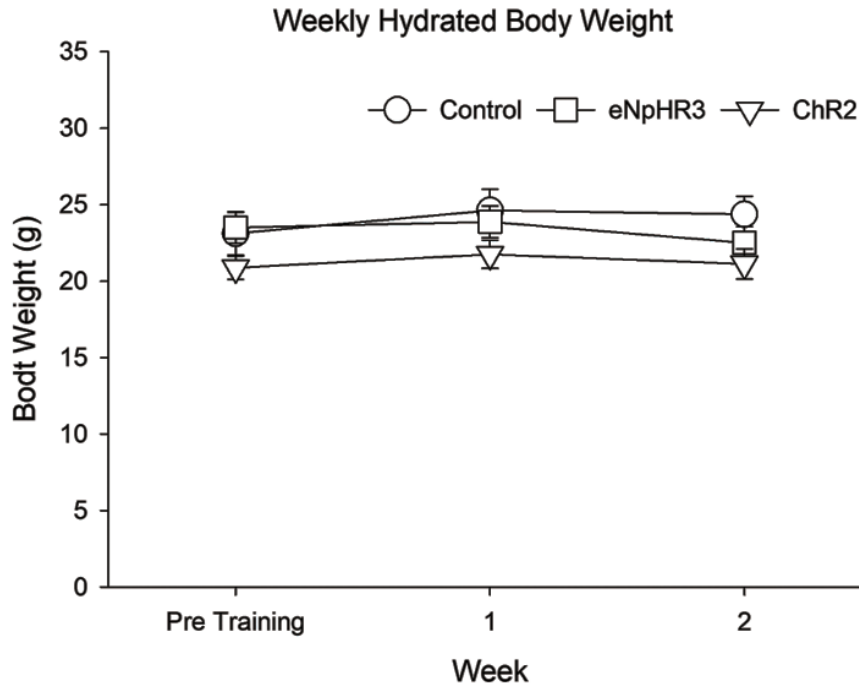


Figure 3.2: Weekly hydrated body weights

Mean weekly hydrated body weight (\pm S.E.) of Control (open circles), eNpHR3 (open squares), and ChR2 (open triangles) HSV injected mice across behavioral testing weeks. Pre training refers to the Sunday morning prior to instatement of water restriction and water training. Week 1 and 2, respectively, refer to Sunday morning body weight prior to reinstatement of water restriction for sucrose and QHCl test sessions. Food was available ad libitum throughout the test sessions except during the last three sucrose sessions during week 1. During these sessions water was available ad libitum (see Methods for details).

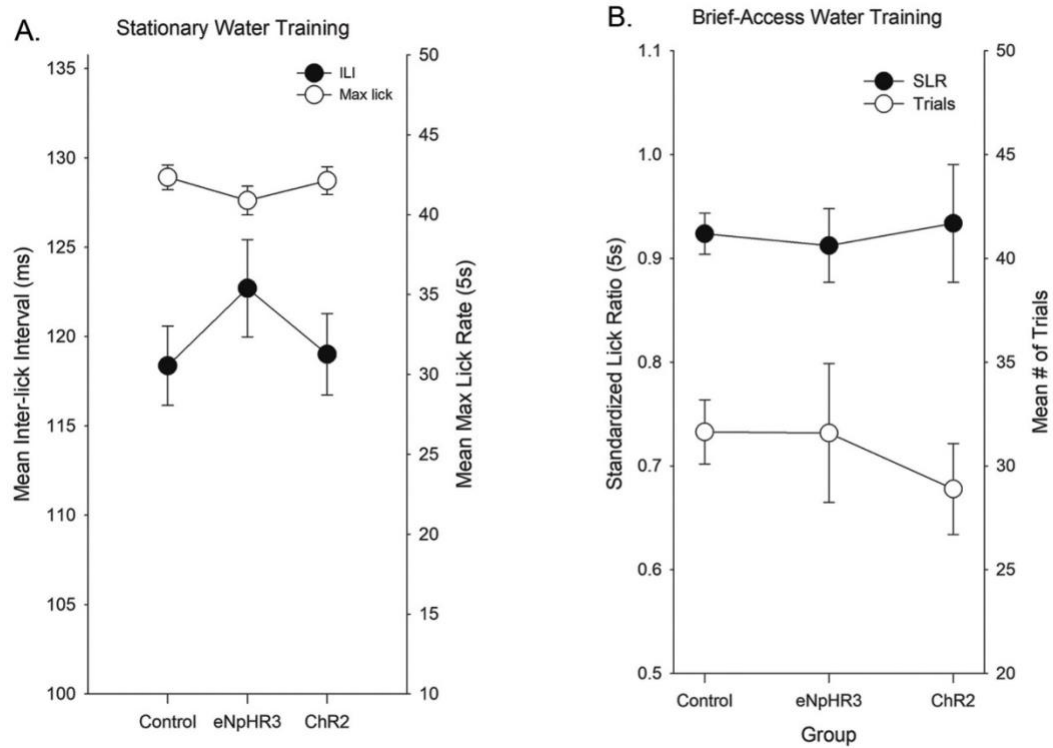


Figure 3.3: Lick performance during water training.

A) Mean inter-lick interval (filled circles) and max lick rate (open circles) (\pm S.E.) of Control, eNpHR3, and ChR2 HSV injected mice during the second day of stationary water training. B) Mean standardized lick ratio (SLR, filled circles) and water trials (open circles) (\pm S.E.) of Control, eNpHR3, and ChR2 HSV injected mice during brief-access water training. A statistically significant difference between groups was not observed for any of these behavioral measures.

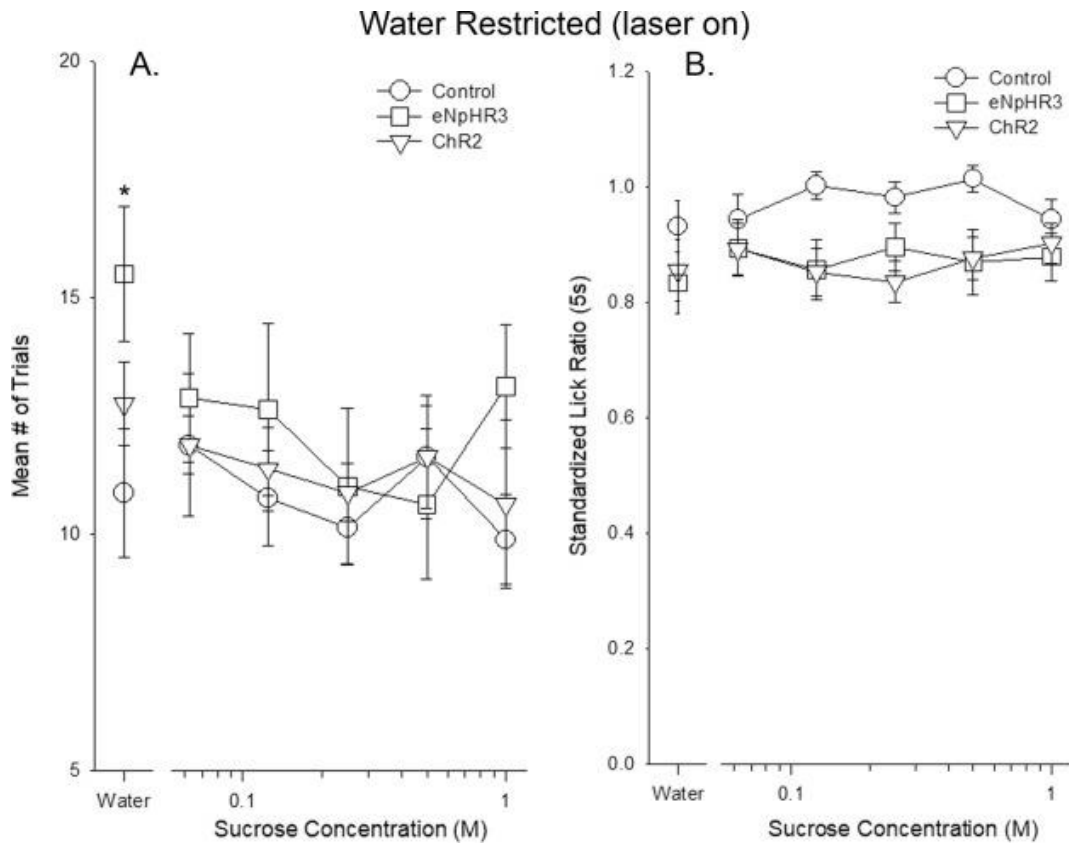


Figure 3.4: Behavioral responses to water and sucrose under water restricted conditions.

The number of trials (A) and standardized lick ratio (B) of the Control (open circles), eNpHR3 (open squares), and ChR2 (open triangles) HSV injected mice for water and the five concentrations of sucrose when water restricted. For sucrose, a statistically significant difference between groups or concentration was not observed for either of these behavioral measures. For water, the inhibitory eNpHR3 group initiated significantly more trials than the Control group, * = $P = 0.04$.

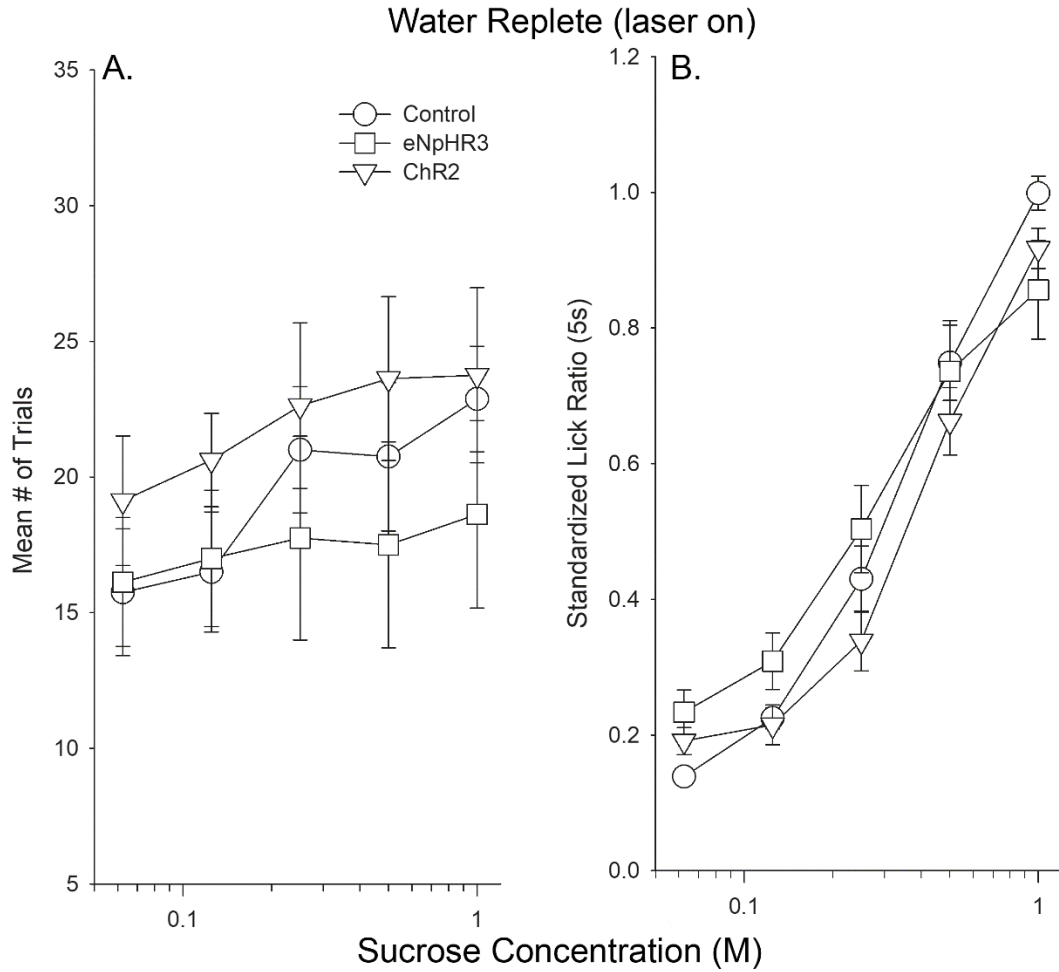


Figure 3.5: Behavioral responses to sucrose under hydrated conditions.

The number of trials (A) and standardized lick ratio (B) of the Control (open circles), eNpHR3 (open squares), and ChR2 (open triangles) HSV injected mice for the five concentrations of sucrose when water replete. Both the number of trials and the standardized lick ratio increased with increasing sucrose concentration. A statistically significant difference between groups was not observed for either of these behavioral measures.

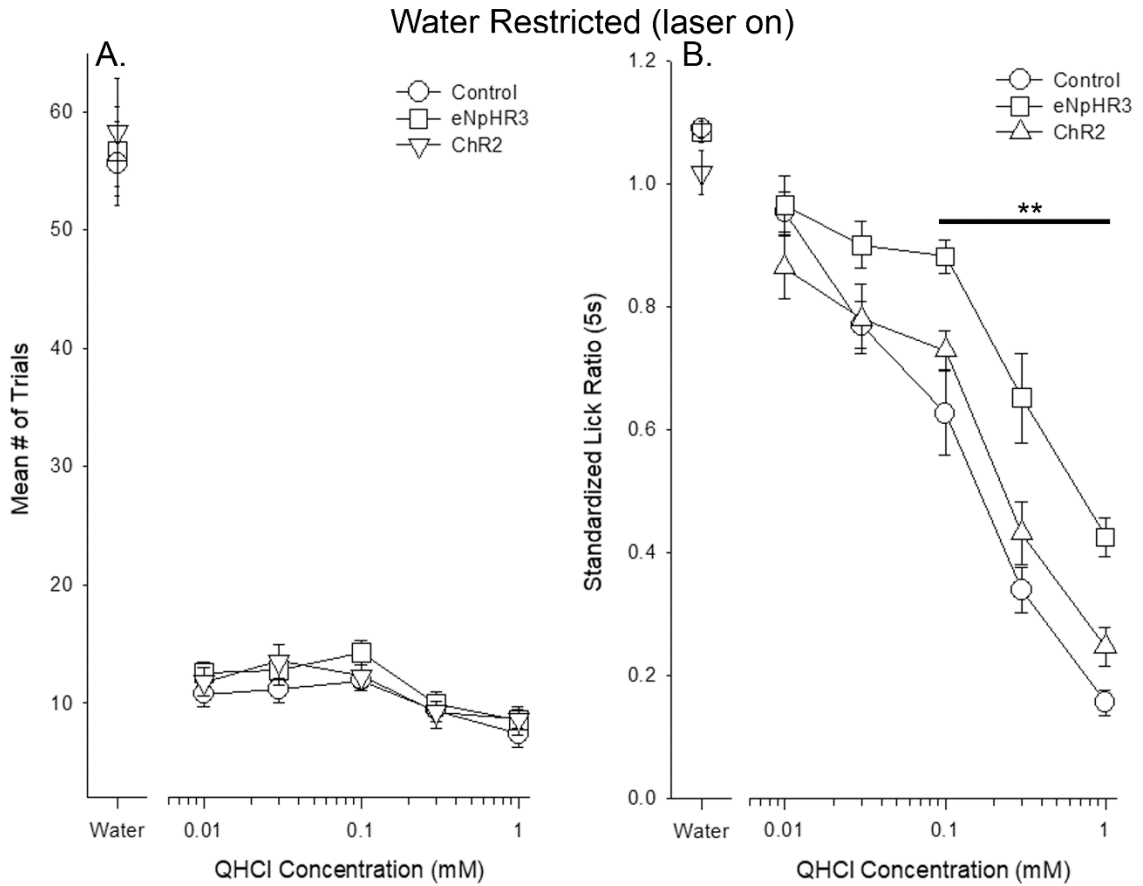


Figure 3.6: Behavioral responses to water and QHCl under water restricted conditions.

The number of trials (A) and standardized lick ratio (B) of the Control (open circles), eNpHR3 (open squares), and ChR2 (open triangles) HSV injected mice for water and the five concentrations of QHCl when water restricted. Both the number of trials and the standardized lick ratio decreased with increasing QHCl concentration. For the three highest QHCl concentrations, the eNpHR3 inhibitory group showed a significantly higher standardized lick ratio compared to the Control and ChR2 activation groups. ** = P's ≤ 0.04.

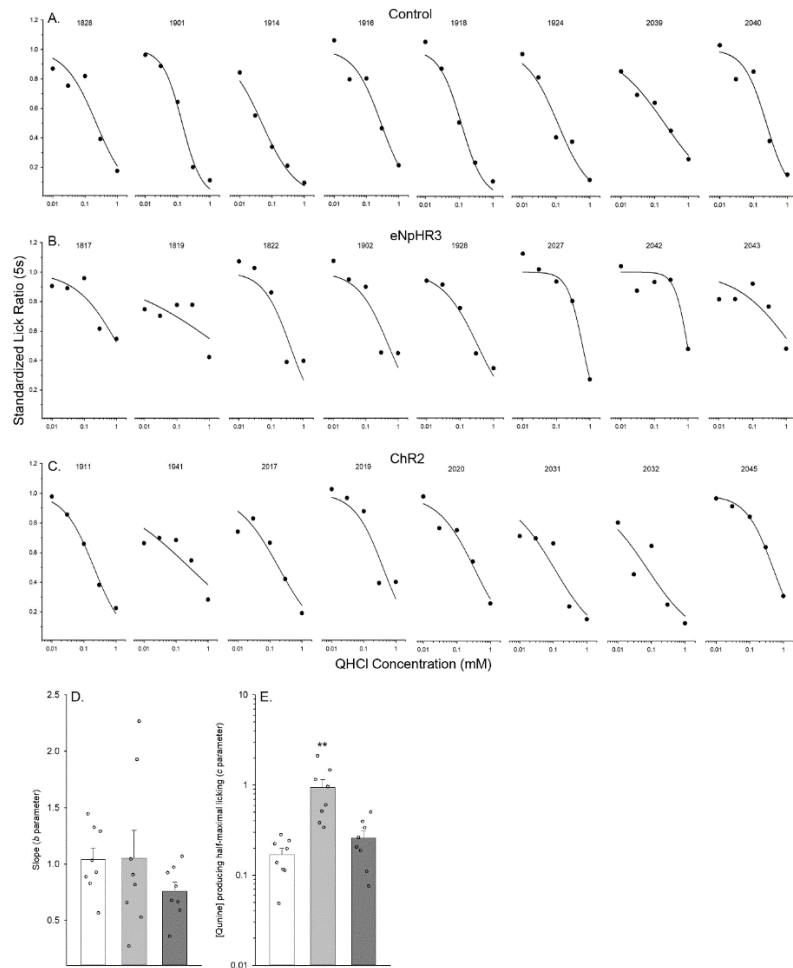


Figure 3.7: Individual mouse performance during QHCI trials

Quinine concentration-response functions for individual control (A), eNpHR3 (B), and ChR2 (C) mice; behavioral responses were quantified as the SLR (standardized lick ratio; see text). Group means for these functions are shown in Figure 3.6. Individual concentration-response functions were fit with a 2-parameter logistic function (see text for details and Table 3.2) which fit data for most mice very well, though some mice had flatter behavioral response functions (e.g., eNpHR3 mouse 1819 and 2043) resulting in lower goodness-of-fit scores but likely indicating a particularly strong effect of the laser inhibition of neural activity. Even discounting these outlier mice, eNpHR3 mice had right-shifted functions relative to control and ChR2 mice, suggesting decreased sensitivity to the aversiveness of quinine. The mean slope (D) and inflection point (E) of Control (open bars), eNpHR3 (light grey bars), and ChR2 (dark grey bars) mice. **, eNpHR3 group differed from Control and ChR2 groups (P 's ≤ 0.01).

Table 3.1: Summary of behavioral procedures

Week	Sessions	Solution	Procedure	Water and Food	Laser
1	2	Water	Stationary	Water restricted, food ad libitum	Off
	3		Brief access	Water restricted, food ad libitum	Off
			Recovery	Water and food ad libitum	
2	2	Sucrose	Brief access	Water restricted	Triggered
	3		Brief access	Food restricted, water ad libitum	Triggered
			Recovery	Water and food ad libitum	
3	1	Water	Brief access	Water restricted, food ad libitum	Off
	3	QHCl	Brief access	Water restricted, food ad libitum	Triggered

Table 3.2: Average nonlinear regression parameters for quinine (water restricted) and sucrose (water replete) lick-concentration functions.

Stimulus	Group	<i>n</i>	<i>r</i> ²	Slope (<i>M</i> ± <i>SE</i>)	Inflection (<i>M</i> ± <i>SE</i>) ^a
Quinine	Control	8	0.95 (0.01)	1.04 (0.10)	0.151 mM (0.09)
	eNpHR3	6 ^b	0.88 (0.03)	1.27 (0.27)	0.596 mM (0.09) ^d
	ChR2	8	0.88 (0.04)	0.76 (0.08)	0.221 mM (0.10) ^d
Sucrose	Control	8	0.93 (0.02)	-2.09 (0.37)	0.269 M (0.02)
	eNpHR3	7 ^c	0.92 (0.01)	-1.55 (0.20)	0.204 M (0.07) ^e
	ChR2	8	0.93 (0.01)	-1.77 (0.30)	0.318 M (0.05) ^e

Note. Individual behavior (quantified by the standardized lick ratio)-concentration functions were fit with a 2-parameter logistic function (see text for details). The logistic function provided good fits in the majority of cases; individual cases with goodness-of-fit (*r*²) values less than 0.7 were considered poor.

^a Averages for inflection point is a geometric mean and represents the interpolated quinine or sucrose concentration producing a standardized lick ratio of 0.5.

^b To be conservative, 2 mice with goodness-of-fit values less than 0.7 were removed from the table. If included, goodness-of-fit is 0.79 (0.07), slope is 1.05 (0.24), and inflection point is 0.781 mM (0.10).

^c Due to a linear concentration-response function, the data for one mouse was not well-described by a sigmoidal function (*r*² = 0.23) and was thus removed from the table.

^d An analysis of variance indicated a significant main effect of Group on the inflection point (log-transformed data); these groups differed from Controls in a post-hoc Tukey test (*p*-values < 0.0132).

^e An analysis of variance indicated a significant main effect of Group on the inflection point (log-transformed data); these groups differed from one another in a post-hoc Tukey test (*p* = 0.028) but not from Controls.

3.4 Discussion

The nucleus of solitary tract is the first central synapse for the ascending gustatory system and is critical for appropriate behavioral responses to changes in the intensity of a gustatory stimulus. Specifically, bilateral damage to the gustatory region of the NST renders animals unresponsive to changes in the concentration of a range of stimuli including sucrose, NaCl, MgCl₂, NH₄Cl, citric acid, and QHCl (Flynn et al., 1991c; Shimura et al., 1997d). It is well established that neural processing of gustatory information in the NST is not static but subject to modulation by many factors (Chang and Scott, 1984b; Davis and Smith, 1997; Giza et al., 1992; Nakamura and Norgren, 1995). In particular, several forebrain areas including the CeA send axonal projections to the gustatory NST that can influence the neural processing of taste information (Cho et al., 2003b; Dilorenzo and Monroe, 1995; Kang and Lundy, 2009a; Kang and Lundy, 2010b; Li et al., 2002b; Smith and Li, 2000). A fundamental question is how centrifugal pathways might regulate taste-guided behaviors subserved by neural processing within the NST.

The present study addressed this question by investigating the contribution of a specific descending pathway from the CeA to the NST on behavioral responsiveness to changes in the intensity of gustatory stimuli. Using somatostatin-cre transgenic mice (Sst) combined with retrograde transported herpes simplex virus, we optogenetically controlled the neural activity of CeA/Sst neurons that project to the NST (CeA/Sst-to-NST pathway) during brief-access licking to several concentrations of normally preferred sucrose and normally

avoided QHCl solutions. Our results showed that licking to sucrose was largely unaffected by either optogenetic activation or inhibition of neural activity in the CeA/Sst-to-NST pathway. In contrast, licking to high concentrations of QHCl was substantially increased by optogenetic inhibition of this descending pathway suggesting increased acceptance of a normally aversive gustatory stimulus. The inability of ChR2 activation of this pathway to alter licking to QHCl is not entirely clear. One possibility is that higher blue light power was needed to penetrate tissue in mice expressing ChR2 compared to eNpHR3. However, light power during behavioral testing far exceeded that required to activate CeA/Sst neurons in our in vitro experiments (see Experimental Procedure). Alternatively, a floor effect at higher concentrations of QHCl is possible but does not seem likely for lower concentrations where licking was comparable to water. In the present experiments, the mice were highly motivated to drink and, thus, it also is possible that ChR2 activation of CeA/Sst-to-NST neurons might alter licking under conditions of low motivation to drink. Despite this caveat, the present experiments revealed that the ability of animals to respond appropriately to changes in the intensity of an aversive taste stimulus can be fine-tuned by descending input to the NST originating from a subset of molecularly defined CeA neurons.

Given that the taste stimuli in the present study differ in terms of palatability and caloric value, an alternative interpretation is that CeA/Sst-to-NST neurons participate in appropriate responding to taste stimuli with no caloric value irrespective of their palatability (e.g., aversive versus appetitive). Two lines of evidence argue against this explanation, however. First, brief-access licking (5s)

measures immediate licking to small stimulus volumes, which minimizes the contribution of post-ingestive factors. Second, optogenetic manipulation of CeA/Sst-to-NST neurons was without effect on licking to water in either the sucrose or QHCl sessions. Although it can be argued that water is more of a tactile stimulus rather than a taste stimulus, neural responses to water have been recorded at each node of the ascending gustatory system (Chen et al., 2021; Rosen et al., 2010; Verhagen et al., 2003; Zocchi et al., 2017), it was certainly an appetitive stimulus to the mice in our experiments, and is non caloric.

To the best of our knowledge only two prior studies have assessed the role of CeA/Sst neurons on drinking behavior. In one study, optogenetic activation of CeA/Sst neurons was shown to suppress licking to water that was rapidly reversed upon cessation of laser light (Yu et al., 2016a). In contrast, the other study showed that optogenetic inhibition of CeA/Sst neurons decreased time spent drinking water during a 5-minute test (Kim et al., 2017). Our present results are inconsistent with both studies because we did not observe any effect on licking to water; rather altered licking behavior was specific for QHCl. These inconsistencies are not easily explained but might be due to procedural differences among studies as well as the fact that our experiments targeted a defined projection of CeA/Sst neurons, the NST, rather than simply targeting a specific neuron type.

Within the NST, a recent study has begun to define neuron types that control responsiveness to the artificial sweetener Acesulfame Potassium (AceK) and QHCl (Jin et al., 2021). The authors show that NST cells responding to AceK express calbindin-2, while those responding to QHCl express Sst. Moreover,

optogenetic inhibition of CeA axon terminals in the NST increased licking to an AceK/QHCl mixture (e.g. increased acceptance) with little or no effect on licking to either stimulus alone. Interestingly, under the same testing procedures, pharmacological inhibition of CeA neurons also suppressed aversion to the mixture as well as QHCl alone. Although the molecular identity of the CeA neurons targeted in the above study are unknown, we recently showed that Sst-expressing neurons comprise approximately 25% of the CeA cell population projecting to the gustatory region of NST (Chapter 2) (Bartonjo and Lundy, 2020). Together, these findings suggest a functional relationship between appropriate responsiveness to QHCl and Sst-expressing neurons in the CeA and NST.

Although the present study targeted a specific cell type with a known projection, it is possible that these CeA/Sst-to-NST neurons also project to other forebrain regions that, in turn, send axons terminals to the NST. For example, prior studies have demonstrated that the CeA is reciprocally connected with the lateral hypothalamus (LH) and bed nucleus of the stria terminalis (BNST) (Giardino et al., 2018; Oler et al., 2017; Ono et al., 1985a; Ottersen, 1980b; Ye and Veinante, 2019). Similar to the CeA, the LH and BNST send axonal projections to the gustatory region of NST (Kang and Lundy, 2009a; van der et al., 1984) and can modulate neural processing of taste information (Cho et al., 2002c; Kang and Lundy, 2010b; Smith et al., 2005). Thus, it cannot be concluded with certainty that the observed increase in acceptance of QHCl resulted solely from inhibiting CeA/Sst neurons with direct projections to the NST. In Chapter 4, the extent to which CeA/Sst-to-NST projecting neurons have divergent input to the LH and

BNST is assessed. Finally, it is possible that independent perturbation of other pathways that innervate the NST might also influence QHCl and/or sucrose sensitivity. The present study shows that one such pathway involves CeA/Sst neurons and provides a framework for future studies to investigate the functional significance of other neural inputs such as LH-to-NST and BNST-to-NST pathways.

Another possibility is that increased acceptance of QHCl observed in the present study resulted from disrupting neural activity of CeA neurons that project to the reticular formation (RF). The medullary RF is located directly ventral to the NST, receives descending input from the CeA (Zhang et al., 2011), and contains neurons that directly influence nuclei controlling muscles for licking and mastication (Travers et al., 1997; Travers and Norgren, 1983). Indeed, inhibition of RF neurons by infusion of the GABA_A receptor agonist muscimol into the RF eliminated ingestion and rejection oromotor responses elicited by sucrose and QHCl, respectively (Chen et al., 2001). In contrast, disinhibition of RF neurons by infusion of the GABA_A receptor antagonist bicuculline into the same area enhanced rejection oromotor responses to sucrose and QHCl (Chen and Travers, 2003). Several lines of evidence argue against this interpretation, however. The HSV injections in the present study were largely confined to the rostral two-thirds of the NST with minimal spread ventrally into the RF. Additionally, CeA/Sst neurons co express GABA (Lundy, 2020b; Saha et al., 2002) and optogenetic silencing these neurons would presumably result in disinhibition of RF neurons. Unlike disinhibition produced by bicuculline infused into the RF, we observed increased acceptance

of QHCl in the absence of an appreciable effect on sucrose licking. Conversely, optogenetic activation of CeA/Sst neurons would presumably result in inhibition of RF neurons. Again, unlike muscimol induced inhibition of RF, we did not observe appreciable changes in licking to either sucrose or QHCl.

In summary, the anatomical and neurophysiological association between the gustatory NST and CeA has been clear for decades, although the nature of the association in terms of taste-guided behavior has remained ambiguous. Much of this uncertainty is because the neurochemical mediators of descending CeA modulation are unknown. To this end, the results reported in Chapter 2 identified CeA/Sst-expressing neurons as a candidate substrate (Bartoinjo and Lundy, 2020). The present behavioral results add to our knowledge of this CeA/Sst-to-NST pathway by demonstrating a role in taste-guided intake. Silencing this subpopulation of CeA neurons disrupts normal affective responding to an exemplary aversive taste stimulus but not responsiveness to a normally preferred stimulus. Interestingly, taste stimulus specificity is not unique to manipulation of the CeA/Sst-to-NST pathway because a recent study has shown that manipulating the activity of CeA/neurotensin neurons that project to the parabrachial nucleus increases intake of sucrose and saccharin but not QHCl (Torruella-Suarez et al., 2020). Given the stimulus specific effect of manipulating descending pathways, future research is needed to determine the molecular identity of other CeA-to-NST and CeA-to-PBN populations as well as their role in taste-guided behaviors.

CHAPTER 4

TARGET SPECIFIC PROJECTIONS OF AMYGDALA SOMATOSTATIN- EXPRESSING NEURONS TO THE HYPOTHALAMUS AND BRAINSTEM.

4.1 Introduction

The nucleus of the solitary tract (NST) is the first central synapse of gustatory afferents originating from branches of the facial and glossopharyngeal nerves (Corson et al., 2012a; Hamilton and Norgren, 1984b). From the NST, gustatory information is sent to the pontine parabrachial nucleus (PBN). In addition to the thalamocortical pathway, PBN gustatory efferents project to ventral forebrain nuclei such as the lateral hypothalamus (LH) and central nucleus of amygdala (CeA) (Norgren and Leonard, 1971). It is well known that these same forebrain areas project back to the NST and PBN to modulate taste-evoked neural responsiveness (Cho et al., 2003b; Kang and Lundy, 2009c; Li and Cho, 2006b; Lundy and Norgren, 2004a). For example, activation of the LH and CeA most often produce an excitatory effect on NST taste neurons. In contrast, inhibition and excitation of PBN taste neurons occurred equally as often during LH activation, whereas CeA activation predominately inhibited PBN taste neurons. Yet, the impact of such neuromodulation on taste-guided behavior as well as the neurochemical identity of relevant descending pathways are not fully understood.

In behaving animals, electrical stimulation of the CeA was shown to increase the number of Fos-immunoreactive neurons in the NST and PBN as well as

aversive taste-reactivity responses to quinine HCl (QHCl). In contrast, stimulation of the LH decreased the number of aversive responses to QHCl with little change in Fos immunoreactivity (Riley and King, 2013). Although these results are suggestive of a role in taste-guided behavior to an aversive stimulus, the use of electrical stimulation is limited in that it cannot distinguish between activation of different neuronal subtypes present in the CeA and LH (Broberger et al., 1998; Kim et al., 2017; McCullough et al., 2018a; Moga and Gray, 1985; Moga et al., 1990a; Moga et al., 1990b; Sakurai et al., 1998). Thus, more work is needed to identify the anatomic substrates through which descending pathways exert their influence on ingestive behavior.

For the CeA, the identity of one such substrate is somatostatin-expressing neurons (Sst). They are a major source of descending input to taste responsive areas of the brainstem and CeA/Sst-to-NST and CeA/Sst-to-PBN projecting neurons are largely distinct from one another (Bartonjo and Lundy, 2020; Magableh and Lundy, 2014; Panguluri et al., 2009). We have shown recently that manipulating the neural activity of CeA/Sst-to-NST neurons altered concentration-dependent intake of QHCl (Chapter 3) (Bartonjo et al., 2022). Specifically, licking to high concentrations of QHCl was substantially increased by optogenetic inhibition of this descending pathway compared to Control mice. This finding suggests that the ability of animals to respond appropriately to changes in the intensity of an aversive taste stimulus can be fine-tuned by descending input from CeA/Sst neurons to the NST. The extent to which increased acceptance of QHCl can be solely attributed to the CeA/Sst-to-NST pathway, however, is tentative

because the CeA is interconnected with other brain regions such as LH that also innervates the NST (Barbier et al., 2018; Ono et al., 1985b; Ottersen, 1980a; Reppucci and Petrovich, 2016).

To address this uncertainty, the present study assessed whether CeA/Sst neurons that project to the NST or PBN have divergent innervation of the LH. We chose to focus on the LH because previous research implicates this region in behavioral responsiveness to QHCl (Ferssiwi et al., 1987; Riley and King, 2013). We used cre-dependent Herpes Simplex Virus (HSV) injections into the NST and ipsilateral LH or PBN and ipsilateral LH of Sst-cre mice to quantify single- and double-labelled CeA/Sst neurons. The HSV used is replication-deficient (e.g. does not result in trans-synaptic transport) and travels in the retrograde direction (e.g. from axon terminal to cell body) (Epstein, 2009; Fenno et al., 2014; Neve et al., 2005; Palmer et al., 2000). Our results show that the CeA is composed of several distinct populations of Sst-expressing neurons that give rise to CeA/Sst-to-NST, CeA/Sst-to-PBN, and CeA/Sst-to-LH pathways. That these cell populations are distinct provides the opportunity for future investigations to delineate their contribution(s) to taste processing and ingestive behavior.

4.2 Materials and Methods

4.2.1 Subjects

Transgenic mice homozygous for cre recombinase in somatostatin (Sst) expressing neurons (Sstm2.1(cre) Zjh/J) and wild type mice (C57BL/J6) were obtained from Jackson Laboratory (Taniguchi et al., 2011). The two strains were bred at the University of Louisville to generate mice heterozygous for cre

recombinase expression in Sst neurons. The mice were maintained in a temperature-controlled colony room on a 12h light/dark cycle with free access to normal rodent chow and distilled water unless otherwise noted. All procedures conformed to NIH guidelines and were approved by the University of Louisville Institutional Animal Care and Use Committee. A total of 12 mice were used for this study, 6 for NST/LH injections (4 male, 2 female) and another 6 for PBN/LH injections (3 male, 3 female).

4.2.2 Surgery

The mice were anesthetized with an intraperitoneal injection of Ketamine (100mg/kg) and Anased (10mg/kg) mixture. If needed, an additional dose of Ketamine (50mg/kg) was administered to maintain a deep level of anesthesia, which was determined using toe pinch reflex. The scalp was shaved and disinfected using Prevanics Swab (Professional Disposables International). Mice were secured in a stereotaxic apparatus and ophthalmic ointment was applied to both eyes. Body temperature was maintained at $35\pm 1^{\circ}\text{C}$ by a feedback-controlled heating pad and rectal temperature probe. A midline incision was made to expose the skull, and the skull was leveled with reference to bregma and lambda cranial sutures. Two small holes were drilled through the bone to allow ipsilateral access to either NST and LH or PBN and LH. The analgesic Meloxicam (5mg/kg) was administered prior to wound incision and again for at least 2 days post-surgery.

4.2.3 HSV injections

The coordinates used for viral injections into NST and PBN were, respectively, 6.1 mm posterior to bregma, 1.3 mm lateral to midline, 3.9 mm ventral to the

surface of the cerebellum and 5.1 mm posterior to bregma, 1.3 mm lateral to midline, 3.6 mm ventral to the surface of the inferior colliculus (Bartonjo and Lundy, 2020). The coordinates for LH injections were 1.3 mm posterior to bregma, 1.1 mm lateral to midline, 4.7 mm ventral to the cortical surface. Viral injections were performed using a 10- μ L nanofil syringe (34 g beveled needle, WPI) mounted in a microprocessor-controlled injector (UltraMicroPump, WPI) attached to the stereotaxic instrument. The syringe was first front-filled with light mineral oil followed by either HSV-EF1alpha-DIO-EYFP (RN415, 2.5×10^9 infectious units/mL) for NST or PBN injections and HSV-EF1alpha-DIO-mCherry (RN413, 2.5×10^9 infectious units/m) for LH injections [Dr. Rachael Neve, Massachusetts General Hospital (Neve et al., 2005)]. Because the mCherry and EYFP genes are preceded by DIO, a double-floxed inverse open reading frame, expression of transgene is restricted to Sst-expressing neurons (Fenno et al., 2014; Li et al., 2013; Taniguchi et al., 2011; Yu et al., 2016b). Prior research indicates that injection of multiple HSV constructs do not negatively interact with one another and are capable of retrograde transport to identify double-labeled neurons that project to distinct target areas (Bartonjo and Lundy, 2020; Kim and Cho, 2017; Lorsch et al., 2019). The microprocessor was set to deliver 300 nL of the virus at a rate of 40 nL/min, and the syringe retracted 5 min post-injection. A different syringe was used for each virus. Once the viral injections were completed, the incision was sealed using Vetbond tissue glue and triple antibiotic ointment was applied to the skin around the incision. Animals were monitored for additional one hour on a heating pad then returned to home cage once ambulatory.

4.2.4 Immunohistochemistry and confocal microscopy

Three weeks post-surgery, the mice received an intraperitoneal injection of a lethal dose of Ketamine/Anased mixture (300 mg/kg [Ketamine]/30 mg/kg [Anased]) followed by thoracotomy and transcardial perfusion with 4% paraformaldehyde. Extracted brains were post fixed overnight in 4% paraformaldehyde at 4 °C. Two brain blocks, one containing NST and PBN and another containing CeA and LH, were made. The blocks were cut (60 um) using a vibrating microtome (Leica). Every other section was collected, blocked with 10% normal donkey serum (NDS) in 0.1% triton-x phosphate buffered saline (TPBS) followed by incubation at 4 °C overnight on a shaker in 1:1000 dilution (in 0.1% TPBS and 5% NDS) of goat anti-GFP (Novus Biologicals) and rabbit anti-DsRed (Novus Biologicals) primary antibodies. After four rinses in TPBS (10min each), the tissue sections were incubated (at room temperature) for 1hr in 1:100 dilution (in 0.1% TPBS and 5% NDS) of Alexa Fluor-488 donkey anti-goat and Alexa Fluor-546 donkey anti-rabbit (Fisher Scientific). After rinsing 3 times in phosphate buffered saline and once in phosphate buffer (10min each), the sections were mounted on microscope slides (HistoBond Adhesive Microscope Slides, VWR) and allowed to dry for 1hr. The sections were rehydrated with deionized water followed by Fluoromount-G mounting medium and coverslips.

4.2.5 Data analysis

Images of injection sites and retrograde-labelled cells positive for EYFP and mCherry were obtained using sequential scanning with an Olympus confocal microscope. In alternate tissue sections (10 per animal), the number of fluorescent

positive cells in each Z stack (3um/slice) of the CeA and LH was calculated (Olympus FluoView software). The CeA was identified as the area approximately 0.7 to 1.8 mm posterior to bregma ventral to the striatum, medial to the basolateral nucleus of the amygdala, and lateral to the optic tract. The LH was identified as the area approximately 1.2 to 2.2 mm posterior to bregma ventral to the zona incerta, medial to the internal capsule/cerebral peduncle, and lateral to the fornix. The color segmentation function in Image J software was used to separate and count labeled neurons (Bartonjo and Lundy, 2020). The separate color channels were converted to 8-bit images, auto threshold adjusted (white objects on black background, otsu or triangle method), and a Gaussian blur applied (sigma radius = 2). The appropriate scale was set (0.85 pixels/um (10x magnification)) and the analyze particles function (size $\geq 20\mu\text{m}^2$) used to count labeled cells (CeA sections: green and red channels; LH sections: green channel only). For CeA, the image calculator function "AND" was used to identify overlapping pixels in the separate channels. Using the analyze particles function on the resultant image, overlapping elements with size $\geq 20\mu\text{m}^2$ were considered double labeled. Manual counts on select sections were similar to automated calculations. Data measurements passed normality (Shapiro-Wilk) and equality of variance tests (Brown-Forsythe) and were statistically analyzed using independent t-tests (SigmaPlot 14.5). The results are presented as mean \pm s.e. and a value of $p < 0.05$ was considered as evidence to reject the null hypothesis.

The software package RStudio was used to calculate complementary estimates of effect size (Hedges' g (g)) and corresponding confidence intervals

(95% CI) (Lakens, 2013; Yigit and Mendes, 2018). Hedges' *g* is considered less biased compared to Cohen's *d* for smaller sample sizes and represents the difference of the means in units of the pooled standard deviation.

4.3 Results

4.3.1 NST-LH injections

Microscopic examination of tissue from HSV-EYFP injections into the NST showed neurons and fibers expressing Sst (green fluorescence) throughout the rostrocaudal extent of the NST with minimal fluorescence in the ventrally located reticular formation or laterally located dorsomedial spinal trigeminal nucleus (Figure 4.1A-D). The green cells in the NST likely reflect Sst-expressing interneurons, while those in surrounding areas indicate Sst neurons that project to the NST or possibly virus spread outside the NST taken up by Sst-expressing interneurons (Balaban and Beryozkin, 1994; Beckman and Whitehead, 1991; Thek et al., 2019; Travers, 1988).

Photomicrograph examples of HSV-mCherry injection into the LH of the same mouse are shown in Figure 4.1E-H where neurons and fibers expressing Sst (magenta fluorescence) were located primarily within the LH and dorsally in the adjacent substantia innominata (Subl) and zona incerta (ZI). The magenta fluorescent cells in the LH likely reflect Sst-expressing interneurons, while those in Subl and ZI indicate Sst neurons that project to the LH or possibly virus spread outside the LH taken up by Sst-expressing interneurons (Grove, 1988a; Grove, 1988b; Li et al., 2021). The green cells represent Sst-positive LH-to-NST projection

neurons, while green fibers likely represent retrograde-labeled axons from higher structures that pass through the LH.

Expression of both fluorescent markers was observed throughout the rostrocaudal extent of the amygdala. Photomicrograph examples of retrograde-labeled Sst-expressing neurons at 4 different levels of the CeA are shown in Figure 4.2A-D. Panels E-H show corresponding stereotaxic atlas drawings depicting the general location of CeA/Sst neurons projecting to the NST (green) and LH (magenta). In the schematic, no attempt was made to signify double-labeled neurons (yellow in Figure 4.2A and B) or provide an exact representation of the total number of cells in each photomicrograph. In one animal, the HSV injection aimed at LH was misplaced medial to the fornix and resulted in retrograde labeled CeA/Sst neurons located in the medial nucleus of the amygdala rather than the central nucleus (not shown).

We counted a total of 658 CeA/Sst neurons that projected to the NST and 437 projecting to the LH. A greater number of retrograde-labeled CeA/Sst neurons was associated with the NST injections (11.1 ± 0.95 cells per section) compared to LH injections (7.4 ± 1.4 cells per sections; Figure 4.3A, $t(10) = 2.36$, $P = 0.03$, $g = 1.26$, 95% CI (0.13, 3.01)). Out of the 1,095 retrograde labeled neurons, only 27 contained both fluorescent markers and were considered dual-target neurons (Figure 4.3A; 0.46 ± 0.12 cells per section). Expressed as a percentage of their respective population, greater than 90% of CeA/Sst cells project either to the NST or LH (Figure 4.3B). Injection site was not associated with differences in the percentage of single-target ($t(10) = 0.67$, $P = 0.52$, $g = 0.35$, 95% CI (-0.86, 1.74))

or dual-target neurons ($t(10) = -0.67$, $P = 0.52$, $g = -0.35$, 95% CI (-1.74, 0.85)). For the LH, the mean number of LH/Sst-to-NST neurons was 5.73 ± 0.89 per section.

4.3.2 PBN-LH injections

Microscopic examination of tissue from HSV-EYFP injections into the PBN showed neurons and fibers expressing Sst (green fluorescence) surrounding the superior cerebellar peduncle (scp) at each level (Figure 4.4A-D). The green cells in the PBN likely reflect Sst-expressing interneurons, while those in surrounding areas such as LC indicate Sst neurons that project to the PBN or possibly virus spread outside the PBN taken up by Sst-expressing interneurons (Giehl and Mestres, 1995; Luppi et al., 1995). The magenta fluorescent cells represent Sst positive PBN-to-LH projection neurons (Norgren, 1976). Photomicrograph examples of HSV-mCherry injection into the LH of the same mouse are shown in Figure 4.4E-H where, again, neurons and fibers expressing Sst (magenta fluorescence) were located primarily within the LH and dorsally in the adjacent Subl and ZI. The green cells represent Sst-positive LH-to-PBN projection neurons, while green fibers likely represent retrograde-labeled axons from higher structures that pass through the LH. Similar to NST/LH injected mice, PBN/LH viral injections resulted in dense expression of fluorescent markers throughout the rostrocaudal extent of the amygdala. Photomicrograph examples of retrograde-labeled Sst-expressing neurons in CeA are shown in Figure 4.5A-D with corresponding stereotaxic atlas drawings in panels E-H.

A total of 1,176 CeA/Sst neurons that projected to the PBN and 607 that projected to the LH were counted. A larger population of CeA/Sst neurons was associated with PBN injections (19.6 ± 2.5 cells per section) compared to LH injections (10.1 ± 1.2 cells per section; Figure 4.6A, $t(10) = 3.7$, $P = 0.004$, $g = 1.97$, 95% CI (0.81, 4.10)). Out of the 1,783 retrograde labeled neurons, only 78 contained both fluorescent markers and were considered dual-target neurons (Figure 4.6A; 1.3 ± 0.2 cells per section). Expressed as a percentage of their respective population, 90% or more of CeA/Sst cells project either to the PBN or LH (Figure 4.6B). Injection site was not associated with differences in the percentage of single-target ($t(10) = 1.74$, $P = 0.11$, $g = 0.93$, 95% CI (-0.21, 2.54)) or dual-target neurons ($t(10) = -1.97$, $P = 0.07$, $g = -1.05$, 95% CI (-2.71, 0.09)). Similar to NST injections, PBN injections resulted in retrograde labeled Sst neurons in the LH (3.83 ± 0.82 cells per section).

Additional analyses comparing NST/LH and PBN/LH injected mice (compare Figure 4.3A and Figure 4.6A) revealed that injection pair was not associated with differences in the number of single-labeled CeA/Sst-to-LH projecting neurons ($t(10) = -1.56$, $P = 0.15$, $g = -0.83$, 95% CI (-2.40, 0.31)). In contrast, PBN injections were associated with a greater number of single-labeled CeA/Sst neurons compared to NST injections ($t(10) = -3.39$, $P = 0.006$, $g = -1.81$, 95% CI (-3.85, -0.66)). Finally, PBN/LH injections were associated with a greater number of dual-labeled CeA/Sst neurons compared to NST/LH injections ($t(10) = -3.64$, $P = 0.004$, $g = -1.94$, 95% CI (-4.04, -0.77)). Albeit the number of dual-target neurons was minimal for both injection groups. Together, the present results show that CeA

neurons marked by Sst expression can be delineated into subpopulations that project to either the NST, PBN, or LH.

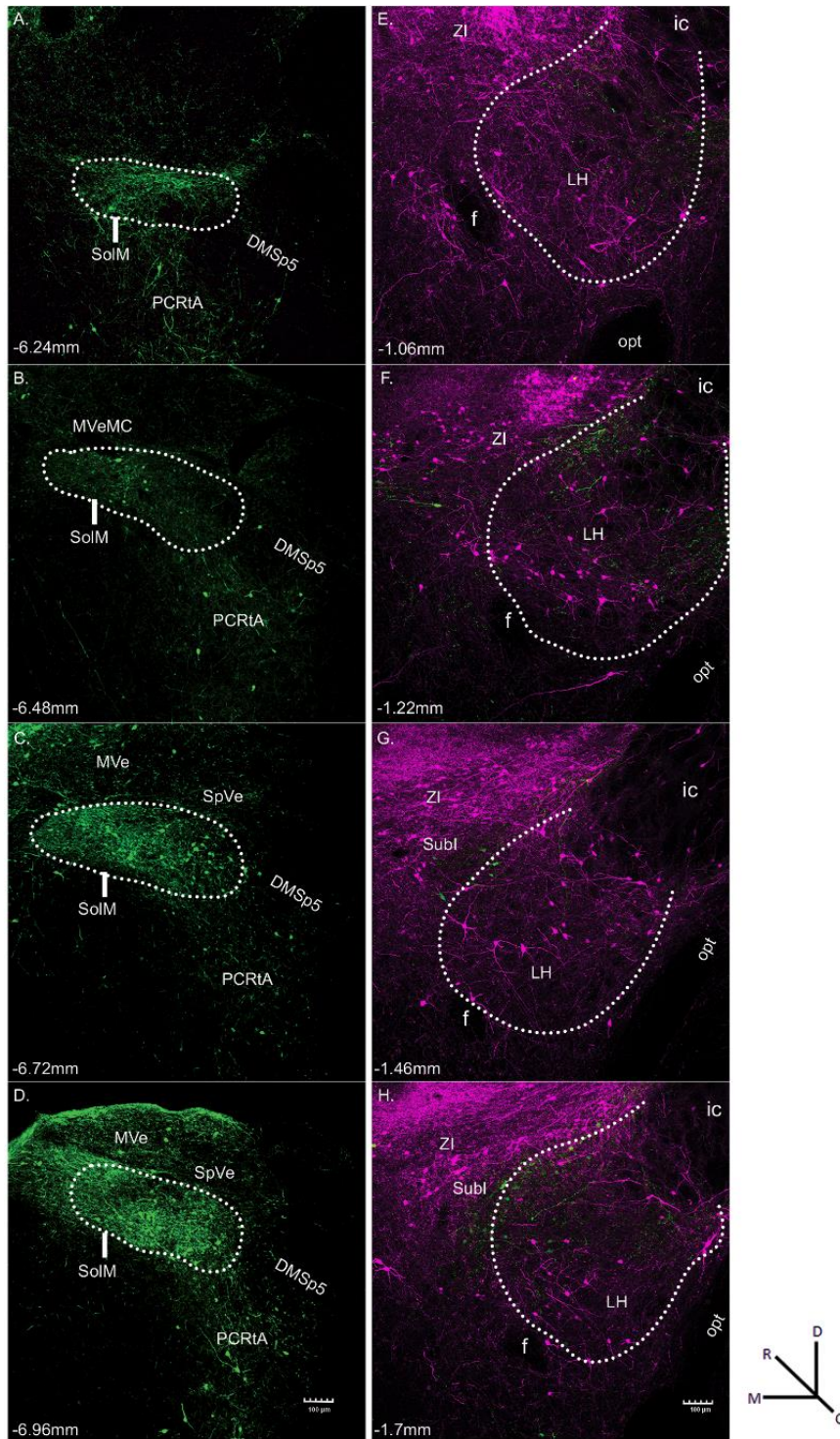


Figure 4.1: Representative fluorescent images of the viral injections into the NSt and LH.

(A-D, green) and HSV-Ef1 α -DIO-mCherry into the LH **(E-H, magenta)** of a *Sst-cre* mouse. Sections are arranged from rostral (top) to caudal (bottom). White

dots outline the approximate boundaries of the NST and the LH. Within the NST, green fluorescence indicates Sst-expressing neurons that project locally within the NST. Within the LH, the magenta, fluorescent cells indicate Sst-expressing interneurons, while those in surrounding areas such as ZI and Subl indicate Sst neurons that project to the LH. The green, fluorescent cells represent Sst-positive LH-to-NST projection neurons, while the green, fluorescent fibers likely represent retrograde-labeled axons from higher structures. The approximate level relative to bregma is shown at the bottom left of each photomicrograph (Paxinos and Franklin, 2001). Magnification was 10x (0.85 pixels/micron). Abbreviations: DMsp5, dorsomedial spinal trigeminal nucleus; anterior part; f, fornix; ic, internal capsule; LH, lateral hypothalamus; MVe, medial vestibular nucleus; MVeMC, medial vestibular nucleus, magnocellular part; opt, optic tract; PCRtA, parvicellular reticular nucleus, alpha part; SolM, nucleus of the solitary tract, medial part; SpVe, spinal vestibular nucleus; Subl, substantia innominata; ZI, zona incerta.

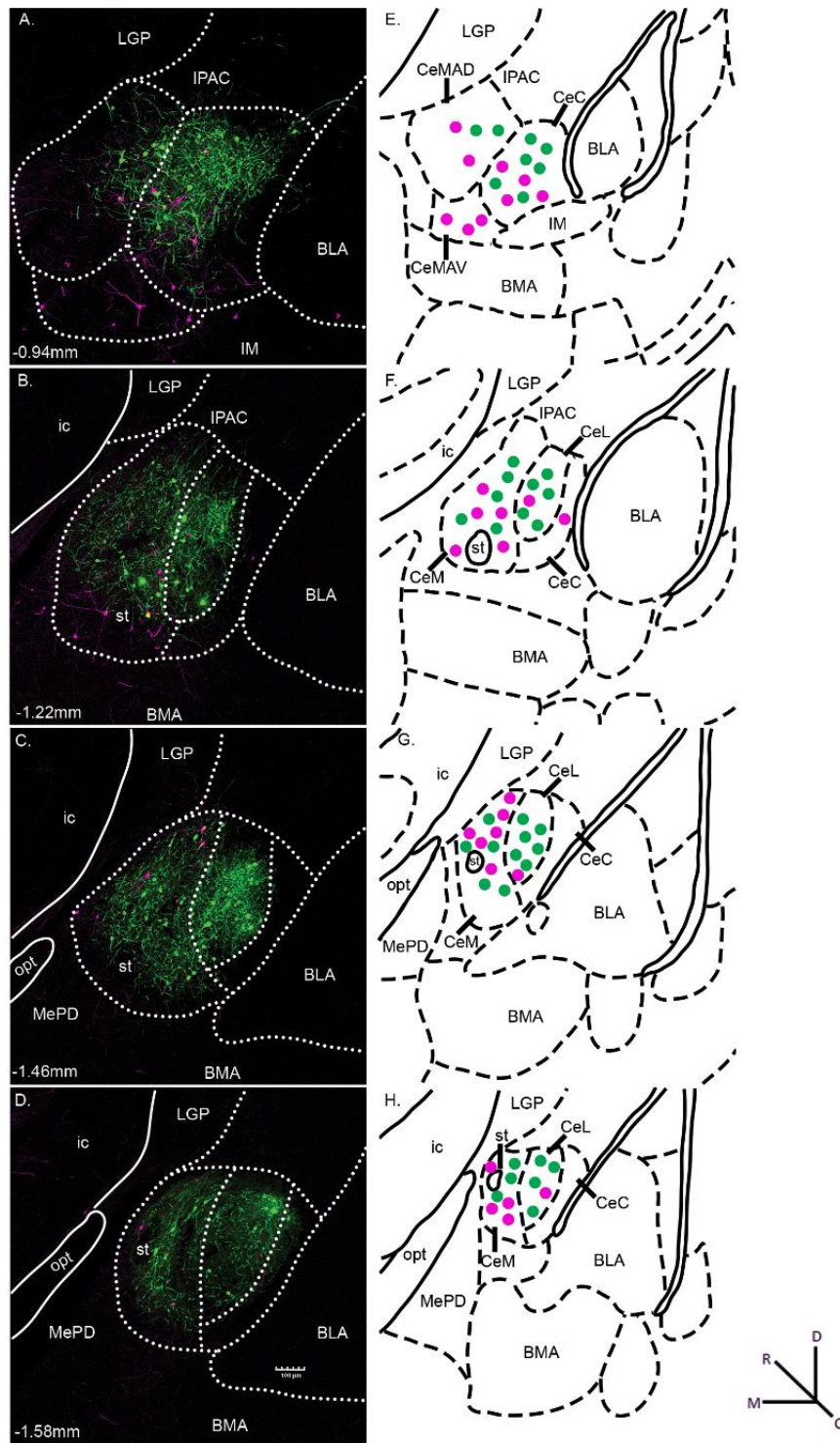


Figure 4.2: Representative photomicrographs of CeA/Sst neurons projections to NST and LH

Figure 4. 1. **(A-D)** Representative photomicrographs of CeA/Sst neurons projecting to the NST (green) and LH (magenta) from HSV injections depicted in Figure 4.1. Yellow fluorescence indicates Sst neurons that project both to the NST and LH. The white dotted lines outline the approximate boundaries of the CeC, CeL, and CeM divisions of the CeA. The approximate levels relative to bregma are indicated at the bottom left corner in each photomicrograph. Magnification of fluorescent images was 10x (0.85 pixels/micron). **(E-H)** Corresponding diagrams labeled with amygdala sub nuclei as defined in Paxinos and Franklin (2001). The general location of retrograde labeled neurons are represented by green (NST projecting) and magenta (LH projecting) dots. Abbreviations: BLA, basolateral amygdaloid nucleus, anterior part; BMA, basomedial amygdaloid nucleus, anterior part; CeC, central amygdaloid nucleus, capsular part; CeL, central amygdaloid nucleus, lateral division; CeM, central amygdaloid nucleus, medial division; CeMAD, central amygdaloid nucleus, medial division, anterodorsal part; CeMAV, central amygdaloid nucleus, medial division, anteroventral part; IM, intercalated amygdaloid nucleus, main part; ic, internal capsule; IPAC, interstitial nucleus of the posterior limb of the anterior commissure; LGP, lateral globus pallidus; MePD, medial amygdaloid nucleus, posterodorsal part; opt, optic tract; st, stria terminalis

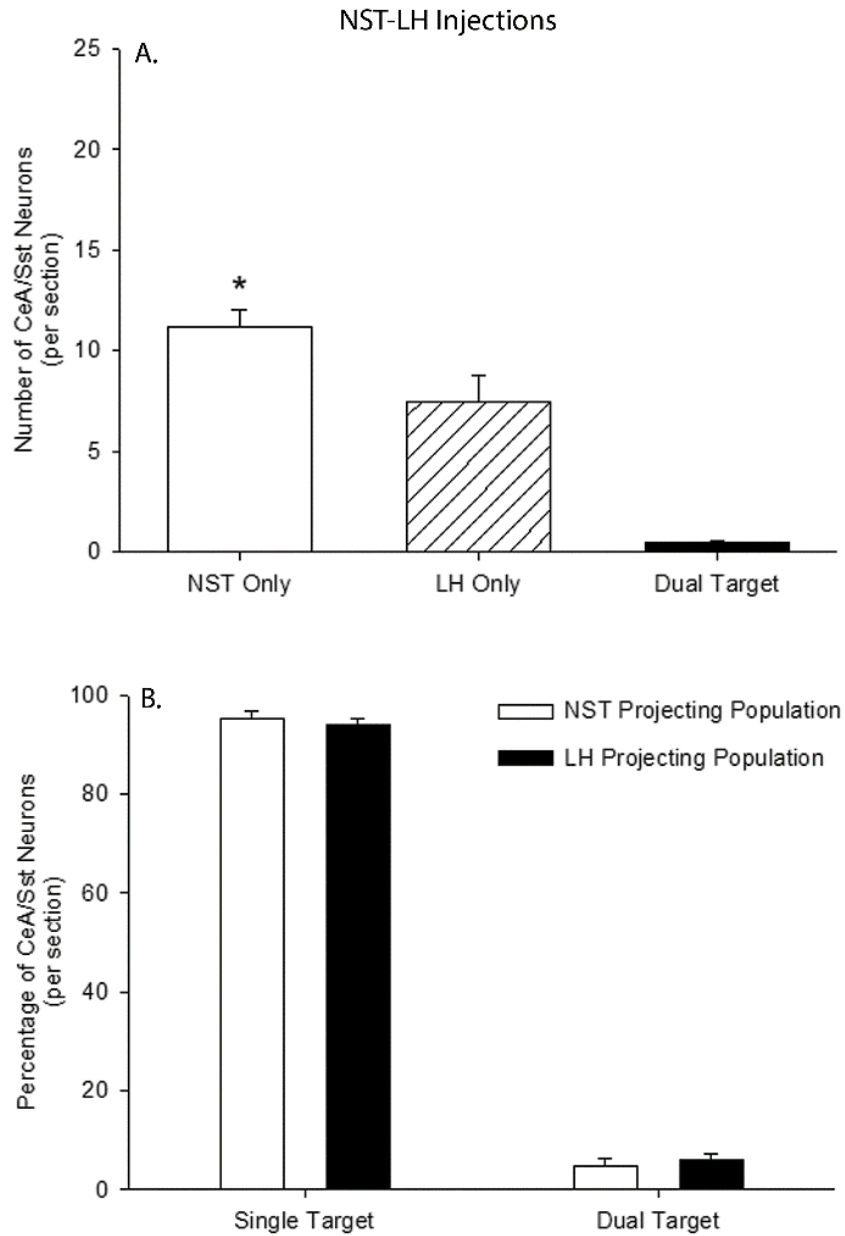


Figure 4.3: The number of retrograde labeled Sst neurons in the CeA projecting into the NST and LH.

(A) The per section average of retrograde labeled Sst neurons in the CeA following HSV injections of into the NST and LH of Sst-cre mice. Open bar represents the average number of Sst cells that only projected to the NST, cross-hatched bar Sst cells that only projected to the LH and filled bar Sst cells that projected both to the NST and LH. *, NST Only > LH Only. **(B)** The mean

percentage of single- and double-labeled Sst neurons in the CeA following HSV injections into the NST (open bars) and LH (filled bars).

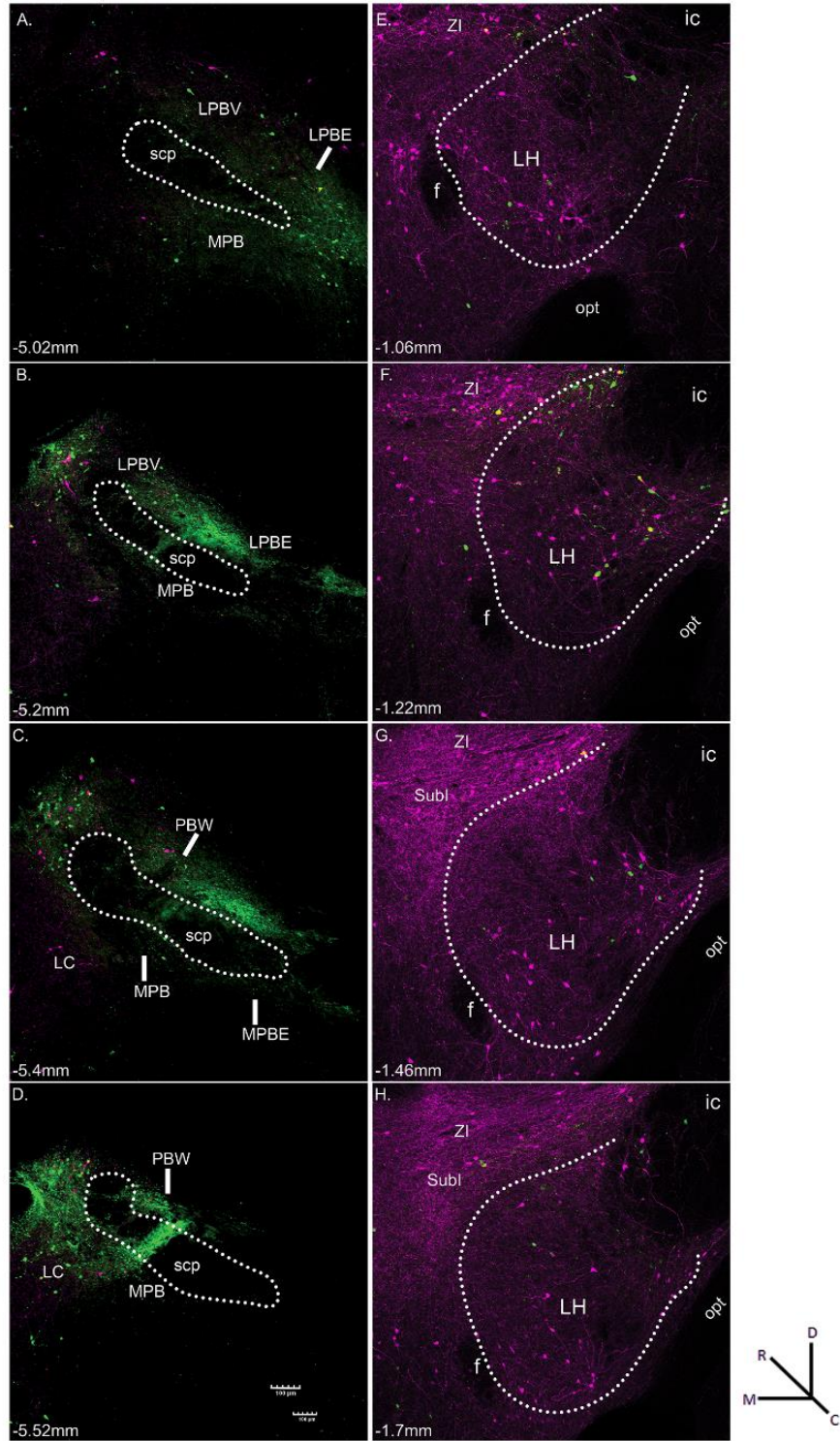


Figure 4.4: Representative fluorescent images of PBN and LH viral injection sites.

Representative fluorescent images resulting from the injection of HSV-Ef1 α -DIO-EYFP into the PBN (**A-D**, green) and HSV-Ef1 α -DIO-mCherry into the LH (**E-H**, magenta) of a Sst-cre mouse. Sections are arranged from rostral (top) to caudal (bottom). White dots outline the approximate boundaries of the LH and superior cerebellar peduncle (scp) in the PBN. Within the PBN, the green, fluorescent cells indicate Sst-expressing interneurons, while those in surrounding areas such as LC indicate Sst neurons that project to the PBN. The magenta, fluorescent cells represent Sst-positive PBN-to-LH projection neurons. Within the LH, the magenta, fluorescent cells indicate Sst-expressing interneurons, while those in surrounding areas such as ZI and Subl indicate Sst neurons that project to the LH. The green, fluorescent cells represent Sst-positive LH-to-PBN projection neurons, while the green, fluorescent fibers likely represent retrograde-labeled axons from higher structures. The approximate level relative to bregma is shown at the bottom left of each photomicrograph. Magnification was 10x (0.85 pixels/micron). Abbreviations: f, fornix; ic, internal capsule; LC, locus coeruleus; LH, lateral hypothalamus; LPBE, lateral parabrachial nucleus, external part; LPBV, lateral parabrachial nucleus, ventral part; MPB, medial parabrachial nucleus; MPBE, medial parabrachial nucleus, external part; opt, optic tract; PBW, parabrachial nucleus, waist part; scp, superior cerebellar peduncle; Subl, substantia innominata; ZI, zona incerta.

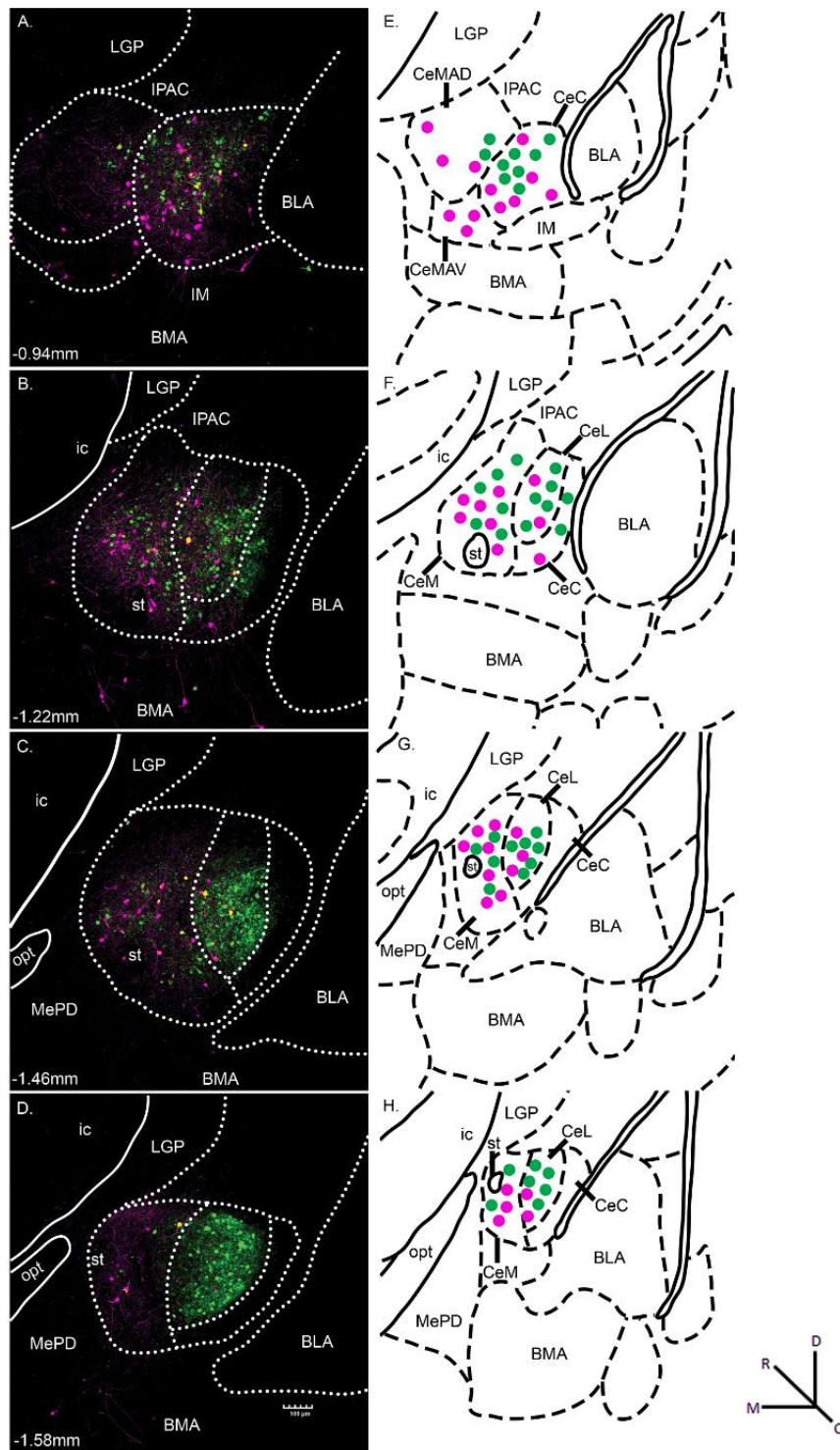


Figure 4.5: Representative photomicrographs showing retrograde labelled cells in CeA.

(A-D) Representative photomicrographs of CeA/Sst neurons projecting to the PBN (green) and LH (magenta) from the HSV injections depicted in Figure 4.4. Yellow fluorescence indicates Sst neurons that project both to the PBN and LH. The white dotted lines outline the approximate boundaries of the CeC, CeL, and CeM divisions of the CeA. The approximate levels relative to bregma are indicated at the bottom left corner in each photomicrograph. Magnification of fluorescent images was 10x (0.85 pixels/micron). **(E-H)** Corresponding diagrams labeled with amygdala sub nuclei as defined in Paxinos and Franklin (2001). The general location of retrograde labeled neurons is represented by green (PBN projecting) and magenta (LH projecting) dots. Abbreviations: BLA, basolateral amygdaloid nucleus, anterior part; BMA, basomedial amygdaloid nucleus, anterior part; CeC, central amygdaloid nucleus, capsular part; CeL, central amygdaloid nucleus, lateral division; CeM, central amygdaloid nucleus, medial division; CeMAD, central amygdaloid nucleus, medial division, anterodorsal part; CeMAV, central amygdaloid nucleus, medial division, anteroventral part; IM, intercalated amygdaloid nucleus, main part; ic, internal capsule; IPAC, interstitial nucleus of the posterior limb of the anterior commissure; LGP, lateral globus pallidus; MePD, medial amygdaloid nucleus, posterodorsal part; opt, optic tract; st, stria terminalis

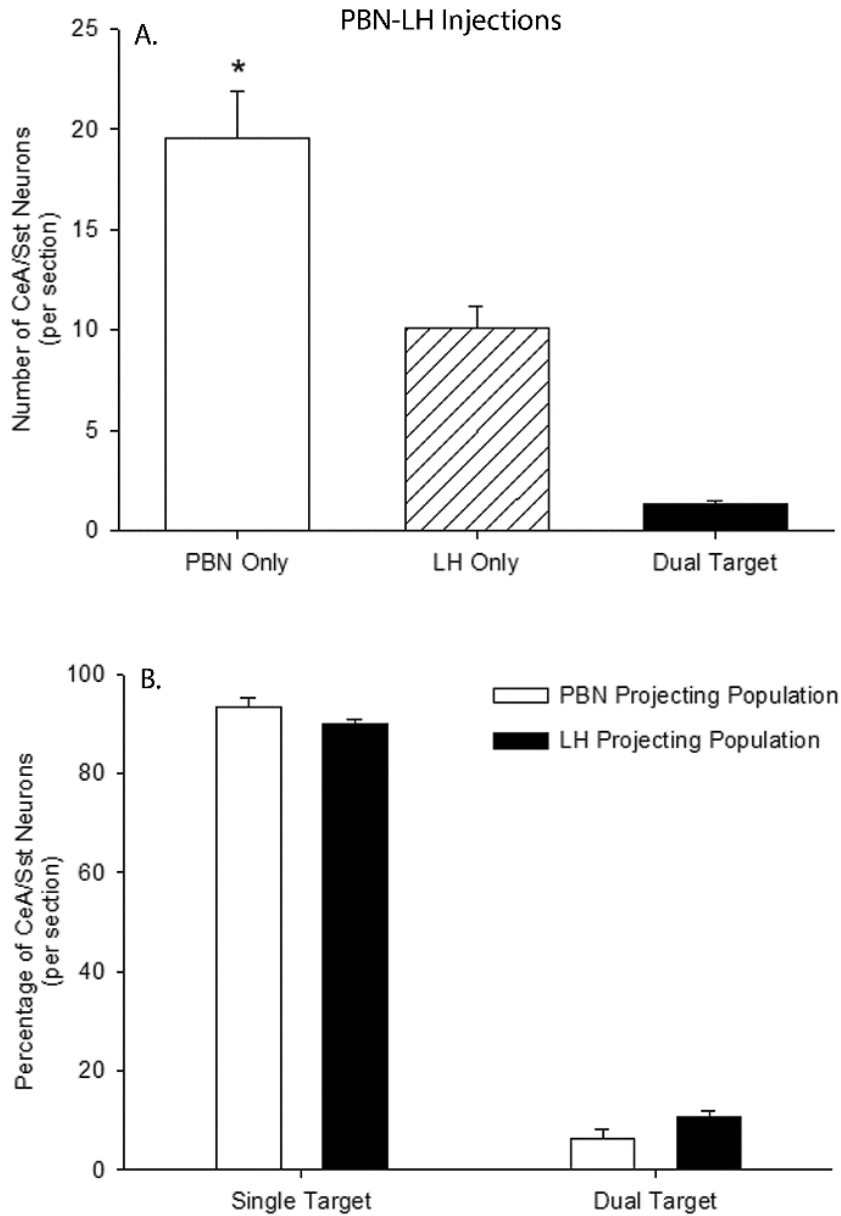


Figure 4.6: The number of retrograde labeled Sst neurons in CeA projecting to PBN and/or LH.

(A) The per section average of retrograde labeled Sst neurons in the CeA following HSV injections of into the PBN and LH of Sst-cre mice. Open bar represents the average number of Sst cells that only projected to the PBN, cross-hatched bar Sst cells that only projected to the LH and filled bar Sst cells that projected both to the PBN and LH. *, PBN Only > LH Only. **(B)** The mean

percentage of single- and double-labeled Sst neurons in the CeA following HSV injections into the PBN (open bars) and LH (filled bars).

4.4 Discussion

The objective of the present experiments was to further elaborate on the heterogeneity of a large subpopulation of CeA neurons that express the neuropeptide Sst. The present findings mirror results from previous studies showing that the medullary reticular formation, NST, and PBN are largely innervated by distinct populations of CeA neurons (Kang and Lundy, 2009a; Zhang et al., 2011) and, at least for the NST and PBN, a subpopulation of these neurons express Sst (Chapter 2) (Bartonjo and Lundy, 2020). The present results extend these observations by demonstrating that an additional subset of CeA/Sst neurons project to the LH and are largely distinct from CeA/Sst-to-NST and CeA/Sst-to-PBN projecting neurons.

To the best of our knowledge only three prior studies have assessed the role of CeA/Sst neurons on ingestive behavior. In two of these studies, CeA/Sst neurons as a whole were targeted for optogenetic manipulation that resulted in either increased or decreased intake of water (Kim et al., 2017; Yu et al., 2016b). The third study used retrograde transported HSV to specifically target CeA/Sst-to-NST neurons for optogenetic manipulation (Chapter 3) (Bartonjo et al., 2022). During brief-access licking sessions, the intake of water and sucrose was unaffected by altering the neural activity of the CeA/Sst-to-NST pathway, while intake of QHCl was increased by inhibiting this pathway. These inconsistencies regarding water intake are not easily explained but are likely due to procedural differences among studies as well as the fact that the latter experiment from our

laboratory targeted a defined projection of CeA/Sst neurons rather than simply targeting the whole population.

Beyond manipulating the neural activity of cell-type/target-specific neurons, the interconnectivity of brain regions also must be considered. Specifically, the LH and the CeA are reciprocally connected to each other, and the LH also innervates the NST to modulate processing of taste information (Barbier et al., 2018; Cho et al., 2002c; Kang and Lundy, 2010b; Ono et al., 1985b; Ottersen, 1980a; Reppucci and Petrovich, 2016). Given this interconnectivity, there was uncertainty that the observed increase in acceptance of QHCl described above resulted solely from inhibiting CeA/Sst neurons with direct projections to the NST. The present anatomical study sheds light on this interpretational caveat by showing that CeA/Sst-to-NST neurons are distinct from CeA/Sst neurons projecting to the LH. Thus, altered responding to QHCl was likely the result of specific manipulation of CeA/Sst-to-NST neurons rather than indirect modulation of CeA/Sst-to-LH neurons that, in turn, project to the NST. It is possible, however, that independent perturbation of CeA/Sst-to-LH as well as CeA/Sst-to-PBN pathways might also influence QHCl and/or sucrose sensitivity.

In summary, the CeA comprises a wide array of molecularly distinct cell populations and contributes to the control of a wide range of behaviors (Douglass et al., 2017; Li et al., 2013; McCullough et al., 2018a; Tye et al., 2011; Yu et al., 2016b). Despite this molecular diversity, a particular cell type can have divergent function such as the contribution of CeA/Sst neurons to expression of conditioned fear and ingestive behavior. In light of previous research and the current study, this

likely relies on engagement of target specific subpopulation(s) of CeA/Sst neurons. At least for the NST, CeA/Sst neurons have been shown to innervate both the rostral and caudal divisions (Bartoinjo and Lundy, 2020; Saha et al., 2002) and, thus, likely function to modulate both oral and visceral sensory information, respectively. In the future, it will be necessary to identify additional cell-type/target-specific pathways to provide a more thorough understanding of the molecular basis of amygdala function (Bartoinjo et al., 2022; Douglass et al., 2017; Torruella-Suarez et al., 2020).

CHAPTER 5

GENERAL DISCUSSION

The gustatory system plays a crucial role in distinguishing between different tastes allowing an organism to identify and consume foods that are rich in essential nutrients while avoiding those that are harmful. This is critical for the survival of organisms in their environment. This process is facilitated by the innate preference for certain tastes, such as sweet and umami, which are often associated with nutrient-rich foods. In contrast, bitter and sour tastes, which are often associated with harmful or toxic substances, can trigger an aversive response and discourage ingestion. The neural circuits that mediate these taste guided behaviors are still not clearly understood. For instance, lesion studies have shown that the nucleus of solitary tract (NST) is important for responding to stimulus intensity and the parabrachial nucleus (PBN) more for associative learning. It has also been demonstrated using electrical stimulation of forebrain regions such as the lateral hypothalamus (LH) and central nucleus of the amygdala (CeA) that taste responses recorded in NST and PBN are differentially modulated. These findings suggest that forebrain regulator nuclei can influence taste perception by modulating neural processing of ascending taste information. Owing to the non-specific nature of lesion and electrical stimulation studies, knowledge of how specific forebrain regulator pathways influence behavior is limited. Given that the CeA is a major source of descending input to the NST and PBN, we investigated

the anatomical and synaptic connectivity of a specific CeA cell population that expresses somatostatin (Sst), as well as its role in taste-guided behavior.

To comprehensively investigate CeA/Sst cells, we employed cutting-edge techniques involving the use of cre-dependent viral vectors in combination with transgenic mice expressing cre recombinase in somatostatin neurons and optogenetics. Specifically, we used cre-dependent retrograde viral vectors containing *HSV-Ef1 α -DIO-EYFP* and *HSV-Ef1 α -DIO-mCherry* reporter genes to map anatomical connections of CeA/Sst cells. By injecting these viruses into the NST, PBN and LH of Sst-cre mice and quantifying retrograde-labelled cell bodies in the central amygdala, we were able to determine whether input to these regions originates from largely separate populations of CeA/Sst cells. For synaptic connectivity, we used a novel, cre-dependent peroxidase reporter (AAV9-Ef1 α -DIO-dAPEX2) to label CeA/Sst cells and their axon terminals in the NST. For optogenetic manipulation during taste-guided behavior, we used cre-dependent HSV viral vectors to express the light-activated opsins ChR2 or eNpHR3 in CeA/Sst cells that project either to the NST or PBN. While the use of optogenetics to manipulate neural activity has been around for over a decade, its use in examining how forebrain regulator pathways influence ingestive behavior is novel.

My experiments revealed that largely separate populations of CeA/Sst cells project either to the NST, PBN, or LH. These results suggest that target specific CeA/Sst cells can be independently activated or inhibited. Further, we analyzed the ultrastructure of CeA/Sst terminals in the NST for co-expression of GABA. We found that virtually all CeA/Sst terminals in rNST co-expressed GABA and

synapsed with non-GABAergic post-synaptic targets. The result is consistent with previous research showing that CeA/Sst axon terminals in PBN co-express GABA and synapse with non-GABAergic dendrites (Lundy, 2020a). Together, these results suggest that CeA/Sst cells provide direct inhibition of projection neurons within NST and PBN. Co-localization of Sst with GABA also has been reported in other brain regions (Oertel; Somogyi et al., 1984). One possibility is that its release modulates the action of GABA on post-synaptic cells.

Because CeA/Sst cell populations are largely distinct, CeA/Sst-to-NST, CeA/Sst-to-PBN, and CeA/Sst-to-LH pathways can be manipulated independently to assess their role in taste-guided behavior. We found that optogenetic inhibition, but not excitation, of CeA/Sst-to-NST neurons increased intake of high concentration of quinine. Photo-activation or inhibition of this pathway was without effect on sucrose or water licking. The lack of effect on sucrose intake is not known, but one possibility is that CeA/Sst-to-NST neurons only respond to aversive gustatory stimuli. This implies that another cell population and/or pathway is involved in processing appetitive gustatory stimuli. For instance, neurons in the NST that represent bitter and sweet tastant are distinct (Jin et al., 2021). Silencing CeA axon terminals in the NST resulted in increased licking to a bitter-sweet taste mixture. Unfortunately, the genetic identity of the CeA cells that were manipulated in this study are unknown. Similarly, within the amygdala, genetically distinct BLA-to-CeA projections mediate appetitive and suppressive behaviors (Kim et al., 2017). Perhaps the most compelling evidence for a distinct cell population and/or pathway for positive stimuli is the recent demonstration that stimulation of CeA

neurotensin (Nts) increase consumption of palatable fluids. When the CeA/Nts-to-PBN pathway was optogenetically activated, animals increased intake of sucrose (caloric stimulus) and sucralose (non-caloric stimulus) but did not influence the licking to quinine (Torruella-Suarez et al., 2020).

The findings from our study suggest that CeA/Sst cells respond to bitter stimuli. Additionally, we determined that the axon terminals of these cells in the NST co-express GABA and establish synapses with non-GABA cells, indicating that these CeA/Sst cells provide inhibitory signals to cells in the NST. Here, we propose a mechanism whereby the activation and inhibition of this pathway impact licking behavior in response to QHCl stimuli. Under normal conditions (controls, Figure 5.1A), oral stimulation by QHCl activates CeA/Sst cells, leading to the release of GABA in the NST. This, in turn, inhibits NST neurons, resulting in the suppression of licking behavior towards QHCl. Upon activation of this pathway, the intake of QHCl was not significantly different from the control group (Figure 5.1B). A potential explanation for this observation is the presence of a floor effect, where the extent of lick suppression cannot surpass the levels observed under normal conditions. Conversely, inhibition of this pathway (inhibition of GABA release) resulted in an increased intake of high concentrations of QHCl. This inhibition of GABA release disinhibits the NST neurons, possibly leading to an upregulation of licking behavior (Figure 5.1C). Hence, these findings highlight the critical role of this pathway in appropriate responding to bitter stimuli.

In summary, our results further the knowledge of forebrain regulator pathways and their contribution to taste-guided behavior. We showed that CeA cells marked by expression of Sst either project to NST, PBN or LH. Moreover, we observed that CeA/Sst-to-NST cells co-express GABA and synapse with non-GABAergic terminals suggesting monosynaptic inhibition of NST projection neurons rather than intrinsic GABAergic neurons. Silencing this specific CeA pathway increased intake of bitter taste stimuli suggesting that inhibitory feedback is required for appropriate responding to bitter taste stimulus. More studies are needed to further characterize other forebrain regulator pathways.

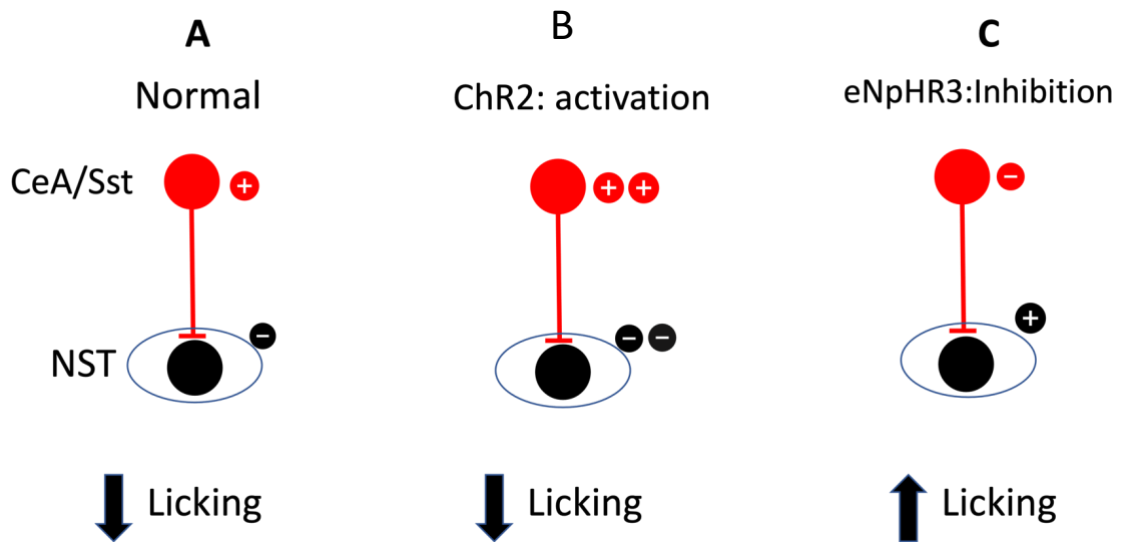


Figure 5.1: Possible mechanisms through which CeA/Sst-to-NST pathway influences licking in mice.

CeA/Sst cells respond to bitter stimuli. Under normal conditions (control), oral stimulation by QHCl activates CeA/Sst to release GABA which inhibits NST cells and suppresses licking behavior. Activation of CeA/Sst cells (ChR2), results in release of GABA and subsequent suppression of licking behavior as observed in controls. Inhibition of CeA/Sst cells suppresses release of GABA which disinhibits NST cells resulting in increased licking to high QHCl concentrations.

REFERENCES

- Baird, J.P., Travers, S.P., Travers, J.B., 2001. Integration of gastric distension and gustatory responses in the parabrachial nucleus. *Am.J.Physiol Regul.Integr.Comp Physiol.* 281, R1581-R1593.
- Balaban, C.D., Beryozkin, G., 1994. Vestibular nucleus projections to nucleus tractus solitarius and the dorsal motor nucleus of the vagus nerve: potential substrates for vestibulo-autonomic interactions. *Exp Brain Res.* 98, 200-12.
- Barbier, M., Fellmann, D., Risold, P.Y., 2018. Morphofunctional Organization of the Connections From the Medial and Intermediate Parts of the Central Nucleus of the Amygdala Into Distinct Divisions of the Lateral Hypothalamic Area in the Rat. *Front Neurol.* 9, 688.
- Barretto, R.P.J., et al., 2015. The neural representation of taste quality at the periphery. *Nature.* 517, 373-376.
- Bartonjo, J., et al., 2022. Perturbation of amygdala/somatostatin-nucleus of the solitary tract projections reduces sensitivity to quinine in a brief-access test. *Brain Res.* 1783, 147838.
- Bartonjo, J.J., Lundy, R.F., 2020. Distinct Populations of Amygdala Somatostatin-Expressing Neurons Project to the Nucleus of the Solitary Tract and Parabrachial Nucleus. *Chem Senses.* 45, 687-698.
- Batten, T.F.C., Gamboa-Esteves, F.O., Saha, S., 2002. Evidence for peptide co-transmission in retrograde- and anterograde-labelled central nucleus of amygdala neurones projecting to NTS. *Autonomic Neuroscience.* 98, 28-32.
- Beckman, M.E., Whitehead, M.C., 1991. Intramedullary connections of the rostral nucleus of the solitary tract in the hamster. *Brain Res.* 557, 265-279.
- Beeler, J.A., et al., 2012. Taste uncoupled from nutrition fails to sustain the reinforcing properties of food. *European Journal of Neuroscience.* 36, 2533-2546.
- Bernstein, I.L., 1978. Learned taste aversions in children receiving chemotherapy. *Science.* 200, 1302-1303.
- Berridge, K.C., et al., 1984. Sodium depletion enhances salt palatability in rats. *Behavioral neuroscience.* 98, 652.
- Berridge, K.C., 2000. Measuring hedonic impact in animals and infants: microstructure of affective taste reactivity patterns. *Neuroscience & Biobehavioral Reviews.* 24, 173-198.
- Botta, P., et al., 2015. Regulating anxiety with extrasynaptic inhibition. *Nature Neuroscience.* 18, 1493-1500.
- Boughter, J.D., Jr, et al., 2002. A Brief-access Test for Bitter Taste in Mice. *Chemical Senses.* 27, 133-142.

- Boughter, J.D., Jr., et al., 2012. Genetic control of a central pattern generator: rhythmic oromotor movement in mice is controlled by a major locus near *Atp1a2*. *PLoS One*. 7, e38169.
- Bradley, R.M., 2000. Sensory receptors of the larynx. *The American Journal of Medicine*. 108, 47-50.
- Breza, J.M., Travers, S.P., 2016. P2X2 Receptor Terminal Field Demarcates a "Transition Zone" for Gustatory and Mechanosensory Processing in the Mouse Nucleus Tractus Solitarius. *Chem Senses*. 41, 515-24.
- Broberger, C., et al., 1998. Hypocretin/Orexin- and melanin-concentrating hormone-expressing cells form distinct populations in the rodent lateral hypothalamus: Relationship to the neuropeptide Y and agouti gene-related protein systems. *Journal of Comparative Neurology*. 402, 460-474.
- Cai, H., et al., 2014. Central amygdala PKC-delta(+) neurons mediate the influence of multiple anorexigenic signals. *Nat Neurosci*. 17, 1240-8.
- Carlezon, W.A., Jr., et al., 1997. Sensitization to morphine induced by viral-mediated gene transfer. *Science*. 277, 812-4.
- Chang, F., Scott, T.R., 1984a. Conditioned taste aversions modify neural responses in the rat nucleus tractus solitarius. *Journal of Neuroscience*. 4, 1850-1862.
- Chang, F.C., Scott, T.R., 1984b. Conditioned taste aversions modify neural responses in the rat nucleus tractus solitarius. *J.Neurosci*. 4, 1850-1862.
- Chen, K., Kogan, J.F., Fontanini, A., 2021. Spatially Distributed Representation of Taste Quality in the Gustatory Insular Cortex of Behaving Mice. *Curr Biol*. 31, 450.
- Chen, Z., Travers, S.P., Travers, J.B., 2001. Muscimol infusions in the brain stem reticular formation reversibly block ingestion in the awake rat. *Am.J.Physiol Regul.Integr.Comp Physiol*. 280, R1085-R1094.
- Chen, Z., Travers, J.B., 2003. Inactivation of amino acid receptors in medullary reticular formation modulates and suppresses ingestion and rejection responses in the awake rat. *Am.J.Physiol Regul.Integr.Comp Physiol*. 285, R68-R83.
- Cho, Y.K., Li, C.-S., Smith, D.V., 2002a. Gustatory Projections from the Nucleus of the Solitary Tract to the Parabrachial Nuclei in the Hamster. *Chemical Senses*. 27, 81-90.
- Cho, Y.K., Li, C.S., Smith, D.V., 2002b. Gustatory projections from the nucleus of the solitary tract to the parabrachial nuclei in the hamster. In: *Chem.Senses*. Vol. 28, ed.^eds., pp. 81-90.
- Cho, Y.K., Li, C.S., Smith, D.V., 2002c. Taste responses of neurons of the hamster solitary nucleus are enhanced by lateral hypothalamic stimulation. *J.Neurophysiol*. 87, 1981-1992.
- Cho, Y.K., Li, C.-S., Smith, D.V., 2003a. Descending Influences from the Lateral Hypothalamus and Amygdala Converge onto Medullary Taste Neurons. *Chemical Senses*. 28, 155-171.
- Cho, Y.K., Li, C.S., Smith, D.V., 2003b. Descending influences from the lateral hypothalamus and amygdala converge onto medullary taste neurons. *Chem.Senses*. 28, 155-171.

- Ciocchi, S., et al., 2010. Encoding of conditioned fear in central amygdala inhibitory circuits. *Nature*. 468, 277-282.
- Contreras, R.J., Beckstead, R.M., Norgren, R., 1982a. The central projections of the trigeminal, facial, glossopharyngeal and vagus nerves: an autoradiographic study in the rat. *J.Auton.Nerv.Syst.* 6, 303-322.
- Contreras, R.J., Beckstead, R.M., Norgren, R., 1982b. The central projections of the trigeminal, facial, glossopharyngeal and vagus nerves: an autoradiographic study in the rat. *Journal of the Autonomic Nervous System*. 6, 303-322.
- Corson, J., et al., 2012a. A survey of oral cavity afferents to the rat nucleus tractus solitarii. *The Journal of comparative neurology*. 520, 495-527.
- Corson, J., et al., 2012b. A survey of oral cavity afferents to the rat nucleus tractus solitarii. *J.Comp Neurol*. 520, 495-527.
- Corson, J., et al., 2012c. A survey of oral cavity afferents to the rat nucleus tractus solitarii. *Journal of Comparative Neurology*. 520, 495-527.
- Cross-Mellor, S.K., Kavaliers, M., Ossenkopp, K.-P., 2005. The effects of lipopolysaccharide and lithium chloride on the ingestion of a bitter-sweet taste: Comparing intake and palatability. *Brain, Behavior, and Immunity*. 19, 564-573.
- Dallel, R., Ricard, O., Raboisson, P., 2004. Organization of parabrachial projections from the spinal trigeminal nucleus oralis: an anterograde tracing study in the rat. *J Comp Neurol*. 470, 181-91.
- Davis, B.J., Smith, D.V., 1997. Substance P modulates taste responses in the nucleus of the solitary tract of the hamster. *Neuroreport*. 8, 1723-1727.
- Davis, J.D., 1973. The effectiveness of some sugars in stimulating licking behavior in the rat. *Physiology & behavior*. 11, 39-45.
- Davis, J.D., Smith, G.P., 1990. Learning to sham feed: behavioral adjustments to loss of physiological postingestional stimuli. *American Journal of Physiology-Regulatory, Integrative and Comparative Physiology*. 259, R1228-R1235.
- Davis, J.D., Kung, T.M., Rosenak, R., 1995. Interaction between orosensory and postingestional stimulation in the control of corn oil intake by rats. *Physiology & Behavior*. 57, 1081-1087.
- Dilorenzo, P.M., Monroe, S., 1995. Corticofugal Influence on Taste Responses in the Nucleus of the Solitary Tract in the Rat. *Journal of Neurophysiology*. 74, 258-272.
- Douglass, A.M., et al., 2017. Central amygdala circuits modulate food consumption through a positive-valence mechanism. *Nat Neurosci*. 20, 1384-1394.
- Eisen, S., et al., 2001. Gastric negative feedback produced by volume and nutrient during a meal in rats. *American Journal of Physiology-Regulatory, Integrative and Comparative Physiology*. 281, R1201-R1214.
- Epstein, A.L., 2009. HSV-1-derived amplicon vectors: recent technological improvements and remaining difficulties--a review. *Mem Inst Oswaldo Cruz*. 104, 399-410.

- Ernits, T., Corbit, J.D., 1973. Taste as a dipsogenic stimulus. *Journal of Comparative and Physiological Psychology*. 83, 27-31.
- Eylam, S., et al., 2005. Melanocortin-4 receptor-null mice display normal affective licking responses to prototypical taste stimuli in a brief-access test. *Peptides*. 26, 1712-1719.
- Fekete, É., et al., 2002. Gastrin-releasing peptide microinjected into the amygdala inhibits feeding. *Brain research*. 955, 55-63.
- Fekete, É.M., et al., 2007. Neuromedin C microinjected into the amygdala inhibits feeding. *Brain research bulletin*. 71, 386-392.
- Fenno, L.E., et al., 2014. Targeting cells with single vectors using multiple-feature Boolean logic. *Nat Methods*. 11, 763-72.
- Ferssiwi, A., Cardo, B., Velley, L., 1987. Gustatory preference-aversion thresholds are increased by ibotenic acid lesion of the lateral hypothalamus in the rat. *Brain Res*. 437, 142-150.
- Flynn, F.W., et al., 1991a. Central gustatory lesions: II. Effects on sodium appetite, taste aversion learning, and feeding behaviors. *Behav. Neurosci*. 105, 944-954.
- Flynn, F.W., et al., 1991b. Central gustatory lesions: II. Effects on sodium appetite, taste aversion learning, and feeding behaviors. *Behavioral Neuroscience*. 105, 944-954.
- Flynn, F.W., et al., 1991c. Central gustatory lesions: I. Preference and taste reactivity tests. *Behav. Neurosci*. 105, 933-943.
- Fonseca, E., et al., 2018. Sucrose intensity coding and decision-making in rat gustatory cortices. *eLife*. 7, e41152.
- Fonseca, E., et al., 2020. Behavioral Disassociation of Perceived Sweet Taste Intensity and Hedonically Positive Palatability. *eNeuro*. 7.
- Frank, M.E., 1991. Taste-responsive neurons of the glossopharyngeal nerve of the rat. *Journal of Neurophysiology*. 65, 1452-1463.
- Fujimoto, S., et al., 1993. Pre- and postnatal development of rabbit foliate papillae with special reference to foliate gutter formation and taste bud and serous gland differentiation. *Microscopy Research and Technique*. 26, 120-132.
- Giardino, W.J., et al., 2018. Parallel circuits from the bed nuclei of stria terminalis to the lateral hypothalamus drive opposing emotional states. *Nat Neurosci*. 21, 1084-1095.
- Giehl, K., Mestres, P., 1995. Somatostatin-mRNA expression in brainstem projections into the medial preoptic nucleus. *Exp Brain Res*. 103, 344-54.
- Giza, B.K., Scott, T.R., VanderWeele, D.A., 1992. Administration of satiety factors and gustatory responsiveness in the nucleus tractus solitarius of the rat. *Brain Res. Bull*. 28, 637-639.
- Glendinning, J.I., Gresack, J., Spector, A.C., 2002. A high-throughput screening procedure for identifying mice with aberrant taste and oromotor function. *Chem Senses*. 27, 461-74.
- Glendinning, J.I., et al., 2005. Contribution of alpha-gustducin to taste-guided licking responses of mice. *Chem. Senses*. 30, 299-316.

- Gravina, S.A., Yep, G.L., Khan, M., 2013. Human biology of taste. *Ann Saudi Med.* 33, 217-22.
- Grigson, P.S., Shimura, T., Norgren, R., 1997a. Brainstem lesions and gustatory function: III. The role of the nucleus of the solitary tract and the parabrachial nucleus in retention of a conditioned taste aversion in rats. *Behav Neurosci.* 111, 180-7.
- Grigson, P.S., Shimura, T., Norgren, R., 1997b. Brainstem lesions and gustatory function: II. The role of the nucleus of the solitary tract in Na⁺ appetite, conditioned taste aversion, and conditioned odor aversion in rats. *Behav. Neurosci.* 111, 169-179.
- Grigson, P.S., Shimura, T., Norgren, R., 1997c. Brainstem lesions and gustatory function: III. The role of the nucleus of the solitary tract and the parabrachial nucleus in retention of a conditioned taste aversion in rats. *Behav. Neurosci.* 111, 180-187.
- Grigson, P.S., et al., 1998a. The parabrachial nucleus is essential for acquisition of a conditioned odor aversion in rats. *Behav. Neurosci.* 112, 1104-1113.
- Grigson, P.S., et al., 1998b. Ibotenic acid lesions of the parabrachial nucleus and conditioned taste aversion: Further evidence for an associative deficit in rats. *Behavioral Neuroscience.* 112, 160-171.
- Grigson, P.S., et al., 1998c. Ibotenic acid lesions of the parabrachial nucleus and conditioned taste aversion: further evidence for an associative deficit in rats. *Behav. Neurosci.* 112, 160-171.
- Grill, H.J., Norgren, R., 1978a. The taste reactivity test. II. Mimetic responses to gustatory stimuli in chronic thalamic and chronic decerebrate rats. *Brain Research.* 143, 281-297.
- Grill, H.J., Norgren, R., 1978b. The taste reactivity test. I. Mimetic responses to gustatory stimuli in neurologically normal rats. *Brain Res.* 143, 263-79.
- Grill, H.J., Schulkin, J., Flynn, F.W., 1986. Sodium homeostasis in chronic decerebrate rats. *Behavioral neuroscience.* 100, 536.
- Grove, E.A., 1988a. Efferent connections of the substantia innominata in the rat. *J Comp Neurol.* 277, 347-64.
- Grove, E.A., 1988b. Neural associations of the substantia innominata in the rat: afferent connections. *J Comp Neurol.* 277, 315-46.
- Hajnal, A., Takenouchi, K., Norgren, R., 1999. Effect of intraduodenal lipid on parabrachial gustatory coding in awake rats. *J. Neurosci.* 19, 7182-7190.
- Halsell, C.B., 1992a. Organization of parabrachial nucleus efferents to the thalamus and amygdala in the golden hamster. *Journal of Comparative Neurology.* 317, 57-78.
- Halsell, C.B., 1992b. Organization of parabrachial nucleus efferents to the thalamus and amygdala in the golden hamster. *J. Comp Neurol.* 317, 57-78.
- Halsell, C.B., Travers, S.P., Travers, J.B., 1996. Ascending and descending projections from the rostral nucleus of the solitary tract originate from separate neuronal populations. *Neuroscience.* 72, 185-97.
- Hamilton, R.B., Norgren, R., 1984a. Central projections of gustatory nerves in the rat. *J. Comp Neurol.* 222, 560-577.

- Hamilton, R.B., Norgren, R., 1984b. Central projections of gustatory nerves in the rat. *J Comp Neurol.* 222, 560-77.
- Han, W., et al., 2017. Integrated Control of Predatory Hunting by the Central Nucleus of the Amygdala. *Cell.* 168, 311-324.e18.
- Jacobs, K.M., Mark, G.P., Scott, T.R., 1988. Taste responses in the nucleus tractus solitarius of sodium-deprived rats. *The Journal of Physiology.* 406, 393-410.
- Jin, H., et al., 2021. Top-Down Control of Sweet and Bitter Taste in the Mammalian Brain. *Cell.* 184, 257-271.e16.
- Jowett, A., Shrestha, R., 1998. Mucosa and taste buds of the human epiglottis. *Journal of Anatomy.* 193, 617-618.
- Kang, Y., Yan, J., Huang, T., 2004. Microinjection of bicuculline into the central nucleus of the amygdala alters gustatory responses of the rat parabrachial nucleus. *Brain Res.* 1028, 39-47.
- Kang, Y., Lundy, R.F., 2009a. Terminal field specificity of forebrain efferent axons to brainstem gustatory nuclei. *Brain Res.* 1248, 76-85.
- Kang, Y., Lundy, R.F., 2009b. Terminal field specificity of forebrain efferent axons to brainstem gustatory nuclei. *Brain Res.* 1248, 76-85.
- Kang, Y., Lundy, R.F., 2009c. Terminal field specificity of forebrain efferent axons to brainstem gustatory nuclei. *Brain research.* 1248, 76-85.
- Kang, Y., Lundy, R.F., 2010a. Amygdalofugal influence on processing of taste information in the nucleus of the solitary tract of the rat. *J Neurophysiol.* 104, 726-41.
- Kang, Y., Lundy, R.F., 2010b. Amygdalofugal influence on processing of taste information in the nucleus of the solitary tract of the rat. *J. Neurophysiol.* 104, 726-741.
- Kaplan, J.M., Roitman, M., Grill, H.J., 2000. Food deprivation does not potentiate glucose taste reactivity responses of chronic decerebrate rats. *Brain research.* 870, 102-108.
- Karimnamazi, H., Travers, J.B., 1998. Differential projections from gustatory responsive regions of the parabrachial nucleus to the medulla and forebrain. *Brain Res.* 813, 283-302.
- Kim, J., et al., 2017. Basolateral to Central Amygdala Neural Circuits for Appetitive Behaviors. *Neuron.* 93, 1464-1479 e5.
- Kim, W.B., Cho, J.H., 2017. Synaptic Targeting of Double-Projecting Ventral CA1 Hippocampal Neurons to the Medial Prefrontal Cortex and Basal Amygdala. *J Neurosci.* 37, 4868-4882.
- Kutscher, C.L., Steilen, H., 1973. Increased drinking of a nonpreferred NaCl solution during food deprivation in the C3H/HeJ mouse. *Physiology & Behavior.* 10, 29-34.
- Lakens, D., 2013. Calculating and reporting effect sizes to facilitate cumulative science: a practical primer for t-tests and ANOVAs. *Front Psychol.* 4, 863.
- Lehman, C.D., et al., 1995. Effect of anesthesia of the chorda tympani nerve on taste perception in humans. *Physiology & Behavior.* 57, 943-951.

- Li, C.-S., Cho, Y.K., Smith, D.V., 2002a. Taste Responses of Neurons in the Hamster Solitary Nucleus Are Modulated by the Central Nucleus of the Amygdala. *Journal of Neurophysiology*. 88, 2979-2992.
- Li, C.-S., Cho, Y.K., Smith, D.V., 2005a. Modulation of Parabrachial Taste Neurons by Electrical and Chemical Stimulation of the Lateral Hypothalamus and Amygdala. *Journal of Neurophysiology*. 93, 1183-1196.
- Li, C.S., Cho, Y.K., Smith, D.V., 2002b. Taste responses of neurons in the hamster solitary nucleus are modulated by the central nucleus of the amygdala. *J.Neurophysiol*. 88, 2979-2992.
- Li, C.S., Cho, Y.K., Smith, D.V., 2002c. Taste responses of neurons in the hamster solitary nucleus are modulated by the central nucleus of the amygdala. *J Neurophysiol*. 88, 2979-92.
- Li, C.S., Cho, Y.K., Smith, D.V., 2005b. Modulation of parabrachial taste neurons by electrical and chemical stimulation of the lateral hypothalamus and amygdala. *J.Neurophysiol*. 93, 1183-1196.
- Li, C.S., Cho, Y.K., 2006a. Efferent projection from the bed nucleus of the stria terminalis suppresses activity of taste-responsive neurons in the hamster parabrachial nuclei. *Am J Physiol Regul Integr Comp Physiol*. 291, R914-26.
- Li, C.S., Cho, Y.K., 2006b. Efferent projection from the bed nucleus of the stria terminalis suppresses activity of taste-responsive neurons in the hamster parabrachial nuclei. *Am.J.Physiol Regul.Integr.Comp Physiol*. 291, R914-R926.
- Li, H., et al., 2013. Experience-dependent modification of a central amygdala fear circuit. *Nat Neurosci*. 16, 332-9.
- Li, Z., Rizzi, G., Tan, K.R., 2021. Zona incerta subpopulations differentially encode and modulate anxiety. *Sci Adv*. 7, eabf6709.
- Lin, J.Y., et al., 2012. Taste neophobia and palatability: the pleasure of drinking. *Physiol Behav*. 106, 515-9.
- Lopez, G.F., Krimm, R.F., 2006. Refinement of innervation accuracy following initial targeting of peripheral gustatory fibers. *Journal of Neurobiology*. 66, 1033-1043.
- Lorsch, Z.S., et al., 2019. Stress resilience is promoted by a Zfp189-driven transcriptional network in prefrontal cortex. *Nat Neurosci*. 22, 1413-1423.
- Lundy, R., 2020a. Comparison of GABA, Somatostatin, and Corticotrophin-Releasing Hormone Expression in Axon Terminals That Target the Parabrachial Nucleus. *Chemical Senses*. 45, 275-282.
- Lundy, R., 2020b. Comparison of GABA, Somatostatin, and Corticotrophin-Releasing Hormone Expression in Axon Terminals That Target the Parabrachial Nucleus. *Chem Senses*. 45, 275-282.
- Lundy, R.F., Jr., Norgren, R., 2001a. Pontine gustatory activity is altered by electrical stimulation in the central nucleus of the amygdala. *J.Neurophysiol*. 85, 770-783.

- Lundy, R.F., Jr., Norgren, R., 2001b. Pontine gustatory activity is altered by electrical stimulation in the central nucleus of the amygdala. *J Neurophysiol.* 85, 770-83.
- Lundy, R.F., Jr., Norgren, R., 2004a. Activity in the hypothalamus, amygdala, and cortex generates bilateral and convergent modulation of pontine gustatory neurons. *J. Neurophysiol.* 91, 1143-1157.
- Lundy, R.F., Jr., Norgren, R., 2004b. Activity in the hypothalamus, amygdala, and cortex generates bilateral and convergent modulation of pontine gustatory neurons. *J Neurophysiol.* 91, 1143-57.
- Luppi, P.H., et al., 1995. Afferent projections to the rat locus coeruleus demonstrated by retrograde and anterograde tracing with cholera-toxin B subunit and Phaseolus vulgaris leucoagglutinin. *Neuroscience.* 65, 119-60.
- Magableh, A., Lundy, R., 2014. Somatostatin and corticotrophin releasing hormone cell types are a major source of descending input from the forebrain to the parabrachial nucleus in mice. *Chem Senses.* 39, 673-82.
- Maier, J.X., Katz, D.B., 2013. Neural dynamics in response to binary taste mixtures. *Journal of Neurophysiology.* 109, 2108-2117.
- McCaughey, S.A., Scott, T.R., 2000. Rapid induction of sodium appetite modifies taste-evoked activity in the rat nucleus of the solitary tract. *American Journal of Physiology-Regulatory, Integrative and Comparative Physiology.* 279, R1121-R1131.
- McCleary, R.A., 1953. Taste and post-ingestion factors in specific-hunger behavior. *Journal of comparative and physiological psychology.* 46, 411.
- McCullough, K.M., et al., 2018a. Quantified Coexpression Analysis of Central Amygdala Subpopulations. *eNeuro.* 5.
- McCullough, K.M., et al., 2018b. Quantified Coexpression Analysis of Central Amygdala Subpopulations. *eneuro.* 5, ENEURO.0010-18.2018.
- Miller, I.J., Jr., Spangler, K.M., 1982. Taste bud distribution and innervation on the palate of the rat. *Chemical Senses.* 7, 99-108.
- Miller Jr., I.J., 1974. Branched chorda tympani neurons and interactions among taste receptors. *Journal of Comparative Neurology.* 158, 155-166.
- Moga, M.M., Gray, T.S., 1985. Evidence for corticotropin-releasing factor, neurotensin, and somatostatin in the neural pathway from the central nucleus of the amygdala to the parabrachial nucleus. *J.Comp Neurol.* 241, 275-284.
- Moga, M.M., Saper, C.B., Gray, T.S., 1989a. Bed nucleus of the stria terminalis: cytoarchitecture, immunohistochemistry, and projection to the parabrachial nucleus in the rat. *J.Comp Neurol.* 283, 315-332.
- Moga, M.M., Saper, C.B., Gray, T.S., 1989b. Bed nucleus of the stria terminalis: cytoarchitecture, immunohistochemistry, and projection to the parabrachial nucleus in the rat. *J Comp Neurol.* 283, 315-32.
- Moga, M.M., et al., 1990a. Organization of cortical, basal forebrain, and hypothalamic afferents to the parabrachial nucleus in the rat. *J Comp Neurol.* 295, 624-61.

- Moga, M.M., Saper, C.B., Gray, T.S., 1990b. Neuropeptide organization of the hypothalamic projection to the parabrachial nucleus in the rat. *J.Comp Neurol.* 295, 662-682.
- Moga, M.M., Saper, C.B., Gray, T.S., 1990c. Neuropeptide organization of the hypothalamic projection to the parabrachial nucleus in the rat. *Journal of Comparative Neurology.* 295, 662-682.
- Monroe, S., Lorenzo, P.M.D., 1995. Taste responses in neurons in the nucleus of the solitary tract that do and do not project to the parabrachial pons. *Journal of Neurophysiology.* 74, 249-257.
- Mook, D.G., Wagner, S., Hartline, D.F., 1991. All-or-none suppression of glucose sham feeding by an intragastric mixed meal in rats. *Behavioral neuroscience.* 105, 712.
- Mook, D.G., et al., 1993. Persistence of sham feeding after intragastric meals in rats. *Appetite.* 20, 167-179.
- Mura, E., et al., 2018. Innate and acquired tolerance to bitter stimuli in mice. *PLoS One.* 13, e0210032.
- Murakami, D.M., et al., 2002. Evidence for vestibular regulation of autonomic functions in a mouse genetic model. *Proc Natl Acad Sci U S A.* 99, 17078-82.
- Nachman, M., Ashe, J.H., 1973. Learned taste aversions in rats as a function of dosage, concentration, and route of administration of LiCl. *Physiology & Behavior.* 10, 73-78.
- Nakamura, K., Norgren, R., 1995. Sodium-deficient diet reduces gustatory activity in the nucleus of the solitary tract of behaving rats. *Am.J.Physiol.* 269, R647-R661.
- Nakashima, M., et al., 2000. An anterograde and retrograde tract-tracing study on the projections from the thalamic gustatory area in the rat: distribution of neurons projecting to the insular cortex and amygdaloid complex. *Neuroscience Research.* 36, 297-309.
- Neve, R.L., et al., 2005. Use of herpes virus amplicon vectors to study brain disorders. *Biotechniques.* 39, 381-91.
- Norgren, R., Leonard, C.M., 1971. Taste Pathways in Rat Brainstem. *Science.* 173, 1136.
- Norgren, R., Leonard, C.M., 1973a. Ascending central gustatory pathways. *J.Comp Neurol.* 150, 217-237.
- Norgren, R., Leonard, C.M., 1973b. Ascending central gustatory pathways. *The Journal of Comparative Neurology.* 150, 217-237.
- Norgren, R., 1976. Taste pathways to hypothalamus and amygdala. *J.Comp Neurol.* 166, 17-30.
- Oertel, W.H.W., Coexistence of glutamic acid decarboxylase- and somatostatin-like immunoreactivity in neurons of the feline nucleus reticularis thalami. *Journal of Neuroscience, The.* 3, 1322-32.
- Ogawa, H., Imoto, T., Hayama, T., 1984a. Responsiveness of solitary-parabrachial relay neurons to taste and mechanical stimulation applied to the oral cavity in rats. *Exp.Brain Res.* 54, 349-358.

- Ogawa, H., Imoto, T., Hayama, T., 1984b. Responsiveness of solitario-parabrachial relay neurons to taste and mechanical stimulation applied to the oral cavity in rats. *Experimental Brain Research*. 54, 349-358.
- Ohla, K., et al., 2019. Recognizing Taste: Coding Patterns Along the Neural Axis in Mammals. *Chemical Senses*. 44, 237-247.
- Oler, J.A., et al., 2017. Connectivity between the central nucleus of the amygdala and the bed nucleus of the stria terminalis in the non-human primate: neuronal tract tracing and developmental neuroimaging studies. *Brain Struct Funct*. 222, 21-39.
- Ono, T., et al., 1985a. Topographic organization of projections from the amygdala to the hypothalamus of the rat. *Neurosci Res*. 2, 221-38.
- Ono, T., et al., 1985b. Topographic organization of projections from the amygdala to the hypothalamus of the rat. *Neuroscience Research*. 2, 221-238.
- Ottersen, O.P., 1980a. Afferent connections to the amygdaloid complex of the rat and cat: II. Afferents from the hypothalamus and the basal telencephalon. *Journal of Comparative Neurology*. 194, 267-289.
- Ottersen, O.P., 1980b. Afferent connections to the amygdaloid complex of the rat and cat: II. Afferents from the hypothalamus and the basal telencephalon. *J Comp Neurol*. 194, 267-89.
- Pallante, L., et al., 2021. On the human taste perception: Molecular-level understanding empowered by computational methods. *Trends in Food Science & Technology*. 116, 445-459.
- Palmer, J.A., et al., 2000. Development and optimization of herpes simplex virus vectors for multiple long-term gene delivery to the peripheral nervous system. *J Virol*. 74, 5604-18.
- Panguluri, S., Saggi, S., Lundy, R., 2009. Comparison of somatostatin and corticotrophin-releasing hormone immunoreactivity in forebrain neurons projecting to taste-responsive and non-responsive regions of the parabrachial nucleus in rat. *Brain Res*. 1298, 57-69.
- Paxinos, G., Franklin, K.B.J., 2001. *The Mouse Brain in Stereotaxic Coordinates*. Academic Press.
- Reilly, S., Grigson, P.S., Norgren, R., 1993a. Parabrachial nucleus lesions and conditioned taste aversion: evidence supporting an associative deficit. *Behav. Neurosci*. 107, 1005-1017.
- Reilly, S., Grigson, P.S., Norgren, R., 1993b. Parabrachial nucleus lesions and conditioned taste aversion: Evidence supporting an associative deficit. *Behavioral Neuroscience*. 107, 1005-1017.
- Reppucci, C.J., Petrovich, G.D., 2016. Organization of connections between the amygdala, medial prefrontal cortex, and lateral hypothalamus: a single and double retrograde tracing study in rats. *Brain structure & function*. 221, 2937-2962.
- Riley, C.A., King, M.S., 2013. Differential effects of electrical stimulation of the central amygdala and lateral hypothalamus on fos-immunoreactive neurons in the gustatory brainstem and taste reactivity behaviors in conscious rats. *Chem Senses*. 38, 705-17.

- Rosen, A.M., Roussin, A.T., Di Lorenzo, P.M., 2010. Water as an independent taste modality. *Front Neurosci.* 4, 175.
- Saggu, S., Lundy, R.F., 2008a. Forebrain neurons that project to the gustatory parabrachial nucleus in rat lack glutamic acid decarboxylase. *Am.J.Physiol Regul.Integr.Comp Physiol.* 294, R52-R57.
- Saggu, S., Lundy, R.F., 2008b. Forebrain neurons that project to the gustatory parabrachial nucleus in rat lack glutamic acid decarboxylase. *American journal of physiology. Regulatory, integrative and comparative physiology.* 294, R52-R57.
- Saha, S., Batten, T.F.C., Henderson, Z., 2000. A GABAergic projection from the central nucleus of the amygdala to the nucleus of the solitary tract: a combined anterograde tracing and electron microscopic immunohistochemical study. *Neuroscience.* 99, 613-626.
- Saha, S., Henderson, Z., Batten, T.F., 2002. Somatostatin immunoreactivity in axon terminals in rat nucleus tractus solitarius arising from central nucleus of amygdala: coexistence with GABA and postsynaptic expression of sst2A receptor. *J.Chem.Neuroanat.* 24, 1-13.
- Sakurai, T., et al., 1998. Orexins and Orexin Receptors: A Family of Hypothalamic Neuropeptides and G Protein-Coupled Receptors that Regulate Feeding Behavior. *Cell.* 92, 573-585.
- Sato, M., Koyano, H., 1987. Autoradiographic demonstration of the distribution of vagal afferent nerve fibers in the epiglottis of the rabbit. *Brain Research.* 410, 101-105.
- Scalera, G., Spector, A.C., Norgren, R., 1995a. Excitotoxic lesions of the parabrachial nuclei prevent conditioned taste aversions and sodium appetite in rats. *Behavioral Neuroscience.* 109, 997-1008.
- Scalera, G., Spector, A.C., Norgren, R., 1995b. Excitotoxic lesions of the parabrachial nuclei prevent conditioned taste aversions and sodium appetite in rats. *Behav.Neurosci.* 109, 997-1008.
- Scalera, G., Grigson, P.S., Norgren, R., 1997. Gustatory functions, sodium appetite, and conditioned taste aversion survive excitotoxic lesions of the thalamic taste area. *Behavioral Neuroscience.* 111, 633-645.
- Shimura, T., Komori, M., Yamamoto, T., 1997a. Acute sodium deficiency reduces gustatory responsiveness to NaCl in the parabrachial nucleus of rats. *Neurosci.Lett.* 236, 33-36.
- Shimura, T., Komori, M., Yamamoto, T., 1997b. Acute sodium deficiency reduces gustatory responsiveness to NaCl in the parabrachial nucleus of rats. *Neuroscience Letters.* 236, 33-36.
- Shimura, T., et al., 1997c. Brainstem lesions and gustatory function: I. The role of the nucleus of the solitary tract during a brief intake test in rats. *Behav Neurosci.* 111, 155-68.
- Shimura, T., et al., 1997d. Brainstem lesions and gustatory function: I. The role of the nucleus of the solitary tract during a brief intake test in rats. *Behav.Neurosci.* 111, 155-168.

- Shimura, T., Tanaka, H., Yamamoto, T., 1997e. Salient responsiveness of parabrachial neurons to the conditioned stimulus after the acquisition of taste aversion learning in rats. *Neuroscience*. 81, 239-247.
- Shuford, E.H., Jr., 1959. Palatability and osmotic pressure of glucose and sucrose solutions as determinants of intake. *Journal of Comparative and Physiological Psychology*. 52, 150-153.
- Smith, D.V., Li, C.S., 2000. GABA-mediated corticofugal inhibition of taste-responsive neurons in the nucleus of the solitary tract. *Brain Res*. 858, 408-415.
- Smith, D.V., Ye, M.K., Li, C.S., 2005. Medullary taste responses are modulated by the bed nucleus of the stria terminalis. *Chem.Senses*. 30, 421-434.
- Somogyi, P., et al., 1984. Different populations of GABAergic neurons in the visual cortex and hippocampus of cat contain somatostatin- or cholecystokinin- immunoreactive material. *The Journal of Neuroscience*. 4, 2590-2603.
- Spector, A.C., Norgren, R., Grill, H.J., 1992a. Parabrachial gustatory lesions impair taste aversion learning in rats. *Behavioral Neuroscience*. 106, 147-161.
- Spector, A.C., Norgren, R., Grill, H.J., 1992b. Parabrachial gustatory lesions impair taste aversion learning in rats. *Behav.Neurosci*. 106, 147-161.
- Spector, A.C., Grill, H.J., Norgren, R., 1993a. Concentration-dependent licking of sucrose and sodium chloride in rats with parabrachial gustatory lesions. *Physiology & Behavior*. 53, 277-283.
- Spector, A.C., Grill, H.J., Norgren, R., 1993b. Concentration-dependent licking of sucrose and sodium chloride in rats with parabrachial gustatory lesions. *Physiol Behav*. 53, 277-283.
- Spector, A.C., 1995. Gustatory parabrachial lesions disrupt taste-guided quinine responsiveness in rats. *Behav.Neurosci*. 109, 79-90.
- St John, S.J., Boughter, J.D., Jr., 2004. The contribution of taste bud populations to bitter avoidance in mouse strains differentially sensitive to sucrose octoacetate and quinine. *Chem Senses*. 29, 775-87.
- Steiger, J.H., 2004. Beyond the F test: Effect size confidence intervals and tests of close fit in the analysis of variance and contrast analysis. *Psychol Methods*. 9, 164-82.
- Stengel, A., et al., 2010. Activation of brain somatostatin 2 receptors stimulates feeding in mice: analysis of food intake microstructure. *Physiol Behav*. 101, 614-622.
- Stone, L.M., et al., 1995. Taste receptor cells arise from local epithelium, not neurogenic ectoderm. *Proceedings of the National Academy of Sciences*. 92, 1916-1920.
- Taniguchi, H., et al., 2011. A resource of Cre driver lines for genetic targeting of GABAergic neurons in cerebral cortex. *Neuron*. 71, 995-1013.
- Thek, K.R., et al., 2019. Extensive Inhibitory Gating of Viscerosensory Signals by a Sparse Network of Somatostatin Neurons. *J Neurosci*. 39, 8038-8050.

- Tokita, K., et al., 2007. Involvement of forebrain in parabrachial neuronal activation induced by aversively conditioned taste stimuli in the rat. *Brain Research*. 1141, 188-196.
- Tokita, K., Inoue, T., Boughter, J.D., Jr., 2009. Afferent connections of the parabrachial nucleus in C57BL/6J mice. *Neuroscience*. 161, 475-488.
- Tokita, K., Inoue, T., Boughter, J.D., Jr., 2010. Subnuclear organization of parabrachial efferents to the thalamus, amygdala and lateral hypothalamus in C57BL/6J mice: a quantitative retrograde double labeling study. *Neuroscience*. 171, 351-365.
- Torruella-Suarez, M.L., et al., 2020. Manipulations of Central Amygdala Neurotensin Neurons Alter the Consumption of Ethanol and Sweet Fluids in Mice. *J Neurosci*. 40, 632-647.
- Travers, J.B., 1988. Efferent projections from the anterior nucleus of the solitary tract of the hamster. *Brain Res*. 457, 1-11.
- Tye, K.M., et al., 2011. Amygdala circuitry mediating reversible and bidirectional control of anxiety. *Nature*. 471, 358-362.
- van der, K.D., et al., 1984. The organization of projections from the cortex, amygdala, and hypothalamus to the nucleus of the solitary tract in rat. *J.Comp Neurol*. 224, 1-24.
- Veening, J.G., Swanson, L.W., Sawchenko, P.E., 1984. The organization of projections from the central nucleus of the amygdala to brainstem sites involved in central autonomic regulation: a combined retrograde transport-immunohistochemical study. *Brain Res*. 303, 337-357.
- Verhagen, J.V., Giza, B.K., Scott, T.R., 2003. Responses to taste stimulation in the ventroposteromedial nucleus of the thalamus in rats. *J Neurophysiol*. 89, 265-75.
- Wang, L., et al., 2018. The coding of valence and identity in the mammalian taste system. *Nature*. 558, 127-131.
- Whitside, B., 1927. Nerve overlap in the gustatory apparatus of the rat. *Journal of Comparative Neurology (and Psychology)*. 44, 363-377.
- Wu, A., et al., 2015. Breadth of tuning in taste afferent neurons varies with stimulus strength. *Nature Communications*. 6, 8171.
- Ye, J., Veinante, P., 2019. Cell-type specific parallel circuits in the bed nucleus of the stria terminalis and the central nucleus of the amygdala of the mouse. *Brain Struct Funct*. 224, 1067-1095.
- Yigit, S., Mendes, M., 2018. Which Effect Size Measure Is Appropriate for One-Way and Two-Way Anova Models? A Monte Carlo Simulation Study. *Revstat-Statistical Journal*. 16, 295-313.
- Yu, K., et al., 2016a. Central Amygdala Somatostatin Neurons Gate Passive and Active Defensive Behaviors. *The Journal of Neuroscience*. 36, 6488.
- Yu, K., et al., 2016b. Central Amygdala Somatostatin Neurons Gate Passive and Active Defensive Behaviors. *J Neurosci*. 36, 6488-96.
- Zhang, C., Kang, Y., Lundy, R.F., 2011. Terminal field specificity of forebrain efferent axons to the pontine parabrachial nucleus and medullary reticular formation. *Brain Res*. 1368, 108-18.

Zhang, Q., et al., 2019. Multiplexed peroxidase-based electron microscopy labeling enables simultaneous visualization of multiple cell types. *Nature neuroscience*. 22, 828-839.

Zocchi, D., Wennemuth, G., Oka, Y., 2017. The cellular mechanism for water detection in the mammalian taste system. *Nat Neurosci*. 20, 927-933.

CURRICULUM VITAE

Jane J. Bartonjo, MSc., MLS (ASCP)^{CM}

Department of Anatomical Science and Neurobiology

511 S. Floyd St.

University of Louisville, School of Medicine

Louisville, KY 40202

Email: jbartonjo@outlook.com

EDUCATION

- | | |
|------------------|--|
| Aug 2018-Present | PhD candidate, Anatomical Sciences and Neurobiology
University of Louisville, School of Medicine, Louisville,
KY |
| May 2021 | MSc., Anatomical Sciences and Neurobiology University
of Louisville, School of Medicine, Louisville, KY |
| Dec 2018 | BSc., Medical Laboratory Science, Western Kentucky
University, Bowling Green, KY |
| May 2015 | MSc., Cell Molecular Biology, Western Kentucky
University, Bowling Green, KY |
| May 2011 | BSc., Biology & Chemistry, Western Kentucky University,
Bowling Green, KY |

HONORS AND AWARDS

2023	Doctoral Dissertation Completion Award, University of Louisville, Louisville KY
2022	Diversity fellowship, Association for Chemoreception Sciences (AChemS)
2022	Graduate Student Travel Award, University of Louisville, Louisville KY
2017	Certificate of Excellent Service to Patients, Owensboro Health Regional Hospital
2011	Outstanding Graduating Senior, Chemistry Department, Western Kentucky University, Bowling Green, KY
2010	Best Undergraduate Poster Award, 40 th Gr
2009	Biology Summer Undergraduate Research Experience funding, Western Kentucky University, Bowling Green, KY
2008-2011	Full athletic Scholarship (track & field), Western Kentucky University, Bowling Green, KY
2008-2010	Sunbelt Conference Commissioner's List (GPA \geq 3.5)
2008-2010	Two-time Dean's Scholar List (3.5 \geq GPA \leq 3.79)
2009-2011	Five-time President's List (GPA \geq 3.8)

TEACHING EXPERIENCE

- 2019 Graduate Teaching Assistant, Anatomical Sciences and Neurobiology University of Louisville, School of Medicine, Louisville, KY
- 2017 (Spring) Adjunct Faculty, Biology Department, Austin Peay State University, Clarksville TN
- 2012- 2015 Graduate Teaching Assistant, Biology Department, Western Kentucky University, Bowling Green KY
- 2014 (Fall) Adjunct Faculty, Biology Department, Brescia University, Owensboro KY

RESEARCH EXPERIENCE

- 2018-2023 Graduate assistant, University of Louisville, School of Medicine
- ◇ Lab rotations in vision lab studying glaucoma in mice model.
 - ◇ Dissertation work in taste lab. Studied the role of central amygdala somatostatin neurons in taste behavior in mice
- 2012-2015 Graduate assistant, Western Kentucky University
- ◇ Developed transgenic plants expressing purple acid phosphatase for phytoremediation of excess soil phosphorus.

- ◇ Collaborated with the University of Texas at El Paso to conduct a research study on the potential uptake of cerium nanoparticles from the environment through the leaves of cucumber plants and its physiological impacts.

2009-2011

Undergraduate research

- ◇ Worked in a biochemistry lab studying gene expression.
- ◇ Collaborated with a graduate student to establish a protocol for the eco-friendly synthesis of gold nanoparticles.

POSTERS/PRESENTATIONS

Jane J. Bartonjo, Robert F Lundy, 2023. Connectivity of amygdala somatostatin-expressing neurons and their role in taste-guided behavior. Graduate Student Regional Research Conference.

Jane J. Bartonjo, Robert F Lundy, 2022. Anatomical Connectivity of Amygdala Somatostatin-Expressing Neurons and Contribution to Taste-Guided Behavior. Sensorium.

Jane J. Bartonjo, Robert F Lundy, 2022. Synaptic connectivity of central amygdala Somatostatin neurons. KY INBRE Electron Microscopy Workshop.

Jane J. Bartonjo, Robert F Lundy, 2022. Somatostatin expressing cells of central amygdala projecting to the nucleus of solitary tract and the lateral hypothalamus are distinct cell populations. Society for neuroscience, University of Louisville Chapter.

Jane J. Bartonjo, Robert F Lundy, 2022. Somatostatin Expressing Cells of Central Amygdala projecting to the Nucleus of Solitary Tract, Parabrachial Nucleus, and the Lateral Hypothalamus are Distinct cell populations. Association for chemoreception sciences.

Jane J. Bartonjo, Sean Masterson, Steven J. St. John, Robert Lundy, 2021. Regulation of licking responses by amygdala somatostatin expressing neurons that project to the nucleus of solitary tract. Society for neuroscience.

COMPUTER SKILLS

- ◇ Adobe suite
- ◇ ImageJ
- ◇ MATLAB
- ◇ Microsoft suite
- ◇ Sigmaplot

PROFESSIONAL AFFILIATIONS

- ◇ Society for Neuroscience
- ◇ Association for Chemoreception Sciences
- ◇ American Society for Clinical Pathology

COMMUNITY SERVICE

- | | |
|------|---|
| 2023 | Louisville Regional Science and Engineering Fair
(Judge) |
| 2023 | duPont Manual Regional Fair Judge (Lead Judge) |
| 2022 | Science Policy & Outreach Group, Louisville KY |

LEADERSHIP

- | | |
|-----------|--|
| 2021-2023 | Student Representative in Graduate Committee,
University of Louisville, Louisville KY |
| 2021 | Co-founder, Core humanitarian Agency Inc, Louisville
KY |

CERTIFICATIONS

- | | |
|------|---|
| 2018 | Medical Laboratory Scientist MLS (ASCP) ^{CM} |
| 2012 | Basic Skills for College Teaching |

JOURNAL PUBLICATIONS

Bartonjo JJ, Lundy RF. Target-specific projections of amygdala somatostatin-expressing neurons to the hypothalamus and brainstem. *Chem Senses*. 2022 Jan 1;47:bjac009. doi: 10.1093/chemse/bjac009. PMID: 35522083; PMCID: PMC9074687.

Bartonjo J, Masterson S, St John SJ, Lundy R. Perturbation of amygdala/somatostatin-nucleus of the solitary tract projections reduces sensitivity to quinine in a brief-access test. *Brain Res*. 2022 May 15;1783:147838. doi: 10.1016/j.brainres.2022.147838. Epub 2022 Feb 16. PMID: 35182570; PMCID: PMC8950164.

Bartonjo JJ, Lundy RF. Distinct Populations of Amygdala Somatostatin-Expressing Neurons Project to the Nucleus of the Solitary Tract and Parabrachial Nucleus. *Chem Senses*. 2020 Nov 7;45(8):687-698. doi: 10.1093/chemse/bjaa059. PMID: 32940663; PMCID: PMC7648651.

Hong, J., Peralta-Videa, J. R., Rico, C., Sahi, S., Viveros, M. N., **Bartonjo, J.**, ... & Gardea-Torresdey, J. L. (2014). Evidence of translocation and physiological impacts of foliar applied CeO₂ nanoparticles on cucumber (*Cucumis sativus*) plants. *Environmental science & technology*, 48(8), 4376-4385.

Badwaik, V. D., **Bartonojo, J. J.**, Evans, J. W., Sahi, S. V., Willis, C. B., & Dakshinamurthy, R. (2011). Single-step biofriendly synthesis of surface modifiable, near-spherical gold nanoparticles for applications in biological detection and catalysis. *Langmuir*,